Atmospheric
Chemistry
and Physics
Discussions

1

2

3

4      **Atmospheric gas-phase composition over the Indian Ocean**

5

6

7      Susann Tegtmeier[1], Christa Marandino[2], Yue Jia[1], Birgit Quack[2], Anoop S. Mahajan[3]

8

9

10     [1]Institute of Space and Atmospheric Studies, University of Saskatchewan, Saskatoon, Canada

11

12     [2]GEOMAR Helmholtz Centre for Ocean Research Kiel, 24105 Kiel, Germany

13

14     [3]Center for Climate Change Research, Indian Institute of Tropical Meteorology, Pune,

15     411016, India

16

Atmospheric
Chemistry
and Physics
Discussions

1    **Abstract**
2
3    The Indian Ocean is coupled to atmospheric dynamics, transport and chemical composition via
4    several unique mechanisms, such as the seasonally varying monsoon circulation. During the
5    winter monsoon season, high pollution levels are regularly observed over the entire northern
6    Indian Ocean, while during the summer monsoon, clean air dominates the atmospheric
7    composition, leading to distinct chemical regimes. The changing atmospheric composition over
8    the Indian Ocean can interact with oceanic biogeochemical cycles and impact marine
9    ecosystems, resulting in potential climate feedbacks.

10    Here, we review current progress in detecting and understanding atmospheric gas-phase
11    composition over the Indian Ocean and its local and global impacts. The review takes into
12    account results from recent Indian Ocean ship campaigns, satellite measurements, station data
13    and information on continental and oceanic trace gas emissions. The distribution of all major
14    pollutants and greenhouse gases shows pronounced differences between the landmass source
15    regions and the Indian Ocean with strong gradients over the coastal areas. Surface pollution and
16    ozone are highest during the winter monsoon over the Bay of Bengal and the Arabian Sea
17    coastal waters due to air mass advection from the Indo-Gangetic Plain and continental outflow
18    from Southeast Asia.

19    We observe, however, that unusual types of wind patterns can lead to pronounced deviations
20    of the typical trace gas distributions. For example, the ozone distribution maxima shift to
21    different regions under different wind scenarios. The distribution of greenhouse gases over the
22    Indian Ocean shows many similarities when compared to the pollution fields, but also some
23    differences of the latitudinal and seasonal variations resulting from their long lifetimes and
24    biogenic sources. Mixing ratios of greenhouse gases such as methane show positive trends over
25    the Indian Ocean, but long-term changes of pollution and ozone, and in particular how they are
26    driven by changing emissions and transport patterns, require further investigation in the future.
27    Although we know that changing atmospheric composition and perturbations within the Indian
28    Ocean affect each other, the impacts of atmospheric pollution on oceanic biogeochemistry and
29    trace gas cycling is severely understudied. We highlight potential mechanisms, future research
30    topics and observational requirements that need to be explored in order to fully understand
31    interactions and feedbacks between the ocean and atmosphere in the Indian Ocean region.
32

33    **1. Introduction**

34    Over the Indian Ocean, intense anthropogenic pollution from Southeast Asia mixes with
35    pristine oceanic air. The interplay of the polluted continental and the clean oceanic air masses,
36    and the resulting atmospheric composition are determined by distinct seasonal circulation
37    patterns. The large-scale monsoon circulations in combination with anthropogenic emissions
38    from southern Asia lead to seasonally contrasting chemical regimes over the Indian Ocean. As
39    the anthropogenic emissions include relatively large contributions from biofuel/biomass
40    combustion and incomplete industrial burning, the atmospheric composition during polluted
41    periods shows unique characteristics when compared to other regimes. The complex mixture
42    of chemical constituents and large-scale transport patterns can have a profound influence on
43    oceanic processes, stratospheric composition and neighbouring regions such as the
44    Mediterranean and Africa. Here, we review recent progress in detecting and understanding
45    atmospheric gas-phase composition over the Indian Ocean and its local and global impact. This
46    article is part of the special issue 'Understanding the Indian Ocean system: past, present and
47    future'.
48
49

Atmospheric
Chemistry
and Physics
Discussions

### 1.1 Region

The Indian Ocean is the world's third largest ocean covering 19.8% of the water on the Earth's surface. In contrast to the Pacific and Atlantic Oceans, it does not stretch from pole to pole, but is enclosed on three sides by major landmasses and an archipelago. The Indian Ocean is centred on the Indian Peninsula, which also forms the northern border together with Iran, Pakistan, and Bangladesh. In the west, the Indian Ocean is bounded by East Africa and the Arabian Peninsula, while the eastern and southern boundaries are set by Southeast Asia, Australia, and the Southern Ocean.

The countries bordering the Indian Ocean include a wide variety of races, cultures, and religions. They are home to one-third of the world's population accounting for approximately 2.5 billion people. The economies of many Indian Ocean countries are expanding rapidly, with India being the fastest growing major economy in the world. Similarly, many Indian Ocean countries show a rapid population growth, which is expected to further increase in the future. Given the quickly growing populations and industries, the Indian Ocean is becoming a pivotal zone of strategic political competition. At the same time, the Indian Ocean hosts a large variety of marine ecosystems including coral reefs, seagrass beds, and mangrove forests. Anthropogenic activities along the coastlines and climate change threaten biodiversity in the Indian Ocean, which contains 25% of the Earth's biodiversity hotspots (Mittermeier et al., 2011).

Growing populations also lead to rapidly increasing anthropogenic emissions. Burning conditions are often poorly controlled, as for instance during biofuel burning in cook-stoves, and fossil fuel burning in vehicles (Li et al., 2017). Together with burning of coal and other fossil fuels for energy production, this leads to large emissions of man-made trace species including greenhouse gases and ozone precursors (e.g., Lawrence, 2004). In addition, primary aerosols, such as soot and dust, and precursors of secondary aerosols are released in relatively large amounts. As a result, air pollution is a serious health issue in many Indian Ocean countries, leading to increases in respiratory and cardiovascular problems (Rajak and Chattopadhyay, 2019). The intense pollution has also been linked to regional weather impacts, such as changes of rainfall patterns and decreasing crop harvests (e.g., Bollasina et al., 2011, Li et al., 2016).

### 1.2 Seasons

Seasonal changes of atmospheric transport patterns are the main driver of Indian Ocean chemical regimes and lead to periods of strong anthropogenic pollution alternating with periods of clean oceanic air. The South Asian monsoon circulation, the strongest monsoon system in the world, dominates the regional meteorology of the Indian subcontinent. The seasonal reversal of the winds is coupled to a strong annual cycle of precipitation with very wet summer and dry winter conditions (Chang, 1967). Being the dominant driver of the annual cycle of rainfall, the South Asian monsoon controls the water and food security of the region and, thus, the well-being and prosperity of large populations.

The monsoon system also has a strong impact on the atmospheric composition over the Indian Ocean. The winter monsoon from November to March is characterized by a strong north-easterly flow that spreads regional pollution from Southeast Asia over the entire northern Indian Ocean (Lelieveld et al., 2001). Continental aerosols as well as man-made trace species and their reaction products dominate the chemical regime. During this time, a layer of air pollution is visible on satellite pictures as a haze of brown colour hanging over much of South Asia and the Indian Ocean. This so-called Indian Ocean brown cloud has been suggested to impact regional climate by masking greenhouse gas induced surface warming (Ramanathan et al., 2005) and to affect monsoon rainfall.

1 In contrast, clean air dominates the atmospheric composition over the Indian Ocean during the
2 summer monsoon from June to September, leading to a completely different chemical regime.
3 Atmospheric pollutant levels are low and typical open ocean background conditions can be
4 observed (Lawrence and Lelieveld, 2010). The surface circulation is accompanied by heavy
5 rainfall over the Indian subcontinent and an anticyclonic circulation, centred at 200 to 100 hPa.
6 While boreal summer surface conditions prevent the anthropogenic pollution from spreading
7 across the Indian Ocean, the anticyclone offers an efficient pathway for continental pollution
8 into the global upper troposphere and lower stratosphere (e.g., Randel et al., 2010).

9 Finally, during the monsoon transition periods from April to May and September to October,
10 zonal flows dominate the surface transport patterns. While this allows for some continental air
11 masses from Southeast Asia and Africa to be transported over the Indian Ocean, the offshore
12 pollution is in general less strong during the transition periods compared to the winter monsoon
13 conditions (Sahu et al., 2006). Strong spatial and temporal variations of trace gas distributions
14 resulting from transitioning transport regimes have been reported during these periods (e.g.,
15 Mallik et al., 2013).

16 ### 1.3    Early work

17 The largest international scientific study exploring the impact of South Asian emissions on the
18 composition of the atmosphere over the Indian Ocean, the Indian Ocean Experiment
19 (INDOEX), took place during the winter monsoon 1999. During the multiplatform field
20 campaign, surprisingly high pollution was detected over the entire northern Indian Ocean all
21 the way to the Intertropical Convergence Zone (ITCZ). Scientific studies revealed that the
22 nature of the pollution was considerably different from that in Europe or North America, with
23 strongly enhanced carbon monoxide concentrations related to widespread biofuel use and
24 agricultural burning (e.g., Lelieveld et al., 2001). Other large pollution sources based on fossil
25 fuel combustion and biomass burning were linked to high loads of sunlight-absorbing aerosols
26 with potential consequences for the regional atmospheric energy balance (Ramanathan et al.,
27 2002).

28 The INDOEX findings, presented in many scientific publications, have drawn attention to this
29 region and several projects and campaigns followed over the next decade. The Bay of Bengal
30 Experiment (BOBEX) research cruise during February to March 2001 detected high ozone and
31 pollution levels over the Bay of Bengal and linked them to transport from the continent (Naja
32 et al., 2004; Lal et al., 2006). The southern Indian Ocean was explored during the Pilot
33 Expedition to the Southern Ocean (PESO) reseach cruise from January to April 2004, which
34 revealed much cleaner air masses with smaller aerosol loadings in the region south of the ITCZ
35 (Pant et al., 2009). Other research cruises such as the Bay of Bengal Processes Studies (BOBPS)
36 during September to October 2002, investigated oceanic productivity and nutrients in relation
37 to air-sea exchange of climate active gases (Sardessai et al., 2007). A detailed overview of
38 research cruises, island measurements and aircraft campaigns investigating the atmosphere over
39 the Indian Ocean is given in Lawrence and Lelieveld (2010). The authors provide a
40 comprehensive review of the state of the art at this time by bringing together observational and
41 modelling studies.

42 ### 1.4 Scope and organization of this study

43 Here we will focus on recent progress in the field by giving an overview of results obtained
44 after 2010. We will synthesize the current understanding of Indian Ocean gas phase
45 atmospheric composition and explore how it is driven by emission sources, transport, and
46 chemistry. This review focuses on three groups of atmospheric gases 1) ozone and pollutants -
47 carbon monoxide (CO), nitrogen oxides ($NO_x$), sulphur dioxide ($SO_2$) and mercury; 2)
48 greenhouse gases - methane ($CH_4$), nitrous oxide ($N_2O$), carbon dioxide ($CO_2$) and carbonyl

1    sulphide (COS) and 3) short-lived biogenic gases - dimethylsulphide (DMS), isoprene and
2    halogen compounds. Section 2 provides an overview of the physical processes in the
3    atmosphere and ocean that are relevant for the atmospheric composition. Section 3 will
4    introduce all campaigns and measurements that are the basis for scientific studies published
5    after 2010 and are discussed here. Regional sources and sinks of greenhouse gases, pollution
6    and biogenic trace gases will be given in Section 4. Short introductions to all gases listed above,
7    including their role in the atmosphere, can also be found in section 4. The focus of section 5 is
8    on our current knowledge of the atmospheric composition over the Indian Ocean and how it is
9    driven by physical processes and by regional sources. We will present a synthesis of the
10   scientific progress made after 2010 in Section 6, where we will also discuss the global and local
11   impacts of the Indian Ocean atmospheric composition. An outlook and a summary of current
12   knowledge gaps are given in Section 7. A key for all abbreviations used in this paper is provided
13   in Appendix A.
14
15   **2 Physical processes**

16   **2.1 Atmospheric processes**

17   The South Asian monsoon circulation dominates the transport patterns and regional
18   meteorology over the Indian Ocean. Strong seasonal circulation changes give rise to three main
19   meteorological regimes: the summer monsoon from June to September, the winter monsoon
20   from November to March and the transition periods from April to May and from the end of
21   September to October.

22   **Near-surface flow patterns**
23   A detailed picture of the near-surface flow patterns is provided in Fig. 1 in the form of seasonal
24   mean surface wind fields and sea level pressure. Seasonal mean plots here and in the rest of the
25   paper are shown for core monsoon and transition periods, i.e., June to August (JJA) for the
26   summer monsoon, December to February (DJF) for the winter monsoon, April to May (Apr-
27   May) for the spring transition period and October (Oct) for the autumn transition period. The
28   equatorial and northern Indian Ocean (north of 10°S) are dominated by seasonally reversing
29   monsoon winds (Schott and McCreary, 2001; Schott et al., 2009). Southeast winds occur during
30   the summer monsoon with the low-pressure system of the ITCZ shifted north of 15°N (Fig. 1a),
31   while northwest winds occur during the winter monsoon with the low-pressure belt situated
32   south of the equator (Fig. 1b). Over the southern Indian Ocean (south of 10°S), steady southeast
33   trades prevail during all seasons, but reach further northward during the northern summer.

34   The seasonally reversing monsoon winds and inter-hemispheric pressure gradients over the
35   equatorial Indian Ocean are a striking feature different from the other tropical oceans, where
36   sustained easterly winds are found along the equator. In contrast, equatorial winds over the
37   Indian Ocean are westerlies during the monsoon transition periods (Fig. 1c and 1d) and show a
38   weak westerly annual mean component (Lamb and Hastenrath, 1979). These equatorial
39   westerlies are driven by an interplay of an eastward pressure gradient along the equator, the
40   latitudinal position of the flow recurvature and the strength of the trade winds (Hastenrath and
41   Polzin, 2004). During the autumn transition period, the equatorial westerlies are the surface
42   manifestation of a zonal–vertical circulation cell between the regions of ascending motion over
43   Indonesia and subsidence over equatorial East Africa (Hastenrath, 2000). Interannual variations
44   of the zonal circulation lead to enhanced subsidence and decreased rainfall at the coast of East
45   Africa during years of intense circulation with accelerated surface westerlies.
46
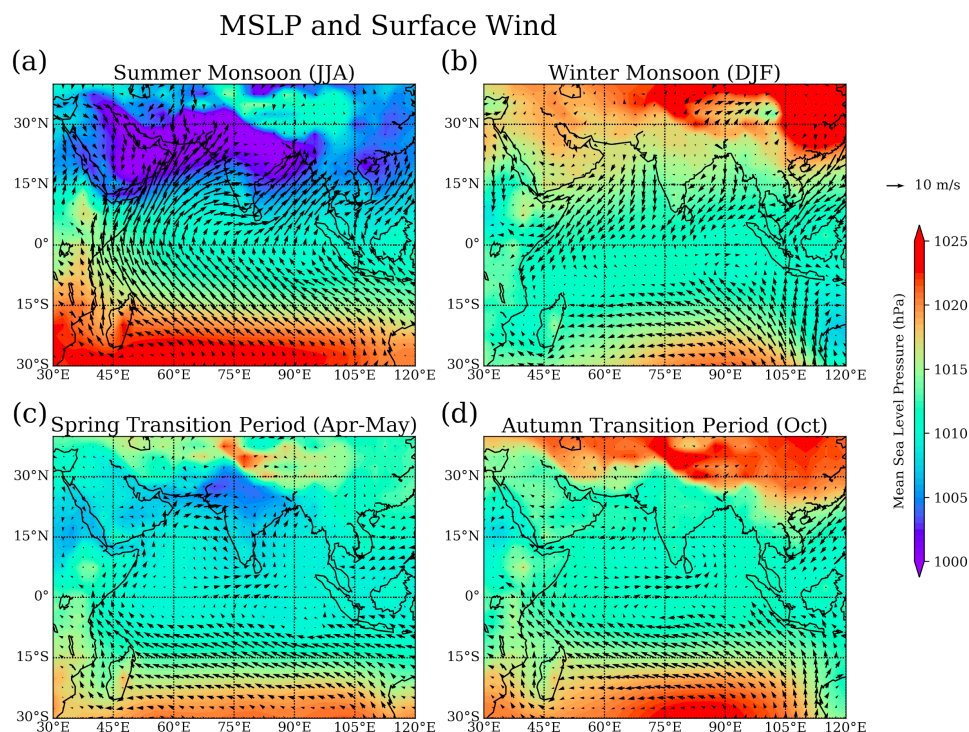
MSLP and Surface Wind

Figure 1. Mean surface level pressure (MSLP) and surface wind for (a) summer monsoon 2018 (June - August), (b) winter monsoon 2018/2019 (December - February), (c) spring transition 2018 (April - May) and (d) autumn transition 2018 (October) periods from ERA-Interim.

**Summer and winter monsoon**

During the summer monsoon, steady onshore winds transport air from the ocean over to the continent, where it rises due to buoyancy and orographic forcing. The resulting deep convection is characterised by massive cirrus anvil clouds and the well-known Indian summer monsoon rains. Air masses experiencing fast upward transport in convective updraughts converge in the upper troposphere forming a high-pressure system. The associated anticyclone circulation is tied to the outflow of the deep convection and is situated directly over the highly polluted southern Asia. As a result, distinct tracer anomalies have been observed in the anticyclone indicating strong upward transport of pollution from the surface (e.g., Randel et al., 2010). Given the dynamical confinement of tropospheric tracers and aerosols in the anticyclone, the Asian monsoon system provides a potentially efficient pathway from the surface to the tropical upper troposphere and lower stratosphere.

During the winter monsoon, prevailing north-easterly winds reverse the meteorological situation. There is little rain over southern Asia marking this as the 'dry season' and the missing convection chemically disconnects the surface layer from the upper troposphere (Kunhikrishnan et al., 2004). Instead, pollution outflow occurs in the marine boundary layer (MBL) via offshore winds towards the northern Indian Ocean down to the equator. Primary MBL flow channels have been identified in the western Arabian Sea, the eastern Arabian Sea just off the Indian west coast, the western Bay of Bengal and Southeast Asia (Krishnamurti 1997a; 1997b; Verver et al., 2001).

Atmospheric
Chemistry
and Physics
Discussions

1    Winter monsoon flow patterns are further complicated by effects of the land-sea breeze, which
2    lofts coastal air masses above the MBL (Simpson and Raman, 2004). The associated offshore
3    flow above the MBL transports air masses over the coastal oceans where they constitute the so-
4    called 'elevated layer'. Due to the relatively rapid outflow, the elevated layer provides an
5    additional effective mechanism for pollution transport from the continents towards the Indian
6    Ocean (Lawrence and Lelieveld, 2010). As a result, outflow during the winter monsoon occurs
7    in two distinct layers, namely the pollutant plume within the MBL (up to 800-1000m) and the
8    elevated layer (1-3km). Once over the northern Indian ocean, the north-easterly trade winds
9    transport the air masses towards the ITCZ typical within 7–10 days (Ethé et al., 2002).
10   Similarly, over the southern Indian Ocean, south-easterly winds transport pristine boundary
11   layer air masses northwards. At the ITCZ, these trade wind flows converge, and associated
12   convection transports the air upwards into the upper troposphere (Iyengar et al., 1999).

13   Over the western part of the tropical Indian Ocean, the ITCZ has been observed to occur
14   simultaneously in two bands on either side of the equator forming the so-called double ITCZ
15   (Meenu et al., 2007). Signatures of the double ITCZ are present practically throughout the year
16   with the largest frequency occurrence in November (~85%) and December (~62%). Based on
17   cloud characteristics and outgoing longwave radiation, the most preferred latitudes for the
18   northern and southern bands of the ITZC were found to be around 5°N and 7.5°S to 10°S.

19   **Intraseasonal and interannual variability**
20   Intraseasonal variability can impact atmospheric transport patterns over the Indian Ocean with
21   the dominant mode being the eastward propagating Madden-Julian Oscillation (MJO).
22   Equatorially trapped, baroclinic oscillations in the tropical wind field propagate slowly
23   eastward across the Indian Ocean, Maritime Continent, and West Pacific with an intraseasonal
24   cycle of 30–60 days (Madden and Julian, 1972). A typical MJO event exhibits large-scale
25   convection anomalies where enhanced convection and rainfall develop over the western Indian
26   Ocean with suppressed convection further east over the western Pacific (Zhang, 2005). The
27   eastward propagation of the convection and circulation anomalies depends on the season and is
28   strongest during the winter monsoon. The summer monsoon shows a north-eastward
29   propagation of the anomalies into Southeast Asia in addition to the eastward propagation along
30   the equator (Waliser, 2006). Among the many impacts of the MJO, strong interactions with
31   ocean surface fluxes of mass, heat, and momentum have been observed (e.g., Matthews et al.,
32   2010).

33   Similarly, modes of tropical interannual variability, such as the irregular oscillation of sea
34   surface temperatures known as the Indian Ocean Dipole (IOD), play a role for Indian Ocean
35   meteorology. The positive phase of the IOD is characterised by positive sea surface temperature
36   anomalies in the western part of the Indian Ocean accompanied by negative anomalies in
37   eastern part (Saji et al., 1999). The initial cooling off the coast of Sumatra–Java leads to a
38   positive feedback mechanism via suppressed local convection, anomalous easterly winds, a
39   shoaling thermocline and stronger upwelling, which in turn reinforce the initial cooling with a
40   peak from September to November (Cai et al., 2014). Extreme positive IOD events can also
41   impact the equatorial ocean by inducing a north-westward extension of the south-easterly trades
42   and drying along the equatorial Indian Ocean (Webster et al., 1999).

43   The dominant mode of interannual climate variability of the Pacific, the El Niño–Southern
44   Oscillation (ENSO), can also impact Indian Ocean sea surface temperatures via anomalous
45   wind stress forcing (Latif and Barnett, 1995). In addition, ENSO modulates the depth of the
46   Indian Ocean thermocline and contributes to changes in salinity due to shifts in rainfall and
47   evaporation. The potential impact of ENSO on the IOD is currently under discussion (Stuecker
48   et al., 2017 and references therein).

Atmospheric
Chemistry
and Physics
Discussions

## 2.2 Oceanic transport

The physical oceanography of the equatorial and southern Indian Ocean, including currents, thermohaline circulation, sea surface temperature (SST), salinity, and upwelling events, does not experience the influence of the seasonal monsoon cycle, however, that of the northern Indian Ocean displays the seasonal changes. Below we will outline the major features of the equatorial and southern Indian Ocean first (Fig. 2) and then describe the influence of the seasonal monsoon on the physical processes in the northern Indian Ocean (Fig. 2). For this review, we concentrate on how physical oceanography affects salinity, SST, and biological productivity, as they play a major role in controlling air-sea exchange and atmospheric composition. For more details about general Indian Ocean physical processes, please see Schott et al. (2009) and references therein.

**Southern Indian Ocean**

The South Equatorial Current (SEC) in the Indian Ocean carries water masses entering through the Indonesian passages, with a relative salinity minimum in the Indian Ocean environment, via broad zonal inflow westward. Driven by the Southeast Trades, the SEC supplies the western boundary currents east of Madagascar. Part of the throughflow water in the SEC forms the northern East Madagascar Current (EMC), which partly passes in southward moving eddies through the Mozambique Channel and merges into the Agulhas (Ridderinkhof and de Ruijter, 2003; Schouten et al., 2003).

Data from satellite altimetry suggest that the eastward South Indian Countercurrent (SICC) is already present in the Mozambique Basin, southwest of Madagascar (Siedler et al., 2006). The eastward frontal SICC coincides with the thermohaline front that separates the saline subtropical surface water from the fresher tropical surface water in the EMC in summer (Palastanga et al., 2007). The variability of SST and salinity is high in the warm waters south to south-east of Madagascar, likely due to eddy activity and upwelling. There is year-round coastal upwelling along the southern stretch of the oligotrophic EMC and in the shallower region just to the south of Madagascar, which leads to enhanced phytoplankton growth (Quartly et al., 2006). All productivity further from the island in bands of relatively high variability along 25°S and along the EMC are due to a combination of local upwelling caused by eddies and, more importantly, the advection of upwelled coastal waters around eddy features. The anticyclones moving through the region wrap both the warm EMC waters and the nutrient-rich upwelled waters into well-defined arcs. Occasionally strands of chlorophyll-rich water can stretch 500 km or more eastward, which are caused by the combined effects of both cyclonic and anticyclonic eddies (Quartly et al., 2006). The southward flowing EMC, as part of the bifurcated SEC, and the SEC form the western and northern boundary currents of the South Indian subtropical gyre, where saline surface water is formed, as there is more evaporation than precipitation in this region (Schott et al., 2009). The south-eastern Indian Ocean shows the strongest interannual to decadal variability of upper-ocean salinity in the Indian Ocean. Seasonality of the mixed layer salinity in the south-eastern tropical Indian Ocean is influenced by the annual cycles of the Indonesian Throughflow and the Leeuwin Current transports, freshwater forcing, and eddy fluxes (Zhang et al., 2016).

Open ocean upwelling associated with the Seychelles dome, a thermocline ridge in the southern tropical gyre can occur between 5 and 10°S, along the northern edge of the southeast trades, where Ekman divergence occasionally appears to be strong enough to upwell subsurface waters into the mixed layer (Schott et al., 2009). In this region, the South Equatorial Countercurrent (SECC) flows eastward year-round, fed by the East African Coastal Current (EACC) and forming the northern flank of the southern Indian Ocean tropical gyre. Low sea surface height is the signature of the Indian Ocean's tropical gyre, bounded in the north by the SECC, to the south by the SEC, and at the western boundary by the EACC.
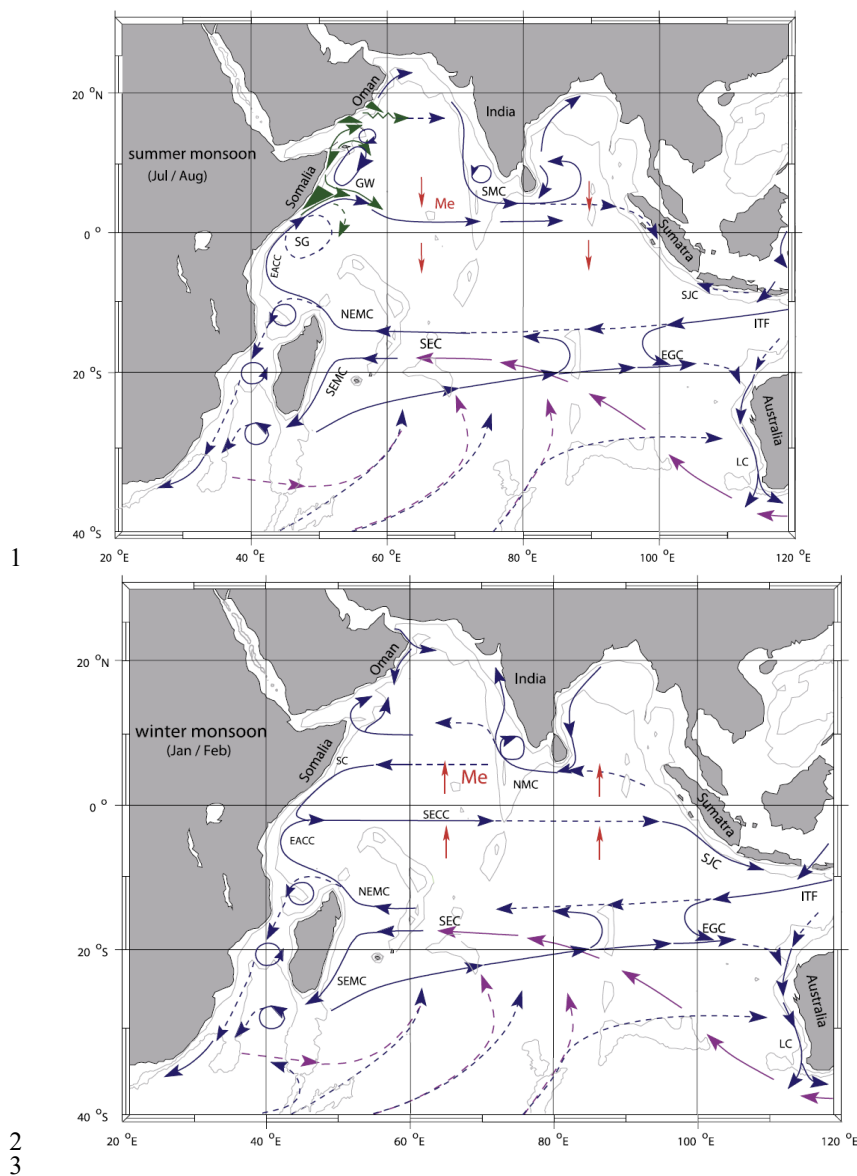
**Figure 2**. Schematic representation of identified oceanic currents during the summer monsoon (a) and winter monsoon (b). Current branches indicated are the South Equatorial Current (SEC), South Equatorial Countercurrent (SECC), Northeast and Southeast Madagascar Current (NEMC and SEMC), East African Coastal Current (EACC), Somali Current (SC), Southern Gyre (SG) and Great Whirl (GW) and associated upwelling wedges (green shades), Southwest and Northeast Monsoon Currents (SMC and NMC), South Java Current (SJC), East Gyral Current (EGC), and Leeuwin Current (LC). The subsurface return flow of the supergyre is shown in magenta. Depth contours shown are for 1000 m and 3000 m (grey). Updated representations are from SMC01; red vectors (Me) show directions of meridional Ekman transports. ITF indicates Indonesian Throughflow (from Schott et al., 2009, copyright 2009 by the American Geophysical Union, reproduced with permission).

Atmospheric
Chemistry
and Physics
Discussions

1 **Northern Indian Ocean**
2 During the summer monsoon, the northward flowing Somali Current is supplied by the SEC
3 and EACC. Once the Somali Current crosses the equator, a part of it turns offshore around 4°N
4 and another part returns across the equator as a part of the southern gyre. A northern gyre occurs
5 north of the Equator and occasionally a third gyre can be observed in many summer monsoons
6 (Schott et al., 2009). These gyres influence the stability of the atmospheric planetary boundary
7 layer, impacting surface wind stress and heat fluxes (Vecchi et al., 2004). Furthermore, the
8 Southwest Monsoon Current flows towards the east, south of Sri Lanka, then turns to flow
9 toward the north, bringing saltier Arabian Sea water into the Bay of Bengal (Jensen, 2003). In
10 contrast, the Somali Current flows southward during the winter monsoon to meet the northward
11 flowing EACC. They supply water for the eastward flowing SECC. The Northeast Monsoon
12 Current flows toward the west, bringing fresher Bay of Bengal water into the Arabian Sea
13 (Schott et al., 2009). In addition, model studies have suggested that Bay of Bengal water flows
14 across the equator in the eastern basin in the winter monsoon (Han and McCreary, 2001; Jensen,
15 2003).

16 Unique to the Indian Ocean are strong eastward ocean surface jets during the inter-monsoon
17 period, called Wyrtki Jets. They are produced by the semi-annual westerly equatorial winds and
18 are important because they carry warm upper layer waters toward the east, which increases sea
19 level and mixed layer depth in the east and decreases them in the west. These semi-annual
20 westerlies are the reason for another unique Indian Ocean feature, namely the eastward
21 Equatorial Undercurrent that is only present for a part of the year (i.e. February – June) when
22 the winds have an easterly component (Schott et al., 2009; Reppin et al., 1999).

23 **Salinity, SSTs and productivity**
24 On seasonal time scales, freshwater input due to rainfall and river discharge is important to the
25 salinity balance in the Bay of Bengal, while horizontal advection related to the monsoon plays
26 a dominant role in the north Indian Ocean (Rao and Sivakumar 2003). In the tropical Indian
27 Ocean, the seasonal cycle of the mixed layer salinity in the south-central Arabian Sea is mainly
28 due to meridional advection driven by the monsoon winds, while freshwater flux due to
29 precipitation may play an important role in the southwestern tropical Indian Ocean (Da-Allada
30 et al., 2015). Rainfall over the Indian Ocean shows a general migration to the summer
31 hemisphere following sunlight and warm SSTs. In addition, the general distribution of rainfall
32 is similar to that for SST, highlighting the strong coupling between the two. Wintertime cooling
33 in the northern Arabian Sea is strong because of latent heat loss caused by cool, dry air from
34 the Asian continent. Interestingly, there is strong summertime cooling in parts of the Arabian
35 Sea as a result of upwelling and offshore advection from the Somali and Omani coasts and due
36 to latent heat loss caused by the strong south-westerly winds. During boreal summer, upwelling
37 induced cooling off Somalia prevents atmospheric convection from the western Arabian Sea.
38 From the eastern Arabian Sea to the South China Sea, north of the Equator, high SSTs promote
39 atmospheric deep convection (Schott et al., 2009).

40 The strong monsoonal winds in the Indian Ocean lead to ocean upwelling, supplying nutrients
41 to the surface layer, where they support elevated rates of primary productivity mainly in the
42 Arabian Sea, the Somali Basin, along the Indian coast and the northern Bay of Bengal,
43 especially during summer months. The seasonal reversals in the boundary currents of the
44 northern Indian Ocean have important biogeochemical and ecological impacts and include
45 seasonal switching from upwelling to downwelling circulations, and modification of primary
46 productivity, nutrient stoichiometry, oxygen concentrations and phytoplankton species
47 composition (Hood et al., 2017). Transient upwelling due to seasonal variations of currents and
48 mesoscale variability can give rise to episodically high levels of primary production throughout
49 the Indian Ocean coastal waters.

1    **2.3 Long-term changes**

2    **Indian Ocean warming**
3    The Indian Ocean has warmed steadily over the past century, with an SST increase of 1°C
4    during 1951–2015, markedly higher than the global average SST warming of 0.7°C, over the
5    same period (Du and Xie, 2008; Han et al., 2014; Krishnan et al., 2020). Overall, this Indian
6    Ocean-averaged warming rate is broadly consistent across observational products (Dong et al.
7    2014; Yao et al., 2016) and historical simulations from the Coupled Model Intercomparison
8    Project - Phase 5 (CMIP5). It can be largely attributed to anthropogenic forcing rather than
9    natural external forcing, such as volcanic and solar variations, which have much weaker effects
10   (e.g., Dong et al., 2014). It has been shown that the basin wide warming due to increasing
11   greenhouse gases is slowed down by the indirect effects of anthropogenic aerosol (Dong and
12   Zhou, 2014). In addition to anthropogenic forcing, the sustained warming over the Indian Ocean
13   warm pool region is caused by local ocean–atmosphere coupled mechanisms, with their relative
14   roles being debated (Dong et al., 2014; Du and Xie, 2008; Rao et al., 2012; Swapna et al., 2014).

15   Some studies suggest that the warming is induced by the increase in downward longwave
16   radiation due to greenhouse gases, and then amplified by the water vapor feedback and
17   atmospheric adjustment (Du and Xie, 2008). Other studies argue that the SST trend is linked to
18   the changes in ocean heat transport and wave-induced thermocline depth (Li et al., 2003) or to
19   a decrease in the upwelling related to a slowdown of the wind-driven Ekman pumping (Alory
20   and Meyers, 2009). Li et al. (2018) showed that the prevailing warming of the western-to-
21   central Indian Ocean for 2000–2014 was largely induced by equatorial easterly winds, Ekman
22   downwelling off the equator, and north-easterly wind trends over the west Asia–East Africa
23   coastal region. The importance of the Indian Ocean in the global ocean heat budget was not
24   recognised until the hiatus period at the beginning of the 21st century, during which the abrupt
25   increase of the upper Indian Ocean heat content served as a major sink of the excessive heat
26   entering the Earth system (Cheng et al., 2015; Nieves et al., 2015; Lee et al., 2015).

27   The Indian Ocean warming is not spatially homogeneous in both models and observations. The
28   western tropical Indian Ocean has been warming for more than a century, at a rate faster than
29   any other region of the tropical oceans and is the largest contributor to the overall trend in the
30   global mean SST (Roxy et al., 2014). For the time period 1901–2012, summer SSTs of the
31   western Indian Ocean experienced anomalous warming of 1.28°C, while the total Indian Ocean
32   warm pool only saw an increase of 0.78°C. In addition to the overall warming trend, positive
33   IOD events, with positive sea surface temperature anomalies in the western part of the Indian
34   ocean, have increased markedly since 1950, while negative IOD events have reduced (Cai et
35   al., 2009). The warming of the generally cool western Indian Ocean against the rest of the
36   tropical warm pool region (Roxy et al., 2014, 2015) and corresponding changes of the zonal
37   SST gradient (Saha et al., 2014) have been both proposed as plausible explanations for the
38   observed decrease of Indian monsoon rainfall over the last three decades. In addition, they have
39   the potential to alter the marine food webs in this biologically productive region.

40   The Indian Ocean warming is projected to further increase over the course of the 21st century
41   in response to unabated greenhouse gas emissions. By the end of the 21st century, strongest
42   warming in the Arabian Sea and western equatorial Indian Ocean is consistently projected in
43   CMIP models, which could yield more Arabian Sea cyclones, more extreme IOD events and
44   further decrease monsoonal rains (Gopika et al., 2020). The mean SST distribution is projected
45   to resemble more positive IOD events, although some change in frequency is expected in the
46   future in response to greenhouse gas warming (Cai et al., 2014). Modelling studies also suggest
47   that the predicted stronger warming of the northern Indian ocean compared to the southern
48   Indian Ocean is most likely overestimated due to internal climate variability, observational
49   biases and uncertainties (Gopika et al., 2020).

1 **Summer monsoon and precipitation**
2 There are large uncertainties related to variability in the South Asian summer monsoon in a
3 changing climate. Several studies debate whether the monsoon is weakening or strengthening,
4 as well as the mechanisms driving the changes (Roxy et al., 2015). According to a review by
5 Singh et al. (2019a), both observational and modelling studies have determined that the
6 potentially weakened monsoon is due to a combination of forcings, such as land use and
7 irrigation changes and increased greenhouse gas and anthropogenic aerosol concentrations.
8 Many of the studies have determined that, due to this combination of forcings, oceanic warming
9 plays a central role in altering the monsoon, but it is currently argued if oceanic warming
10 weakens the monsoon over the Indian Ocean or if the weakened monsoon has accelerated the
11 warming (Rao et al. 2012; Swapna et al. 2014). Roxy et al. (2015) provide compelling evidence
12 that Indian Ocean warming potentially weakens the land-sea thermal contrast and dampens the
13 summer monsoon Hadley circulation, leading to reduced rainfall over parts of South Asia.

14 The Indian Ocean is one of the greatest moisture sources accounting for nearly one-third of the
15 total net transport of water toward the continents (Bengtsson, 2010). Both remote and local SST
16 anomalies can induce hydrological cycle changes over the Indian ocean. An increase in
17 evaporation is due to the robust warming of SSTs during recent decades, via changes of the
18 near surface specific humidity gradient, near-surface wind and the turbulent exchange
19 coefficient (Yu, 2007; Richter and Xie, 2008). Accompanied by atmospheric circulation
20 changes, water vapor can be redistributed and affect local and remote precipitation.

21 Han et al. (2019) show that the moisture sources (evaporation minus precipitation) in the
22 tropical central-eastern and south-western Indian Ocean experienced a significant increase
23 during boreal summer between 1979 to 2016. During those decades, the enhanced east–west
24 thermal gradient in the Pacific strengthened the Walker Circulation, leading to a westward shift
25 in convection and thus weakened convection and ascent over the tropical central-eastern Indian
26 Ocean. Enhanced moisture sources over these regions led to strengthened wind in the lower
27 troposphere over the south-western Indian Ocean, which is associated with an enhanced land–
28 sea thermal gradient under global warming (Han et al., 2019). In addition, there has been a
29 significant reduction in the annual frequency of tropical cyclones and their associated rainfall
30 over the northern Indian Ocean since the middle of the twentieth century (Krishnan et al., 2020).
31 In contrast, the frequency of very severe cyclonic storms during the post-monsoon season has
32 increased significantly during the last two decades. At the same time, an enhanced rainfall
33 contribution has occurred due to a higher precipitation efficiency (Singh et al., 2016; 2019b)
34 possibly leading to a dry atmosphere.

35 A significant reduction in the Indian summer rainfall over most of the Indian states during the
36 second half of the twenty-first century is projected by some modelling studies (Ramanathan et
37 al., 2005; Roxy et al., 2015). Other modelling studies project an increase in rainfall during the
38 East Asian summer monsoon region at the end of the twenty-first century (e.g., Zou and Zhou,
39 2013; Kitoh et al., 2013), with a large increase in rainfall over the ocean (Chen and Bordoni,
40 2016) and a slight increase in precipitation over central India (Asharaf and Ahrens, 2015). The
41 contradicting results indicate that the projection of the Indian summer monsoon rainfall is still
42 a key challenge for global and regional climate models. Enhanced evaporation variability,
43 which, in turn, intensifies the variability of Indian monsoon rainfall (Meehl and Arblaster,
44 2003) and a weakening in the monsoonal circulation are opposing effects, which remain a topic
45 of debate (Asharaf and Ahrens, 2015).

46 The mechanisms that alter regional precipitation vary at different time scales. A fast response
47 to an increase in $CO_2$ concentration before SST changes occurs at shorter time scales and is
48 associated with changes in large-scale wind patterns in the atmosphere. Changes in surface
49 wind are expected to be moderate for the first half of the 21st century, with a noticeable decline

1  of wind speed over the tropical Indian Ocean due to reduced thermal land-sea contrasts. The
2  southern extratropical region and Southern Ocean, on the other hand, show a significant
3  strengthening of the wind fields by the end of the twenty-first century (Mohan and Bhaskaran,
4  2019). Not well represented ocean–atmosphere feedback and coarse model resolutions,
5  however, are known to lead to large uncertainties in model estimates of wind speed changes
6  (Annamalai et al. 2017; Mohan and Bhaskaran, 2019).

7  **Salinity and productivity**
8  Idealised model experiments suggest that multidecadal changes of subsurface ocean salinity
9  during 1950–2000 were a result of an amplification of the mean surface salinity pattern and
10 isopycnal migration due to the ocean surface warming (Lago et al. 2016). However, the
11 enhanced precipitation in the Maritime Continent and the strengthening of the Indonesian
12 Throughflow are thought to be the likely causes of the freshening trend in the south-east Indian
13 Ocean since early 2000s, rather than local Ekman pumping and freshwater flux anomalies
14 (Llovel and Lee 2015; Hu and Sprintall, 2017). Du et al. (2015) noted a contrasting sea surface
15 salinity trend pattern characterised by freshening in the south-eastern tropical Indian Ocean and
16 salinification in the western tropical Pacific starting in the mid-1990s, which is attributed to a
17 strengthening trend of the Indo-Pacific Walker circulation combined with ocean advection
18 processes.

19 While Behrenfeld et al. (2006) indicate a reduction in net primary productivity over most of the
20 tropics as a result of surface thermal stratification, they have suggested an increase in primary
21 productivity for the western Indian Ocean from 1998 to 2004. Recent biogeochemical
22 simulations of the Arabian Sea ecosystem also predict that a projected intensification of
23 monsoon winds strongly increases the ecosystem productivity, thereby amplifying the oxygen
24 biological consumption and intensifying the oxygen minimum zone (OMZ) at depth (Lachkar
25 et al., 2018). At the same time, the near-surface will experience increased ventilation due to the
26 predicted stronger winds. On the contrary, a study using chlorophyll data and Earth system
27 model simulations over a larger region of the western Indian Ocean, points out an alarming
28 decrease of up to 20% in marine phytoplankton during the past six decades (Roxy et al., 2016).
29 The authors suggest that this decrease is driven by enhanced ocean stratification due to the rapid
30 warming in the Indian Ocean, which suppresses nutrient mixing from subsurface layers. Gregg
31 and Rousseaux (2019) also conclude from the assimilation of ocean colour satellite data (1998-
32 2015) into an ocean biogeochemical model, that the decline in global ocean primary
33 productivity of 2.1% per decade is mainly driven by the northern and equatorial Indian Ocean.
34 Reduced production by large, fast-growing diatoms along with chlorophytes characterizes this
35 decline, while cyanobacteria and coccolithophores benefit in the model.

36
37 **3. Campaigns, station data and satellite measurements**

38 Physical processes in the Indian Ocean are captured better now than in previous decades due to
39 the deployment of Argo floats and moored tropical buoy arrays, as well as the application of
40 satellite instruments (Hermes et al., 2019). Tropospheric composition over the Indian Ocean,
41 on the other hand, is still poorly sampled. In order to investigate oceanic emissions, chemical
42 transformation and transport of key substances, accurate atmospheric measurements are
43 needed. A few Indian Ocean coastal or island stations have been operated as part of long-term
44 scientific measurement programmes or operational air quality networks providing limited area
45 observations. Intensive ship and aircraft campaigns have been conducted for detailed
46 investigations of atmospheric processes during short episodes. These data can be complemented
47 by satellite observations of the tropospheric composition, which provide the large-scale picture
48 for a number of substances, albeit often with limited vertical resolution and reduced accuracy

1 for individual measurements. In this section we will give an overview of campaigns, station
2 data and satellite measurements that have been applied to study the atmospheric composition
3 over the Indian Ocean over the last decade.

### 3.1 Campaigns and station data

5 In the 21st century, several new attempts have been made to explore the processes occurring in
6 and above the Indian Ocean, which span several disciplines including oceanography,
7 atmospheric chemistry and physics, and biogeochemistry. Here we will introduce all the
8 campaigns that have contributed to the recent progress in the field and led to publications after
9 2010. General information on the time periods, regions and objectives of the campaigns is
10 summarized in Table 1.

11 The southern Indian Ocean was explored during the PESO cruise in 2004, with measurements
12 south of the ITCZ highlighting the clean air masses dominated by pristine oceanic conditions.
13 Since then, a series of campaigns, the Indian Southern Ocean Expeditions (ISOEs), were
14 initiated, with key components including hydrodynamics, biogeochemistry, air-sea interactions,
15 and more recently trace gases in the MBL. Since the inception of ISOE, 11 expeditions have
16 been carried out with trace gas emissions being one of the key objectives since ISOE-8 in 2014.

17 Efforts during the multi-platform field experiment 'Integrated Campaign for Aerosols, gases
18 and Radiation Budget' (ICARB) have focused on the northern Indian Ocean, Arabian Sea and
19 Bay of Bengal with the cruise tracks designed to cover maximum areas of these regions. The
20 experiment consisted of a first phase exploring post winter monsoon composition in 2006
21 (ICARB), a second phase taking place during the winter monsoon 2008/2009 (referred to as
22 W_ICARB) and a third phase during the winter monsoon of 2018 (referred to as ICRAB-218).
23 All ICARB campaigns focused on the physico-chemical properties and radiative effects of
24 aerosols and trace gases and how they are affected by polluted continental air-mass transported
25 over the oceans by the various wind regimes.

26 Since 2014, several campaigns focused on the South Asian summer monsoon time period have
27 taken place. The Organic VSLS and their air sea exchange from the Indian Ocean to the
28 Stratosphere (OASIS) campaign in 2014 aimed at analysing the impact of oceanic gases on the
29 remote stratospheric ozone chemistry. In 2015, the Oxidation Mechanism Observations (OMO)
30 aircraft campaign addressed the "self-cleaning capacity" of the atmosphere by focusing on
31 oxidation mechanisms and radical chemistry. During the OMO campaign, air pollutants such
32 as non-methane volatile organic compounds (NMVOC), oxidized volatile organic compounds
33 (OVOC) and nitrogen oxides were measured over continental regions (South Asia, Arabian
34 Peninsula, and east Africa) as well as over the Mediterranean and the Indian Ocean. In a similar
35 region, the Air Quality and climate change in the Arabian BAsin (AQABA) shipborne
36 campaign, was carried out in 2017, during which non-methane hydrocarbons (NMHCs) were
37 measured.

38 The 2nd International Indian Ocean Expedition program (IIOE-2) was launched in 2015 with
39 the goal to advance the understanding of interactions between geologic, oceanic, and
40 atmospheric processes of the Indian Ocean region, and the impact on other Earth components
41 and socio-economic activities. The scientific program organizes collaborative research
42 investigating the Indian Ocean from coastal environments to the deep sea. Campaigns
43 conducted within IIOE-2, focus on the ocean but also help characterise related atmospheric
44 processes at a wide spectrum of spatial and temporal scales.

45 In addition to dedicated campaigns, some island and coastal stations have conducted long-term
46 measurements that provide valuable information about the atmospheric composition over the
47 Indian Ocean.

1    **Table 1.** Summary of campaigns in the Indian Ocean for the 21st century.
2

| Campaign | Time | Region | Objective | Reference |
|---|---|---|---|---|
| PESO (Pilot Expedition to the Southern Ocean) | 2004 Jan - Apr | Southern Indian Ocean | Multi-disciplinary expeditions to understand the forcing mechanisms behind widely geographically separated climate change. | Pandey et al. (2006) |
| ISOE 1-11 (1st-11th Indian Southern Ocean Expedition) | Since 2004 | Southern Indian Ocean | Identify role and response of Southern Ocean to the regional and global climate variability (emissions of trace gases since ISOE 8) | ISOE Reports Mahajan et al. (2019a, b) Inamdar et al. (2020) |
| ICARB (Integrated Campaign for Aerosols, gases and Radiation Budget) | 2006 Mar - May; 2008/09 Dec - Jan; 2018 Jan-Feb | Indian mainland, northern Indian Ocean, Bay of Bengal | Characterize the physico-chemical properties and radiative effects of atmospheric aerosols and trace gases over the Indian landmass and the adjoining oceanic regions. | Moorthy et al. (2008) David et al., 2011 |
| Campaign aboard the Ocean Research Vessel Sagar Kanya (SK-277) | 2010 Oct-Nov | Bay of Bengal | Analyze atmospheric composition over the Bay of Bengal and how it is driven by air mass origin from Indian Ocean, Southeast Asia, and the Indian subcontinent | Mallik et al. (2013) |
| OASIS (Organic VSLS and their air sea exchange from the Indian Ocean to the Stratosphere) | 2014 Jul-Aug | West Indian Ocean | Investigate oceanic emissions of very short-lived substances and their transport and chemistry from the tropical Indian Ocean to the atmosphere, in particular to the stratosphere | Fiehn et al. (2017) Zavarsky et al. (2018b) |
| OMO (Oxidation Mechanism Observations aircraft campaign) | 2015 Jul - Aug | Indian Ocean and the Mediterranean | Identify atmospheric impacts of associated air pollution emissions at regional and global scales during the South Asian summer monsoon | Lelieveld et al. (2018) |
| IIOE-2 (Second International Indian Ocean Expedition) | 2015-2020 | Indian Ocean | Advance Indian Ocean initiatives and projects addressing emerging scientific issues of the Indian Ocean in the 21st century | Hood et al., 2016 |
| AQABA (Air Quality and climate change in the Arabian BAsin) | 2017 Jul-Aug | Mediterranean and Arabian Peninsula | Study air quality and climate change in the Arabian Basin | Bourtsoukidis et al., 2019 |

3
4

5    $CO_2$ surface flask measurements from the Cape Rama site on the Indian coastline have been
6    used to analyse the distribution and variability of $CO_2$ over this region for 2009-2012 (Nalini
7    et al., 2018). Measurements of $CH_4$, another important greenhouse gas, and the pollutant CO

1 are available from ground-based in situ cavity ring-down spectroscopy analysers and Fourier
2 transform infrared spectrometers at two sites on Reunion Island in the southern Indian Ocean
3 (Zhou et al., 2018). These multi-annual time series (2011-2017) allowed to investigate the
4 impact of emissions from biomass burning in Africa and South America on atmospheric
5 pollutant levels over the Indian Ocean. CO surface data are also available from the
6 NOAA/ESRL Global Monitoring Division network station in Mahé (Wai et al., 2014).

7 In situ tropospheric ozone measurements have been collected from 2003 to 2007 from balloon-
8 borne electrochemical concentration cell sensors launched above Ahmedabad in western India
9 (Lal et al., 2014). The continuous dataset enabled studies of the impact of transport processes
10 on the seasonal cycle and on the vertical distribution of ozone. The observation site in
11 Trivandrum situated on the southwest coast of India collected measurements of nitrogen oxides
12 with a chemiluminescence $NO_x$ analyser from 2007 to 2009 (David and Nair, 2011).

13 **3.2 Satellite measurements**

14 Satellite measurements of atmospheric composition over the Indian Ocean have provided
15 valuable information over the last decades that allowed for studies of the overall distribution
16 and long-term changes of key substances. Most instruments used today apply passive remote
17 sensing with observations being mainly done in nadir geometry. Here we will give a short
18 overview of satellite instruments that provide measurements used in scientific studies of the
19 Indian Ocean atmosphere. In addition, we have compiled plots of the seasonal CO, $NO_2$ and
20 $CH_4$ surface distribution for this review article and will describe the respective satellite
21 measurements more in detail.

22 **Ozone and pollutants from OMI and TROPOMI**
23 The Ozone Monitoring Instrument (OMI) is a key instrument onboard NASA's Aura satellite.
24 OMI is a nadir-viewing, wide-field-imaging spectrometer that measures backscattered
25 radiances at a spectral resolution of 0.42–0.63 nm (Levelt et al., 2006). Its wide field-of-view
26 of 114° with a swath width of 2600 km yields daily global coverage with a spatial resolution of
27 13 km×24 km (Liu et al., 2010). OMI measures ozone profiles as well as other key air quality
28 components such as $NO_2$, $SO_2$, and aerosol characteristics. In this article, we use the OMI
29 tropospheric $NO_2$ column product from 2003 to 2020 to analyse long-term changes over
30 different coastal and open ocean regions of the Indian Ocean (Section 6.2).

31 The TROPOspheric Monitoring Instrument (TROPOMI) is a nadir-viewing imaging
32 spectrometer on board the Copernicus Sentinel-5 Precursor satellite, which was launched in
33 October 2017 for a mission of seven years. The satellite has a sun-synchronous orbit achieving
34 near full-surface coverage on a daily basis. The TROPOMI instrument contains four
35 spectrometers with three covering the ultraviolet-near infrared and one for the shortwave
36 infrared range. Key atmospheric species observed by TROPOMI include ozone, $NO_2$, $SO_2$, CO
37 and aerosol properties. The TROPOMI tropospheric $NO_2$ column product (Boersma et al.,
38 2018) shows improved spatial resolution over previous. The $NO_2$ retrieval algorithm is based
39 on the $NO_2$ DOMINO retrieval previously used for OMI spectra with improvements made for
40 all retrieval steps. In this article, we use the TROPOMI Level 2 $NO_2$ tropospheric column data
41 product to show its distribution and seasonal variations (Section 5.1).

42 **Pollutants (CO) from MOPITT**
43 The Measurements of Pollution in the Troposphere (MOPITT) instrument is onboard NASA's
44 Earth Observing System Terra spacecraft, measuring tropospheric CO since March 2000. The
45 satellite is in a sun-synchronous polar orbit of 705 km allowing the instrument to make
46 measurements in a 612 km cross-track scan with a footprint of 22 km × 22 km providing global

1  coverage every 3 days. The MOPITT measurements provide vertical profiles and total columns
2  of CO, which are useful to analyse the distribution, transport, sources and sinks on a global
3  scale. CO retrieval products are generated with an iterative optimal-estimation-based retrieval
4  algorithm based on the MOPITT calibrated radiances and a priori knowledge of CO variability.
5  The recently released version 8 (V8) products benefit from updated spectroscopic information
6  used in the radiative transfer model and improved methods for radiance bias corrections (Deeter
7  et al., 2019). In this article, we use MOPITT V8 Level 3 monthly data to analyse the seasonal
8  variation of surface CO distribution (Section 5.1).

9  **Greenhouse gases ($CH_4$ and $CO_2$) from AIRS and GOSAT**
10  The Atmospheric Infrared Sounder (AIRS) provides measurements of temperature and water
11  vapor through the atmospheric column along with a number of trace gases, surface and cloud
12  properties. The instrument is mounted on the sun-synchronous, near polar orbiting NASA
13  satellite, AQUA, and measures the brightness temperature of infrared radiation emitted by the
14  Earth's surface and atmosphere. $CO_2$ measurements from AIRS ($XCO_2$, ~ 2 ppm accuracy)
15  show a good coverage over the Indian Ocean mid-tropospheric region and have been used in
16  studies by Nayak et al. (2011) and Nalini et al. (2018). The AIRS retrieval algorithm is a
17  sequential retrieval, in which the quality of the $CH_4$ retrievals strongly depends on the AIRS
18  temperature and moisture profiles as well as surface temperature and emissivity products in
19  previous steps. In this article, we use AIRS version 6 level 3 data to depict the seasonal variation
20  of surface $CH_4$ distribution.

21  The Greenhouse Gases Observing Satellite (GOSAT/Ibuki) is a sun-synchronous polar orbit
22  satellite that measures $CO_2$ and $CH_4$ from the stratosphere to the Earth's surface. The retrieval
23  precision for $CO_2$ is smaller than 3.5 ppm (Yoshida et al., 2011) utilising the Thermal and Near
24  Infrared Sensor for Carbon Observation – Fourier Transform Spectrometer, which operates in
25  the shortwave and thermal emission bands. The GOSAT Level 3 product at a horizontal
26  resolution of $2.5° \times 2.5°$ has data gaps over the globe including a major portion of the Indian
27  region during the monsoon season due to its limitation in retrieving $CO_2$ in the presence of
28  clouds. This is rectified in the level 4 product that uses the Atmospheric Tracer Transport Model
29  to incorporate ground-based observations and achieves a better distribution of $CO_2$ over the
30  Indian Ocean (Nalini et al., 2018).

31  **Pollutants ($NO_x$) from GOME and SCIAMACHY**
32  The Global Ozone Monitoring Experiment (GOME) is a UV/Visible spectrometer on the
33  European polar sun-synchronous orbiting satellite ERS-2, launched in April 1995. It measures
34  in 230–800 nm wavelength range, with a spectral resolution of 0.2–0.4 nm, and obtains global
35  coverage at the equator after 3 days (Burrows et al. 1999). Problems with tape storage on ERS-
36  2 led to the replacement of GOME by the Scanning Imaging Absorption Spectrometer for
37  Atmospheric Chartography (SCIAMACHY), which was launched in 2002 on the European
38  ENVISAT platform. It measures in the spectral range 240–2380 nm (Bovensmann et al., 1999).
39  Both instruments provide measurements of the mean columnar amount of tropospheric $NO_2$
40  and allowed to study its variations and long-term changes over the Indian subcontinent (Ghude
41  et al., 2013; Mahajan et al., 2015a).
42
43
44  **4. Regional sources and sinks**
45
46  Atmospheric composition over the Indian Ocean is known to be impacted by the trace gas
47  outflow from the surrounding continental land masses, long range transport and regional
48  oceanic air-sea fluxes (Lawrence and Lelieveld, 2010). Here, we describe the distribution,
49  seasonality and trends of continental and oceanic trace gas emissions important for the

1   atmospheric composition over the Indian Ocean. Our study region includes East Africa, the
2   Middle East, South Asia, East Asia, and Southeast Asia and is depicted in Fig. 3.

3   We use the latest versions of the Emissions Database for Global Atmospheric Research
4   (EDGAR), in order to present continental pollution and greenhouse gas emissions over the last
5   two decades. For air pollutants, EDGAR v5.0_AP for the period 1970-2015 is available (Crippa
6   et al., 2020) and for greenhouse gases EDGAR v5.0_GHG for the period 1970-2015 (Crippa et
7   al., 2019) can be used. The EDGAR datasets include continental emissions from the energy
8   sector (i.e., power industry), industrial processes (i.e., manufacturing, industrial combustion),
9   the transport sector (i.e., road transport, aviation), residential sources (small-scale combustion
10  and waste treatment), and agriculture. Exhausts from ship engines as one of the major sources
11  of air pollution over the open ocean are also included in the EDGAR emissions. The datasets
12  are given at a high spatial resolution of 0.1° x 0.1°. The results shown in this section focus on
13  the main pollutants CO, $NO_x$, and $SO_2$, and the greenhouse gases $CH_4$, $N_2O$, and $CO_2$. We also
14  briefly discuss mercury emissions. The most recent year for which data is given (year 2015 for
15  both air pollutants and greenhouse gases) is used here to present emissions strength and patterns
16  representative for the last decade. Emission changes are calculated for the time period 2000-
17  2015 and are shown in relative terms compared to the emissions in 2000. Emissions are
18  averaged over East Africa, the Middle East, South Asia, East Asia, and Southeast Asia for a
19  direct comparison of the regional contributions and the text and tables.

20  The ocean is an important source and sink to/from the atmosphere for many of the same gases
21  mentioned above, as well as other climate- and chemically active compounds, such as DMS,
22  isoprene, and halogen species. Below we will describe the net ocean fluxes of CO, $CH_4$, $CO_2$,
23  $N_2O$, DMS, isoprene, and bromoform ($CHBr_3$) as obtained from recent publications, placing
24  special attention on monsoon related variability.

25  **4.1 Pollutants**

26  Among atmospheric pollutants, CO is considered to be one of the most important gases as it is
27  highly toxic at elevated concentrations. Due to its intermediate lifetime of a few months
28  (Seinfeld and Pandis, 2006), CO is much more variable in the troposphere than other
29  atmospheric constituents with longer lifetimes and often used as a transport tracer. CO has an
30  indirect radiative effect, since it scavenges the hydroxyl radical (OH), the cleaning agent of the
31  atmosphere that otherwise would destroy the greenhouse gases $CH_4$ and $O_3$ (Daniel and
32  Solomon, 1998). Another important pollutant is the family of the nitrogen oxides ($NO_x$)
33  consisting of nitrogen dioxide ($NO_2$) and nitrogen oxide (NO). Tropospheric $NO_x$ acts as a
34  precursor for a number of harmful secondary air pollutants such as ozone and particulate matter
35  and plays a role in the formation of acid rain. Breathing in raised levels of $NO_2$ can cause
36  respiratory problems independently of negative health effects of other secondary pollutants.
37  Once transported into the stratosphere, reactive odd-nitrogen species destroy ozone, in
38  particular in the middle stratosphere near the ozone maximum (Portmann et al., 2012). $SO_2$ is
39  another key component of gaseous air pollution. As for $NO_2$, exposure to $SO_2$ can harm the
40  human respiratory system. In addition, $SO_2$ can react with other compounds in the atmosphere
41  to form small particles that contribute to particulate matter pollution. If oxidised within airborne
42  water droplets, $SO_2$ produces sulphuric acid, which can be transported by wind over many
43  hundreds of kilometres and deposited as acid rain. Atmospheric ammonia ($NH_3$) is a pollutant
44  which plays an important role in the formation of particulate matter, as well as in acidification
45  and eutrophication of ecosystems (Lelieveld et al., 2015; Bauer et al., 2016).

46  The distributions of CO, $NO_x$, and $SO_2$ emissions are shown in Figures 3, 4 and 5, respectively.
47  One of the common features of the spatial distribution of these emissions is that they generally
48  coincide with the population distribution, such that high emissions appear in the densely
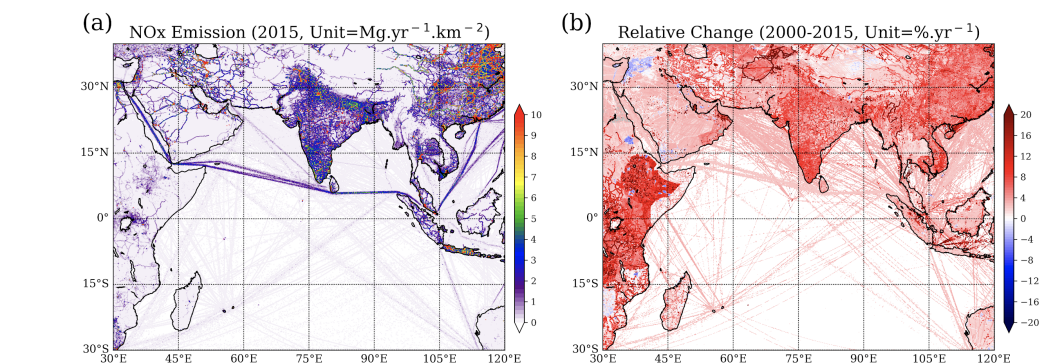
1    populated areas. In East Asia, high-emission areas include northern China, the Yangtze River
2    delta, Sichuan Basin, Korea, and Japan (not shown in the Figure). In South Asia, high emissions
3    are distributed throughout northern India, Nepal, the southern point of India, and Bangladesh.
4    In Southeast Asia, high emissions appear around some major cities including Bangkok, Hanoi,
5    and Ho Chi Minh City, as well as Java. Similar to Southeast Asia, high-emission regions in
6    East Africa are also around major cities like Kampala, Nairobi, and Addis Ababa. In the Middle
7    East, high-emission regions are distributed around the Persian Gulf. Among the different source
8    regions, East Asia and South Asia are main emitters. In 2015, the two regions accounted for
9    41% (East Asia) and 27% (South Asia) of the total CO emissions discussed here. East Asia is
10    also a large emitter of $NO_x$ (54%) and $SO_2$ (57%).

11    It is well known that pollution sources from Asia are characterized by inefficient combustion
12    processes during biofuel and fossil fuel burning. For instance, the burning of biofuels such as
13    wood, dung, and agricultural waste accounts for 18% of all CO emissions in Southeast Asia.
14    Globally it only accounted for ~9% of all CO emissions in 2015, highlighting the role of biofuel
15    burning in regions around the Indian Ocean. Inefficient combustion processes also occur during
16    fossil fuel burning at lower temperatures and result in relatively low $NO_x$ emissions and higher
17    $CO/CO_2$ ratios, when compared to other industrialized areas around the globe. The incomplete
18    fossil fuel combustion from the residential sector and road transportation are the two main
19    sources contributing to the CO production, accounting for 29.5% and 29.0% of all CO
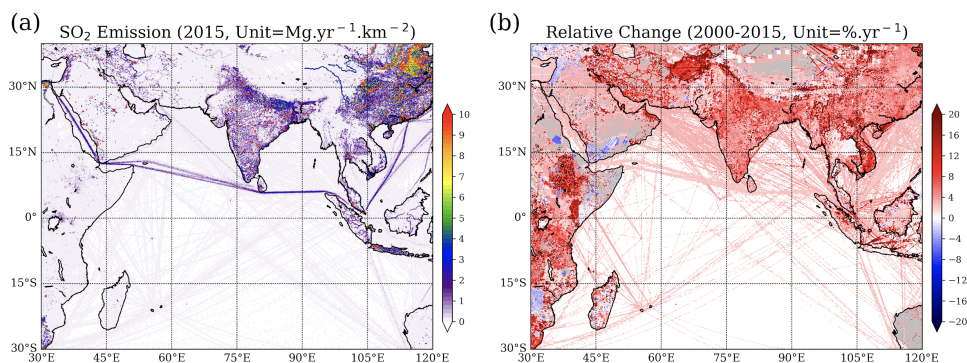20    emissions in our study region in 2015.



(a) CO Emission (2015, Unit=Mg.yr$^{-1}$.km$^{-2}$)  (b) Relative Change (2000-2015, Unit=%.yr$^{-1}$)
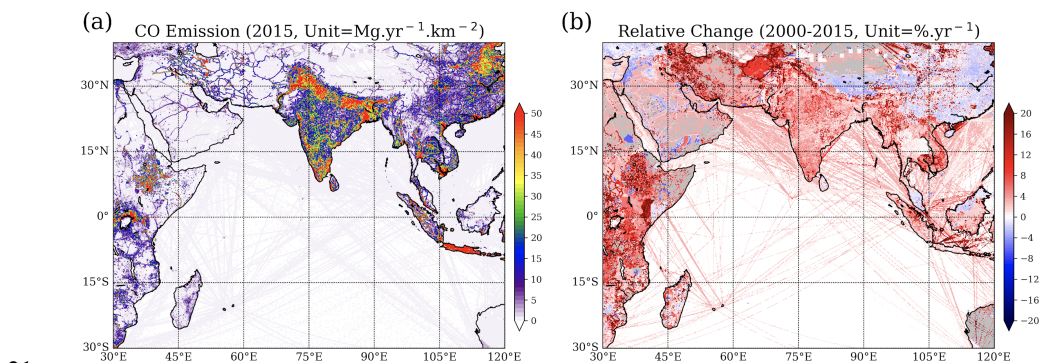
21

22 **Figure 3.** Annual mean CO emissions for 2015 (a) and relative change with respect to 2000 (b) from
23 EDGAR V5.0_AP.



(a) NOx Emission (2015, Unit=Mg.yr$^{-1}$.km$^{-2}$)  (b) Relative Change (2000-2015, Unit=%.yr$^{-1}$)

24

25 **Figure 4.** Same as Figure 3, but for $NO_x$.

Atmospheric
Chemistry
and Physics

Discussions



(a) SO$_2$ Emission (2015, Unit=Mg.yr$^{-1}$.km$^{-2}$)   (b) Relative Change (2000-2015, Unit=%.yr$^{-1}$)

1

2   **Figure 5.** Same as Figure 3, but for SO$_2$.

3

4   NO$_x$ emissions mainly stem from high temperature combustion. Energy production,
5   manufacturing industries and road transportation caused 30.7%, 25.8%, and 25.6% of all NO$_x$
6   emissions in our study region in 2015, respectively. Manufacturing industries and energy
7   (electricity production and heat production) are also the two main contributors to the SO$_2$
8   emissions, accounting for 41% and 40%, respectively, of all SO$_2$ emissions in our study region
9   in 2015. As per the 2000 Asian emission inventory, India has the second highest SO$_2$ emission
10  (14%) after China (65%) with coal-burning power plants contributing to around half (47%) of
11  the emissions in India (Ohara et al., 2007). About 40% of the thermal plants in India are located
12  over the Indo-Gangetic Plains causing relatively high SO$_2$ emissions from this region (Fig. 5;
13  Aswini et al., 2020). In addition, ship traffic leads to anthropogenic NO$_x$ and SO$_2$ emissions
14  directly over the open ocean with emissions concentrated along the major shipping lanes (e.g.
15  Franke et al., 2009).

16  Over the period 2000-2015, the emissions of all pollutants increased in almost all regions
17  around the Indian Ocean, with CO emissions changing from 275.9 Tg yr$^{-1}$ to 350.3 Tg yr$^{-1}$, NO$_x$
18  from 35.3 Tg yr$^{-1}$ to 58.3 Tg yr$^{-1}$, and SO$_2$ from 41.8 Tg yr$^{-1}$ to 61.1 Tg yr$^{-1}$. Between 2000 and
19  2015, CO emissions increased particularly along the Mekong River, north of the Persian Gulf,
20  in Afghanistan and East Africa, while CO emissions in most regions of East Asia decreased
21  despite a comparably low overall increase (15%, Table 2, Fig. 3b). NO$_x$ emission increases
22  show a different pattern and are relatively high in most regions around the Indian Ocean, with
23  peaks in East Asia, South Asia and East Africa (Fig. 4b) SO$_2$ emission changes show a similar
24  distribution as the NO$_x$ changes, with peaks along the Mekong River and in East Africa (Fig.
25  5b). Ship traffic in the Indian ocean has seen the largest increase worldwide between 1992 and
26  2012, especially on well-defined shipping lanes, such as the Red Sea-Arabian Gulf-Asia route
27  or the Asia-Cape Town route (Tournadre, 2014). The overall increase of the pollutant emissions
28  shows pronounced variations from region to region (Table 2) with the highest rate of all three
29  pollutants emission increases found in South Asia.

30  In particular, for the time period after 2012, satellite measurements have shown pronounced
31  regional SO$_2$ and NO$_2$ pollution changes. A decrease of SO$_2$ pollution from the North China
32  Plain has been noted since 2011 as a result of government efforts, while SO$_2$ and NO$_2$ emissions
33  from India have continued to grow at a fast rate (Krotkov et al., 2016). Recent emission
34  estimates suggest that during 2013–2017, anthropogenic emissions from China decreased by
35  23 % for CO, 21 % for NO$_x$, and 59 % for SO$_2$ over this period as a consequence of the
36  implementation of active clean air policies (Zheng et al., 2018).

Atmospheric
Chemistry
and Physics
Discussions

1 **Table 2.** Emissions of CO, NO$_x$, and SO$_2$ from different regions in 2015 and their increase with respect
2 to 2000.
3

| | Emission in 2015 (Increase with respect to 2000) | | | | |
|---|---|---|---|---|---|
| | East Africa | Middle East | South Asia | East Asia | Southeast Asia |
| CO | 26.48 Tg yr$^{-1}$ (40%) | 16.76 Tg yr$^{-1}$ (18%) | 93.97 Tg yr$^{-1}$ (50%) | 144.21 Tg yr$^{-1}$ (15%) | 68.91 Tg yr$^{-1}$ (25%) |
| NO$_x$ | 0.89 Tg yr$^{-1}$ (76%) | 7.27 Tg yr$^{-1}$ (65%) | 12.47 Tg yr$^{-1}$ (101%) | 31.39 Tg yr$^{-1}$ (56%) | 6.28 Tg yr$^{-1}$ (54%) |
| SO$_2$ | 0.43 Tg yr$^{-1}$ (67%) | 7.55 Tg yr$^{-1}$ (54%) | 13.09 Tg yr$^{-1}$ (120%) | 34.63 Tg yr$^{-1}$ (29%) | 5.42 Tg yr$^{-1}$ (40%) |

4

5 Unfortunately, measurements of oceanic CO emissions from the Indian Ocean are sparse. We
6 only know of unpublished data sets (D. Arevalo-Martinez, personal communication) from one
7 GEOMAR campaign (OASIS) and a series of NASA-SAGA cruises
8 (www.saga.pmel.noaa.gov, eastern open Indian Ocean, summer 1987). Net fluxes covering the
9 northern to southern extent of the Indian Ocean range from ~0.1 to ~1.4 Mg km$^{-2}$ yr$^{-1}$, as CO is
10 always supersaturated in the surface ocean (Conte et al., 2019 and references therein), and
11 values are similar to ship emissions but considerably smaller than continental emissions (Fig.
12 3). CO is produced in the surface ocean from organic material photochemistry and biological
13 processes (Conte et al., 2019). Available data from the western Indian Ocean suggests that the
14 most significant meridional gradients occur due to open ocean upwelling at 5°S-10°S. CO
15 emissions are high from 5°-15°S, but to the north and south of this region, emissions decrease
16 to zero with seasonal variations occurring due to upwelling changes. In the eastern Indian
17 Ocean, seasonal variability is expected in association with surface productivity changes in the
18 Seychelles–Chagos Thermocline Ridge. However, here no seasonal cycle can be detected in
19 available measurements and it is not clear if this is a real feature or caused by the lack of data.
20 Additional variability is expected in coastal regions, since large amounts of seasonally
21 discharged runoff supply terrestrial organic material that serves as a precursor to CO marine
22 photoproduction.

23 The atmospheric pollutant mercury is transported around the globe as gaseous elemental
24 mercury, eventually oxidizing to divalent mercury. The latter is known to deposit to the surface
25 from where it can be taken up into food webs and be transformed to highly toxic species
26 endangering humans and ecosystems (Selin et al., 2007). Atmospheric mercury is released from
27 anthropogenic activities, such as coal-fired power plants, metal smelting, and waste incineration
28 (Pacyna et al., 2005; Streets et al., 2005). Emissions associated with artisanal and small-scale
29 gold mining account for almost 38% of the global total emission (UN-Environment, 2019).
30 Mercury is also emitted from the oceans, soils, terrestrial vegetation, and biomass burning.
31 These 'natural' emissions include some anthropogenic fraction related to the recycling of
32 previously deposited mercury (Mason and Sheu, 2002). Based on 2015 inventories, Asia is
33 responsible for a large part of the emissions (49%), which primarily stem from East and
34 Southeast Asia. While emissions in North America and the European Union have shown
35 moderate decreases, increased economic activity, notably in Asia, and the use and disposal of

1   mercury-added products have led to a global increase of approximately 20% between 2010 and
2   2015 (UN-Environment, 2019).

3   For $NH_3$, East Asia and South Asia are the two main contributors, which account for 38.9% and
4   32.3% of the total emissions, respectively (not shown here). From 2000 to 2015, emissions of
5   $NH_3$ in the regions around the Indian Ocean documented by EDGAR increased by 22.5%.
6   Agricultural activities dominate the ammonia emissions, with about 56.7%, 18.4% of the
7   emissions from the sectors of direct soil emission and manure management. Besides, long-term
8   satellite measurements (van Damme et al., 2018) show other hotspots of ammonia emission not
9   well represented in EDGAR inventory, most of which are associated with either high-density
10  animal farming or industrial fertilizer production.

11  **4.2 Greenhouse gases**

12  $CO_2$ concentrations have been increasing steadily over the last decades reaching a new record
13  high in 2018 of $407.4 \pm 0.1$ ppm (Blunden and Arndt, 2019). Due to its high atmospheric
14  abundance and long atmospheric lifetime, $CO_2$ is the most important of Earth's long-lived
15  greenhouse gases. In addition to its impact on climate, $CO_2$ is responsible for ocean
16  acidification as it produces carbonic acid when it dissolves in the ocean. $CH_4$ is also a very
17  effective greenhouse gas and the second-largest contributor to anthropogenic radiative forcing
18  since preindustrial times after $CO_2$. In the troposphere, $CH_4$ acts to reduce the atmosphere's
19  oxidizing capacity. It has a relatively short atmospheric lifetime of about 9 years (Prather et al.,
20  2012) and exhibits a strong seasonal cycle as well as a distinct gradient across the equator.
21  Despite its relatively low atmospheric concentrations, $N_2O$ is the third anthropogenic
22  greenhouse gas after $CO_2$ and $CH_4$ in terms of radiative forcing (Ciais et al., 2014). Due to its
23  long atmospheric lifetime of about 116 years (Prather et al., 2015) and large infrared absorption
24  capacity per molecule, $N_2O$ is a much more efficient greenhouse gas than $CO_2$ with a global
25  warming potential of 265 over a 100-year time span. In the stratosphere, reaction with $O(^1D)$
26  leads to the production of NO (Seinfeld and Pandis, 2006), which is involved in chemical ozone
27  depletion. As a consequence, $N_2O$ has been estimated to be the main emitted ozone-depleting
28  substance of the 21st century (Ravishankara et al., 2009; Butler et al., 2016).

29  Anthropogenic greenhouse gas emissions in the regions surrounding the Indian Ocean generally
30  correspond to economic activities. As the largest emerging economies, East Asia and South
31  Asia are the main emitters of $CH_4$ (Fig. 6) and $N_2O$ (Fig. 7) with emission centres in the Indo-
32  Gangetic Plain, northern China and Java. In 2015, East Asia and South Asia accounted for 37%
33  and 26% of the total $CH_4$ emission, as well as 43% and 26% of the total $N_2O$ emission discussed
34  here. Among the regions surrounding the Indian Ocean, East Asia is also the largest $CO_2$ emitter
35  causing 68% of the total $CO_2$ emissions in our study region in 2015 (Fig. 8).

36  Atmospheric $CH_4$ has anthropogenic and natural sources, with the latter including natural
37  wetlands, livestock, termites, hydrates and forest fires. Anthropogenic sources account for the
38  majority of all emissions and can be split into biogenic and non-biogenic sectors. Almost a
39  quarter (23%) of the $CH_4$ emissions in our study region stems from enteric fermentation
40  (livestock farming), which acts as the primary source in South Asia and East Africa. Rice
41  cultivation in Asia is responsible for 19% of $CH_4$ emissions in our study region causing a
42  systematic seasonal pattern with peak emissions during the fully-grown stage in September and
43  October (Pathak et al., 2005). Other main sources of $CH_4$ are solid fuels (17%), mainly from
44  East Asia and Southeast Asia, and oil and gas production (14%), mainly from the Middle East.

45  $N_2O$ emissions are linked to the biogeochemical cycle of nitrogen and are thus impacted by
46  anthropogenic use of fertilizer and industrial activities that lead to the atmospheric deposition
47  of reactive nitrogen (e.g., Davidson, 2009). More than half of the $N_2O$ emissions in our study
48  region (56%) are directly from managed soils and can be quite heterogeneous with spatial

1   patterns revealing hot spots in agricultural areas in China and the Indo-Gangetic Plains (Ito et
2   al., 2018; Fig. 7). Furthermore, the $N_2O$ emissions from managed soils are characterized by a
3   pronounced seasonal cycle and interannual variability, primarily in response to meteorological
4   conditions and nitrogen inputs. In particular, $N_2O$ emissions are correlated with soil moisture
5   (Raut et al., 2015), leading to strongly enhanced emissions in South Asia during summertime
6   when high precipitation events occur.
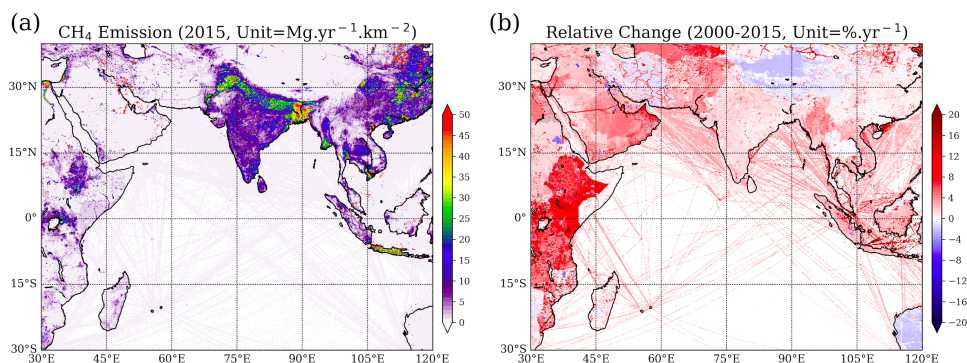


7
8   **Figure 6.** Annual mean $CH_4$ emissions for 2015 (a) and relative change with respect to 2000 (b) from
9   EDGAR V5.0_GHG.
10

11   Similar to the air pollutants discussed above, the overall $CH_4$ and $N_2O$ emissions increased
12   significantly over the period 2000-2015 from 135.7 Tg yr$^{-1}$ to 182.4 Tg yr$^{-1}$ and from 2.80 Tg
13   yr$^{-1}$ to 3.51 Tg yr$^{-1}$, respectively. Increasing $CH_4$ emission in South Asia (Fig. 6b) have been
14   linked to increased rice cultivation area, natural wetlands and warmer climate (Tian et al.,
15   2015). Increasing $N_2O$ emissions (Fig. 7b) are believed to stem from intensified crop production
16   and nitrogen fertilizer use as well as higher air temperatures (Raut et al., 2015). While not being
17   the main emitter, East Africa is the region with the fastest increase of $CH_4$ and $N_2O$ emissions
18   among the regions discussed here (Fig. 6b and 7b, Table 3). A recent study suggested that east
19   African wetlands could account for up to a third of the spike in global $CH_4$ emissions between
20   2010 and 2016, with most of this coming from the South Sudanese wetland, one of the largest
21   freshwater ecosystems in the world (Lunt et al., 2019).

22   **Table 3.** Emissions of $CH_4$, $N_2O$, and $CO_2$ from different regions in 2015 and their increase in respect
23   to 2000.

| | Emission in 2015 (Increase respect to 2000) | | | | |
|---|---|---|---|---|---|
| | East Africa | Middle East | South Asia | East Asia | Southeast Asia |
| $CH_4$ | 12.33 Tg yr$^{-1}$ (50%) | 21.47 Tg yr$^{-1}$ (50%) | 47.65 Tg yr$^{-1}$ (24%) | 68.08 Tg yr$^{-1}$ (34%) | 32.83 Tg yr$^{-1}$ (38%) |
| $N_2O$ | 0.36 Tg yr$^{-1}$ (51%) | 0.20 Tg yr$^{-1}$ (21%) | 0.91 Tg yr$^{-1}$ (36%) | 1.52 Tg yr$^{-1}$ (15%) | 0.52 Tg yr$^{-1}$ (26%) |
| $CO_2$ | 69.3 Tg yr$^{-1}$ (137%) | 2062.30 Tg yr$^{-1}$ (93%) | 2565.10 Tg yr$^{-1}$ (125%) | 13041.02 Tg yr$^{-1}$ (127%) | 1430.79 Tg yr$^{-1}$ (79%) |
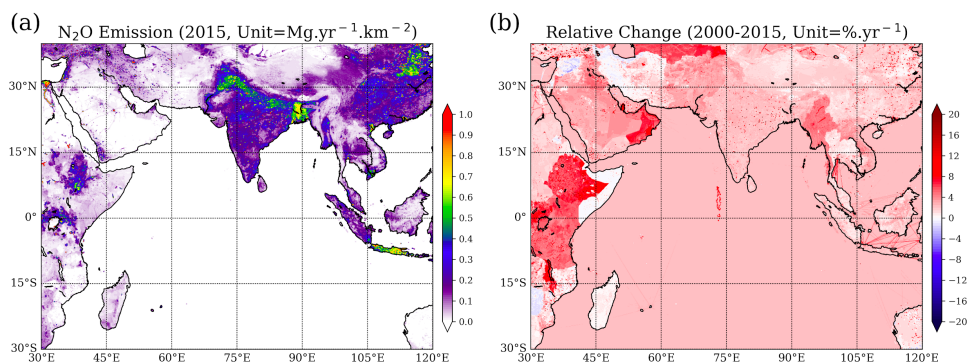
**Figure 7.** Same as Figure 6 but for $N_2O$

For $CO_2$, the majority of the emissions in our study region stem from East Asia related to two main sectors: electricity and heat production (41%) and manufacturing industries (23%). Over the period 2000-2015, the $CO_2$ emissions in our study region more than doubled from 8790 Tg yr$^{-1}$ to 19168 Tg yr$^{-1}$. Especially in East Asia and South Asia, they grew at very fast rates with increases of 127% and 125%, respectively. Despite the apparent policy breakthrough leading to the Paris Agreement in 2015, $CO_2$ emissions from fossil fuel and industry have continued to increase over the recent years. According to the latest estimates from the Global Carbon Project, the expected growth of global emissions in 2019 will be almost entirely due to China and India with expected annual growth rates of 2.6% and 1.8%, respectively (Peters et al., 2020).

The ocean is also a source and sink of greenhouse gases. Compared to the terrestrial sources, the ocean is just a minor contributor to the atmospheric $CH_4$, accounting for 1%-13% of the global atmospheric $CH_4$ budget (Saunois et al., 2016). The concentration of $CH_4$ in the Indian Ocean is characterized by a sharp decrease offshore (Naqvi et al., 2010a). Due to the large geographical changes in surface saturation and wind speed, the sea-to-air flux of $CH_4$ varies strongly in the northern Indian Ocean. Highest emissions were observed during the southwest monsoon in the Arabian Sea (~64 μmol m$^{-2}$ d$^{-1}$), and the estimated overall $CH_4$ emission from Arabian Sea amounts to 0.1–0.2 Tg yr$^{-1}$ (Naqvi et al., 2005), which is much smaller than the total terrestrial emissions mentioned above (~182 Tg yr$^{-1}$ in 2015).

Unlike $CH_4$, the ocean is a major source of $N_2O$, accounting for at least one third of global $N_2O$ emissions (Bange, 2006). Intense $N_2O$ emissions are usually found in upwelling regions with OMZs (Codispoti, 2010), such as in the Arabian Sea and Bay of Bengal (not shown). The South Asian monsoon drives intense seasonal changes of upwelling in both of the OMZs, thus affecting the regional $N_2O$ productivity and emissions. The upwelling in the Arabian Sea is most intense during the South Asian summer monsoon, leading to high oceanic $N_2O$ production (Naqvi et al., 2010a) and emissions of 0.34–0.99 Tg $N_2O$ yr$^{-1}$(Naqvi et al., 2010b), representing 2–31% global oceanic $N_2O$ emissions (Suntharalingam et al., 2019). However, the estimate by Sudheesh et al. (2016) in the south-eastern Arabian Sea, based on the measurements from Mangalore and Kochi, is almost four times lower than previous estimates. Raes et al. (2016) proposed that the south-eastern Indian Ocean could be both a source and sink of $N_2O$, suggesting great uncertainty of the oceanic emission of $N_2O$ in the Indian Ocean. The upwelling driven by the summer monsoon also occurs in the Bay of Bengal, however, it is attenuated by the intense precipitation and pronounced freshwater discharge from the Ganges, yielding lower $N_2O$ productivity (Singh and Ramesh, 2015) and much smaller emission (~0.03–0.11 Tg $N_2O$ yr$^{-1}$, Naqvi et al., 1994, 2010b). There is some indication that increased nitrogen deposition,

Atmospheric
Chemistry
and Physics
Discussions

Open Access
EGU

1   due to anthropogenic perturbation, already influences the air-sea flux of $N_2O$ in the northern
2   Indian Ocean and will continue to do so into the future (Suntharalingam et al., 2019). Due to
3   sparse measurements, it is impossible to compare the oceanic $N_2O$ emission of the Indian Ocean
4   with the terrestrial emissions directly. However, the emissions from the Arabian Sea alone are
5   about 9.6%-28% of the terrestrial emissions of the study region (~3.5 Tg $yr^{-1}$ in 2015),
6   suggesting the importance of the oceanic source in the Arabian Sea region. Enhanced $N_2O$ sea-
7   to-air fluxes were also found in a zonal band between 5°S and 10°S as a result of wind-driven
8   upwelling during the OASIS research cruise in 2014 (Ma et al., 2018).
9
10
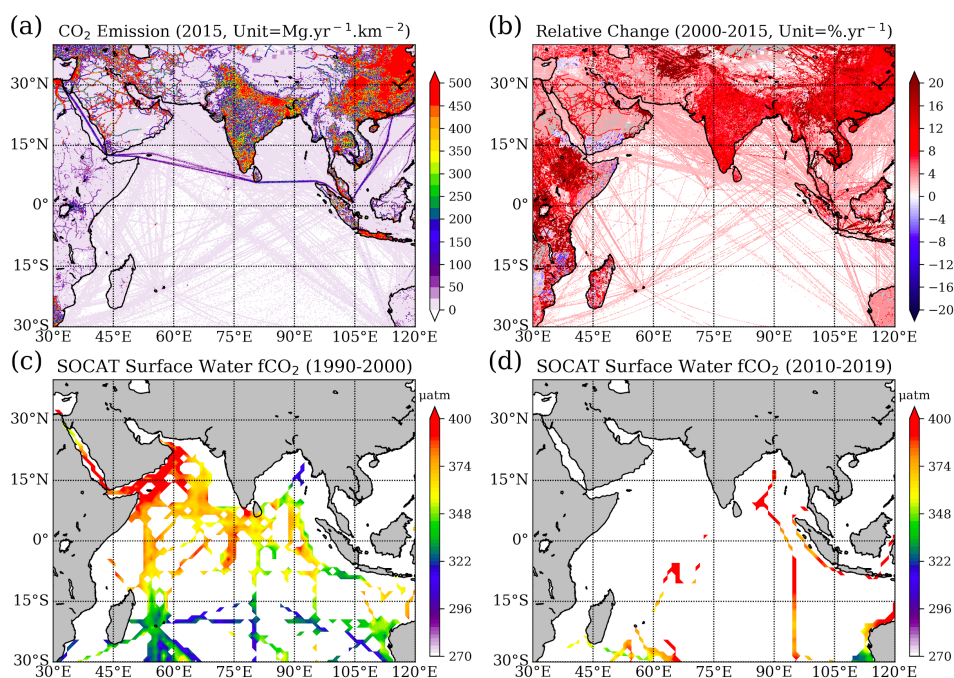


11
12   **Figure 8.** Annual mean $CO_2$ emissions for 2015 (a) and relative change with respect to 2000 (b) from
13   EDGAR V5.0_GHG. Surface water $fCO_2$ observations (color shading, unit: µatm) over the Indian
14   Ocean for 1990-2000 (c) and 2010-2019 (d) from SOCATv2019 (Bakker et al., 2016).

15
16   While the global oceans act as a net sink of $CO_2$, absorbing about 25% of the annual
17   anthropogenic $CO_2$ emission (Le Quéré et al., 2018), the air-sea exchange of $CO_2$ varies at
18   different spatial and temporal scales. The northern Indian Ocean is a net source of $CO_2$ to the
19   atmosphere, while the southern Indian Ocean is a net sink. On an annual scale, the Bay of
20   Bengal emits 2.45±0.49 Mg $CO_2$ $yr^{-1}$ $km^{-2}$ (Ye et al., 2019) with lowest emission of ~1.61 Mg
21   $CO_2$ $yr^{-1}$ $km^{-2}$ found for 2014 in the western Bay of Bengal (Dixit et al. 2019). Significant
22   impacts of tropical cyclones (Ye et al., 2019) and freshwater discharge (Sarma et al., 2011) on
23   the $CO_2$ air-sea exchange have been suggested for the Bay of Bengal. If compared to
24   anthropogenic emissions of more than 500 Mg $CO_2$ $yr^{-1}$ $km^{-2}$ over large areas (Fig. 8a), the
25   contribution of the northern Indian Ocean to the atmospheric $CO_2$ is relatively low. Analysing
26   the Surface Ocean $CO_2$ Atlas (SOCATv2019; Bakker et al., 2016) demonstrates that in the
27   Indian Ocean only a few $CO_2$ measurements are available for the last decade, especially when

1    compared with the 1990s (Fig. 8c and d), making it impossible to assess the long-term changes
2    of $CO_2$ air-sea exchange in this region.

3    During the OASIS campaign in the western Indian Ocean (Zavarsky et al., 2018a), both positive
4    and negative $CO_2$ fluxes were observed based on the direct eddy covariance flux technique.
5    South of the equator, average values were 0.2 Mg day$^{-1}$ km$^{-2}$ and -0.28 Mg day$^{-1}$ km$^{-2}$,
6    respectively, making this region a net sink of $CO_2$. These results are consistent with Chen et al.
7    (2011), who found significant spatial and temporal variability in the southern Indian Ocean
8    carbon sink. However, by comparing campaigns that occurred from 1999-2000 to those from
9    2004-2005, Chen et al. (2011) imply that the sink of the southern Indian Ocean is weakening.
10    A decadal variability analysis from 1991-2007 of dissolved $CO_2$ in surface seawater in the
11    southern Indian Ocean (20°S-55°S) suggests that it increased at a faster rate than atmospheric
12    $CO_2$ (Metzl, 2009), indicating that the ocean carbon sink weakened. The authors suggested that
13    the reduction was related to variability in the Southern Annular Mode. The weakening of Indian
14    Ocean carbon sink has also been found in a recent modelling study (DeVries et al. 2019).

15    Carbonyl sulphide (COS) is another important long-lived trace gas that acts as a greenhouse
16    gas in the troposphere and as the main precursor of aerosols in the stratosphere (Brühl et al.
17    2012; Kremser et al. 2016). The ocean is the main source of COS to the atmosphere, previously
18    estimated at 441-542 Gg COS yr$^{-1}$, globally, but a revision of the vegetation sinks has led to the
19    hypothesis that the ocean source might be stronger than previously calculated. The missing
20    ocean source is hypothesised to be in the tropics (e.g., Suntharalingam et al., 2008; Glatthor et
21    al., 2015). Launois et al. (2015) modelled oceanic concentrations and emissions for this region
22    that are approximately an order of magnitude higher, but the values do not agree with the albeit
23    sparse COS measurements that exist in the Indian Ocean. A recent measurement and modelling
24    study on the OASIS campaign has shown that, in fact, the ocean source of COS is not higher
25    than previously determined (Lennartz et al., 2017). Daily integrated air-sea fluxes computed
26    for the southern Indian Ocean ranged between -0.045 and -0.000375 g COS km$^{-2}$, indicating
27    that the Indian Ocean may be a net sink for COS. In addition, COS is produced in the
28    atmosphere from DMS and carbon disulphide ($CS_2$) oxidation, both of which are emitted from
29    the ocean (Chin and Davis, 1993; Watts, 2000). These pathways increase the ocean source of
30    COS indirectly, but do not account for the full missing ocean source (Lennartz et al., 2017).
31    Campbell et al. (2015) and Lennartz et al. (2017) point to anthropogenic emissions of COS
32    from Asia to close the gap and, indeed, Lee and Brimblecombe (2016) find twice as much COS
33    in the atmosphere from anthropogenic emissions than previously thought. They report that
34    anthropogenic COS emissions account for approximately one third of global emissions and
35    originate from the paper industry and biofuel and coal combustion. Another study suggests that
36    COS emission from domestic use coal combustion only in China would be at least $57.2 \pm 10.5$
37    Gg COS yr$^{-1}$, an order of magnitude greater than recent estimates of COS emissions from the
38    total coal combustion in China (Du et al., 2016).

39    **4.3 Short-lived gases DMS, isoprene and bromoform**

40    **Dimethylsulphide (DMS)**
41    The largest source of biogenic sulphur to the atmosphere is from marine DMS. DMS is
42    produced from the algal derived precursor, dimethylsulphoniopropionate (DMSP), which is
43    cleaved by marine microbes to form DMS. Only a small fraction of this DMS is released to the
44    atmosphere. The seminal CLAW hypothesis proposed a feedback loop between marine
45    biogenic DMS production, emissions and climate, via aerosol and cloud formation (Charlson
46    et al., 1987), triggering decades of research on DMS cycling in the ocean and emission to the
47    atmosphere. Lana et al. (2011) is the most comprehensive and up-to-date monthly DMS
48    concentration and flux climatology resulting from this large body of research. Unfortunately,

1  measurements in the Indian Ocean are sparse and most values in the climatology are
2  interpolated, with only 6271 non-uniformly spaced data points over 40 years available in the
3  Indian Ocean.

4  DMS emissions exhibit clear seasonality, with the highest fluxes, basin wide, evident during
5  the summer monsoon period. According to Lana et al. (2011), the summertime values in the
6  Indian Ocean are a global hotspot for DMS emissions. The largest values are found in the
7  Arabian Sea (Fig. 9). High biological productivity associated with the upwelling areas off north-
8  east Africa and the Arabian Sea are strongly correlated with the monsoon cycle (Yoder et al.,
9  1993). Combined with the strong, steady winds during the summer monsoon, fluxes of DMS
10 reach their peak. Lowest fluxes are computed during the spring transition period, likely
11 associated with low productivity and low wind speeds. Year round, there is a relatively large
12 flux area around 15°S, which migrates north and south according to the summer hemisphere
13 and is related to biogenic processes in the upwelling. Winds are always relatively high in this
14 region throughout the year, which also enhances the flux (Fig. 1). Maximum emissions of over
15 650 kg DMS $k^{-2}$ $yr^{-1}$ for the Arabian Sea (Lana et al., 2011) translate to slightly larger S flux to
16 the atmosphere from DMS than that from $SO_2$ ship emissions (approximately 335 kg S $k^{-2}$ $yr^{-1}$
17 from DMS and 250 kg S $k^{-2}$ $yr^{-1}$ from $SO_2$).

18 Gali et al. (2018) used satellite-based proxies to estimate the DMS concentration climatology
19 and reported that the Lana et al. (2011) climatology overestimates the DMS in the Indian Ocean
20 region by 25-50% in all the seasons. DMS direct flux measurements using the eddy covariance
21 technique and ocean concentration measurements were performed during the OASIS campaign
22 in order to compare directly with the Lana climatology in the western tropical Indian Ocean
23 (Zavarsky et al., 2018a). The oceanic DMS concentrations were found to be lower than those
24 in the climatology, but the difference was more pronounced south of 16°S where measured
25 values were a third of those in the climatology. North of 16°S, the measured ocean
26 concentrations were in better agreement with those in the climatology until the vicinity of the
27 Maldives, where they again were lower by a factor of three. The measured fluxes, subsequently,
28 were lower than the climatology for the region by approximately 60% on average. This was
29 attributed to lower measured oceanic concentrations, as well as lower measured wind speeds
30 than used in the climatology and a different gas transfer parameterisation. The directly derived
31 gas transfer parameterisation was linearly dependent on wind speed, while the climatology uses
32 a quadratic wind speed dependence. Nonetheless, the Indian Ocean appears to be a hotspot for
33 DMS emissions during the summer monsoon, but with more likely sulphur loading to the
34 atmosphere on the order of half of that from $SO_2$ ship emissions.
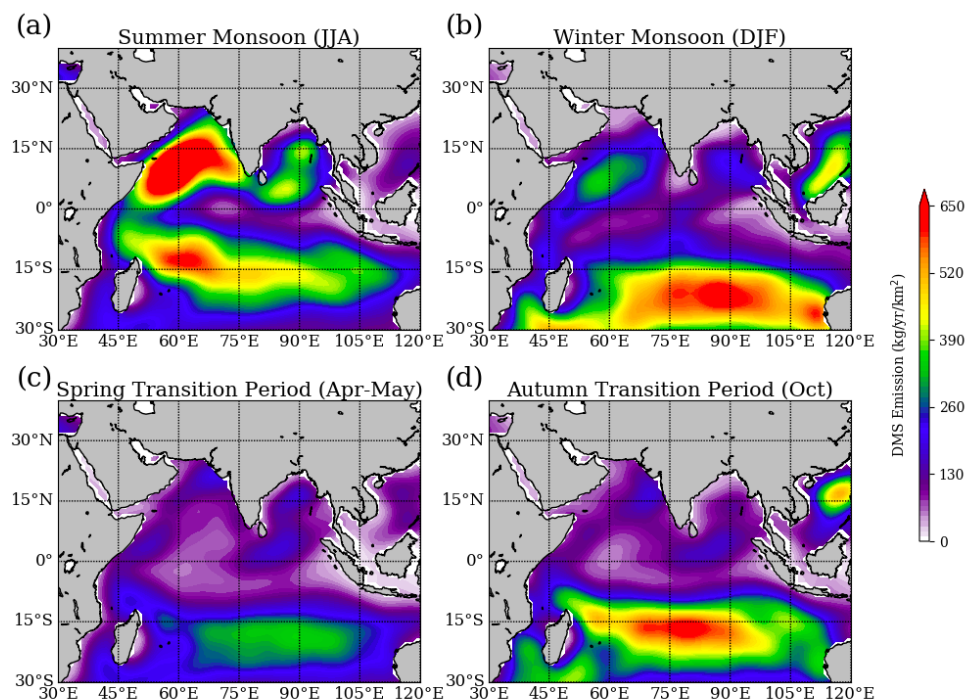
**Figure 9**. DMS emission for (a) summer monsoon (June - August), (b) winter monsoon (December - February), (c) spring transition (April - May) and (d) autumn transition (October) periods from Lana et al. (2011).

**Isoprene**

Isoprene (2-methyl-1,3-butadiene) is a biogenic volatile organic compound (VOC) and accounts for half of the total global biogenic VOCs in the atmosphere (Guenther et al., 2012). Most is emitted from terrestrial vegetation (400–600 TgC yr$^{-1}$, Guenther et al., 2006; Arneth et al., 2008). The ocean source strength is much lower, and the magnitude is debated (Carlton et al., 2009), with most estimates lower than 1 TgC yr$^{-1}$ (Palmer and Shaw, 2005; Arnold et al., 2009; Gantt et al., 2009; Booge et al., 2016). It is known from laboratory studies that phytoplankton produce isoprene (Exton et al., 2013 and references therein), but only a few studies have performed direct measurements of marine isoprene concentrations worldwide.

Emitted isoprene affects the oxidative capacity of the atmosphere through ozone and OH interactions and is a source for secondary organic aerosols (SOAs) (Carlton et al., 2009). Due to the short atmospheric lifetime of minutes to a few hours, terrestrial isoprene does not reach the atmosphere over much of the ocean and, thus, marine emissions of isoprene could play an important role in SOA formation on regional and seasonal scales, especially in association with increased production during phytoplankton blooms (Hu et al., 2013). Furthermore, isoprene SOA yields increase under acid-catalysed particle phase reaction in low-NO$_x$ conditions, which dominate over open oceans regions (Surratt et al., 2010), and which are significantly higher than that during neutral aerosol experiments (Henze and Seinfeld, 2006). Here we use data from the OASIS campaign and a modelling study with input variables from 2014 to assess seasonal isoprene fluxes to the atmosphere from the Indian Ocean (Booge et al., 2016, 2018).
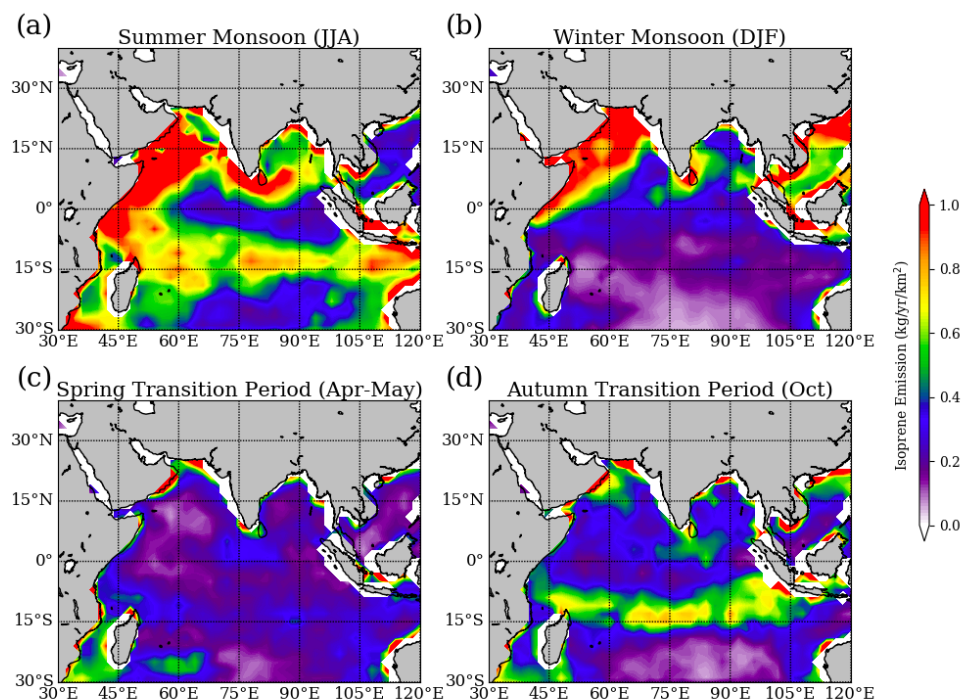
**Figure 10**. Same as Figure 9 but for isoprene from Booge et al. (2016).

Isoprene fluxes to the atmosphere change seasonally, with the highest values computed during the summer monsoon over the entire Indian Ocean extent (Fig. 10). The summer values are the second highest values, globally, during that season, following the Southern Ocean. Lowest isoprene emissions in the Indian Ocean are found in the spring transition period. This seasonal pattern is similar to the DMS emissions pattern. Computed fluxes during the winter monsoon are high in the northern region of the Indian Ocean, especially in the Arabian Sea. A belt of relatively high isoprene fluxes can be seen in the autumn transition period around 15°S, but the values are lower than the highs seen during the summer (basin wide) and winter (Arabian Sea) monsoon season. Unlike DMS, this is only visible in the summer and autumn seasons. Isoprene production rates are phytoplankton functional type dependent and are driven further by light, SST, salinity, and nutrients (Booge et al., 2018). High light and high SST favour higher production, while high salinity and high nutrients lead to lower production. The combination of the direct influence of wind speeds on fluxes and the interaction of the environmental factors and isoprene production leads to the seasonal patterns.

**Halogens**

Halogenated very short-lived substances (VSLSs) from the ocean, such as bromoform ($CHBr_3$), dibromomethane ($CH_2Br_2$) and methyliodide ($CH_3I$), contribute to atmospheric halogen loading and ozone depletion (Engel and Rigby et al., 2019). The oceanic $CHBr_3$ surface concentrations are spatially and temporally highly variable. Natural production of $CHBr_3$ involves marine organisms such as macroalgae and phytoplankton (Gschwend et al., 1985), while $CH_2Br_2$ is formed in parallel and correlates with $CHBr_3$ in water and air (Tokarczyk and Moore, 1994). A recent study suggests that heterotrophic processes in the ocean can increase the flux of

1   CH$_2$Br$_2$ from the sea to the atmosphere (Mehlmann et al., 2020). Enhanced emissions of
2   brominated VSLS coincide with biologically active equatorial and coastal upwelling regions
3   (Quack et al., 2007) and the distribution of macroalgae and anthropogenic sources along the
4   coasts (Carpenter and Liss, 2000; Maas et al, 2020). Iodinated VSLS such as CH$_3$I, on the other
5   hand, show elevated oceanic abundances in the subtropical gyre regions in agreement with
6   identified production by photochemical reactions (Richter and Wallace, 2004).

7   Various CHBr$_3$ emission inventories have been derived from the extrapolation of measurement-
8   based data (Ziska et al., 2013; Fiehn et al., 2017), oceanic modelling (Stemmler et al., 2015),
9   top-down atmospheric modelling approaches (Liang et al., 2010) and a data-oriented machine-
10  learning algorithm (Wang et al., 2019). Overall, large differences between CHBr$_3$ emission
11  inventories exist with the observation-based, bottom-up emissions (Ziska et al., 2013) being
12  most consistent with atmospheric measurements in the tropics (Hossaini et al., 2013). All
13  inventories agree on the tropical Indian Ocean being a productive source region of CHBr$_3$.
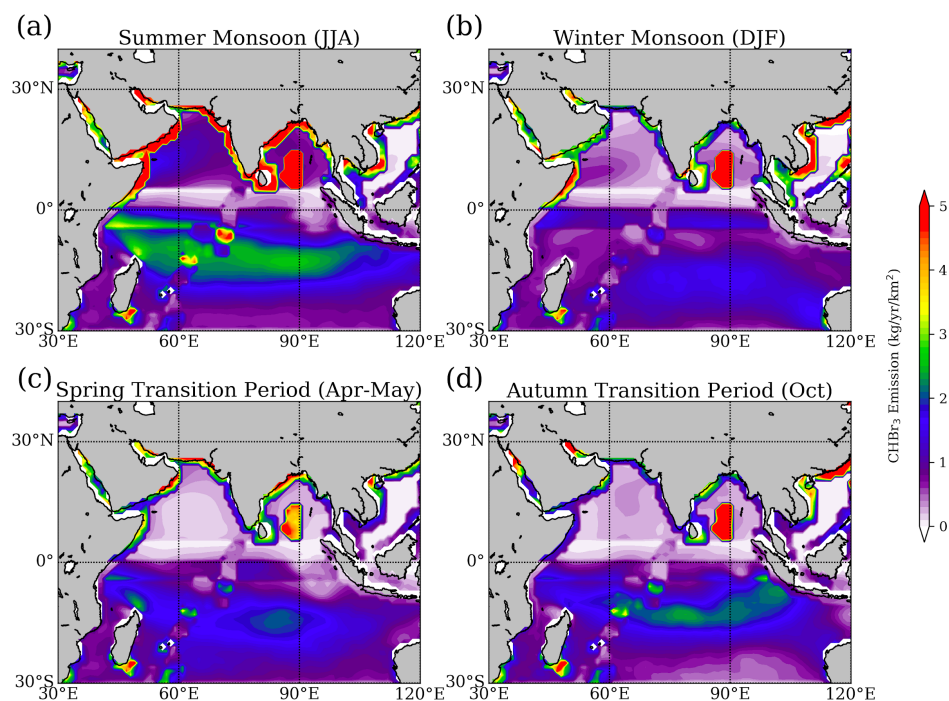


14
15  **Figure 11**. Bromoform (CHBr$_3$) emission for (a) summer monsoon (June - August), (b) winter monsoon
16  (December - February), (c) spring transition (April - May) and (d) autumn transition (October) periods
17  based on static surface concentrations and ERA-Interim meteorology for 2014 (Fiehn et al., 2018).
18
19
20  Here we show the most recent bottom-up CHBr$_3$ emission inventory (Fiehn et al., 2018) based
21  on two campaigns in the marginal seas (Yamamoto et al., 2001; Roy et al., 2011), one campaign
22  in the open Indian Ocean (Fiehn et al., 2017) and extrapolations of measurements from other
23  oceans (Ziska et al., 2013) in Fig. 11. The emission inventory is based on static surface
24  concentration maps generated from atmospheric and oceanic surface ship-borne in-situ
25  measurements collected within the HalOcAt (Halocarbons in the ocean and atmosphere)

1    database project (https://halocat.geomar.de, last access July 2020). While the concentration
2    maps do not provide any temporal variability, the emission parameterisation is based on
3    monthly mean meteorological ERA-Interim data allowing for relative emission peaks related
4    to maxima in the horizontal wind fields and sea surface temperature.

5    The $CHBr_3$ emissions peak along the Northern Hemisphere (NH) coastlines due to macroalgae
6    production and anthropogenic sources (3.3-6.6 kg $yr^{-1}$ $km^{-2}$), the central Bay of Bengal (up to
7    11.1 kg $yr^{-1}$ $km^{-2}$) and the southern tropical Indian Ocean (2.2 kg $yr^{-1}$ $km^{-2}$). The coastal
8    emissions in the Indian Ocean of the bottom-up inventory presented here agree well with other
9    emission estimates (Fiehn et al., 2018). High emissions along the coasts of Somalia and Oman
10   due to coastal upwelling detected in biogeochemical modelling studies (Stemmler et al., 2015)
11   are not captured here due to missing $CHBr_3$ measurements in this biogeochemical regime. The
12   emissions show a pronounced seasonal cycle with a peak during the summer monsoon period
13   (Fig. 11) due to higher wind speeds over the whole Indian Ocean during this time of year (Fig.
14   1).

15   Once destroyed in the atmosphere, brominated VSLS contribute to the family of inorganic
16   bromine ($Br_y$) consisting of bromine radicals such as bromine monoxide (BrO) and non-radical
17   reservoir species such as HBr and HOBr. Inorganic bromine has also other anthropogenic and
18   natural sources including methyl bromide, which is a product of biomass burning, leaded fuel
19   combustion, plant and marsh emissions, as well as soil fumigation (Mano and Andreae, 1994).
20   Inorganic bromine can also be released when sea salt is exposed to the atmosphere from young
21   sea-ice surfaces, frost flowers, snowpack, seawater and marine aerosols (Hay et al., 2007).

22   Similar to bromine, inorganic iodine such as iodine oxide (IO) is produced through the
23   degradation of its organic precursor $CH_3I$ and other short-lived iodinated VSLS. The primary
24   source of iodine to the marine boundary layer, however, are believed to be inorganic iodine
25   emissions at the ocean surface from reactions of dissolved iodide with deposited gas-phase
26   ozone (Carpenter et al., 2013). Once in the atmosphere, inorganic iodine plays an important
27   role for the boundary layer chemistry by influencing the oxidising capacity through catalytically
28   removing $O_3$ and altering the $HO_x$ and $NO_x$ balance.
29

30   **5. Atmospheric composition**

31   During the South Asian summer monsoon, clean air dominates the atmospheric composition
32   over the Indian Ocean, leading to a completely different chemical regime than observed during
33   wintertime. As the ITCZ moves over the Indian subcontinent (Waliser and Gautier, 1993), air
34   mass transport via steady winds is directed from the ocean towards the land and anthropogenic
35   pollutants are confined to the continents. During this period, the intense summer monsoon
36   rainfalls also effectively remove many soluble species from the continental boundary layer.
37   During the winter monsoon and transitional months, the wind pattern is reversed with
38   continental air masses being transported towards and over the open ocean environment. This
39   leads to an increase in the anthropogenic origin trace gases and aerosol loading over the Indian
40   Ocean. Based on studies and campaigns that took place before 2010, Lawrence and Lelieveld
41   (2010) provided a comprehensive review of atmospheric composition over the Indian Ocean.
42   Here we summarize their most important findings and report on new datasets and results that
43   have emerged since then.

44   **5.1 Pollution and $O_3$**

45   The surface distributions of anthropogenic pollutants and ozone levels are often highly
46   correlated as the majority of tropospheric ozone formation occurs when CO, $NO_x$, and other

1   ozone precursor gases react in the atmosphere in the presence of sunlight. Tropospheric ozone
2   is a greenhouse gas with a relatively short lifetime and is therefore considered a near-term
3   climate forcer. The direct radiative forcing of ozone is estimated to be $0.40 \pm 0.20$ W m$^{-2}$ (IPCC,
4   2013) and additional indirect radiative forcings can result from its impact on vegetation, carbon
5   uptake and methane lifetime (e.g., Lombardozzi et al., 2015; Fiore et al., 2008). Ozone also acts
6   as an environmental pollutant detrimental to human health, and crop and ecosystem
7   productivity (e.g. Monks et al., 2015). Changes of ozone precursor emissions, low-frequency
8   climate variability and long-term anthropogenic climate change all impact the quantity and
9   distribution of tropospheric ozone (e.g. Barnes et al., 2016).

10  The distribution and variations of pollutants and ozone over the Indian Ocean have been
11  investigated during individual campaigns (e.g., ICARB) and can be derived from continuous
12  in-situ (e.g., ozone profiling at Indian coastal stations) and satellite measurements (e.g., OMI
13  and MOPITT). The various data sets offer different advantages, allowing for a wide range of
14  applications. While the in-situ measurements are characterised by higher resolution and lower
15  uncertainties, they are usually limited in space (stations) or time (campaigns). The satellite
16  measurements on the other hand, offer comprehensive spatial coverage and extend over longer
17  time periods, but suffer from limited vertical resolution and higher uncertainties. Most available
18  Indian Ocean campaigns and studies investigate $O_3$, CO and $NO_x$. As a result, the following
19  sections focus on the distribution and variability of these three gases, while $SO_2$ and mercury
20  are only discussed briefly.

21  **Carbon monoxide (CO) and nitrogen oxides ($NO_x$)**
22  The distribution of the major pollutant CO over the Indian Ocean is well known from MOPITT
23  satellite measurements (e.g., Ghude et al., 2011; Srivastava et al., 2012a). Seasonal mean
24  surface values for 2014/15-2018/19 show a clear gradient between CO over the Indian Ocean
25  and over the landmass source regions (Fig. 12). Highest CO surface values over the Indian
26  Ocean occur during the winter monsoon with multiannual mean mixing ratios of around 150
27  ppb over the open ocean and 350-400 ppb over Bay of Bengal coastal waters (Fig. 12b). CO
28  mixing ratios over marine regions of more than 150 ppb are considered as polluted continental
29  air (Nowak et al., 2004), and during the winter monsoon most parts of the NH Indian ocean fall
30  into this category. South of 5°S, mixing ratios drop below 100 ppb during winter and can be
31  considered as part of the pristine oceanic regime.

Atmospheric
Chemistry
and Physics
Discussions

Open Access

EGU
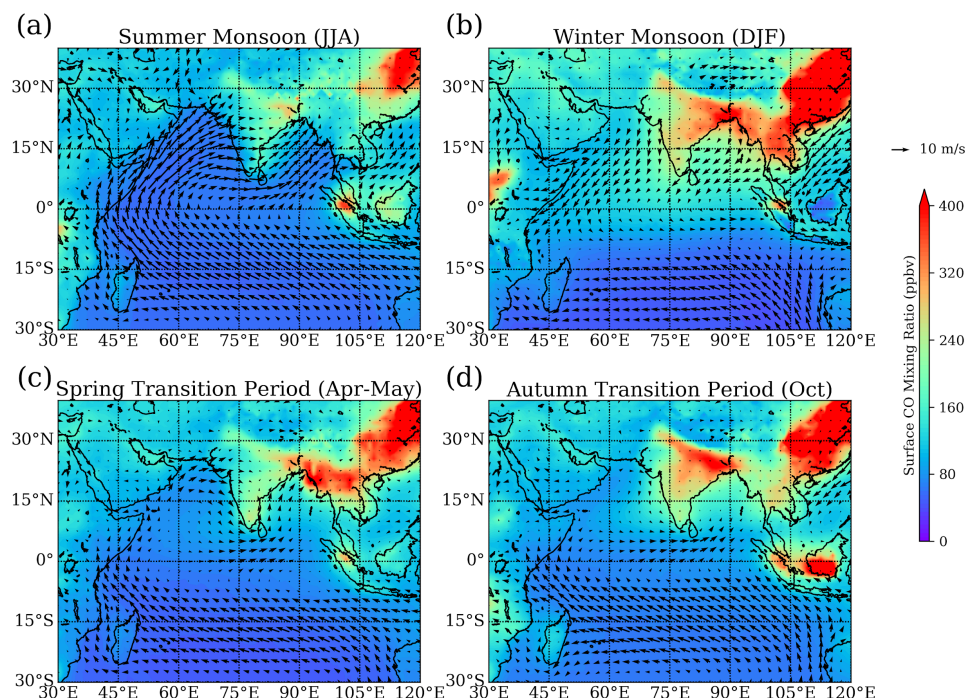
**Figure 12.** Surface carbon monoxide (CO) mixing ratios from MOPITT (coloured shading) and surface wind from ERA-Interim (black arrows) for (a) summer monsoon 2014 - 2018 (June - August), (b) winter monsoon 2014/2015 - 2018/2019 (December - February), (c) spring transition 2014 - 2018 (April - May) and (d) autumn transition 2014 - 2018 (October) periods.

The tropospheric distribution of $NO_x$ is very similar to that of CO. Figure 13 shows the tropospheric $NO_2$ column from TROPOMI, which, due to the fast photochemical cycling between NO and $NO_2$, can be taken as a robust measure for concentrations of nitrogen oxides. Seasonal mean values for 2018/19 show a clear gradient of $NO_2$, with maxima over the landmass source regions and minimum values over the equatorial western Indian Ocean (Fig. 13). Coastal gradients are particularly pronounced around the Indian coastline during the autumn transition period and winter monsoon. One clear difference in comparison to the CO distribution is the appearance of enhanced $NO_2$ columns along the shipping lanes, in particular along the major route from the tip of India to Malaysia.

The INDOEX campaign showed that the winter monsoon season is characterized by strongly enhanced CO abundances over the northern Indian Ocean, with values comparable to air downwind of Europe and North America (Lawrence and Lelieveld, 2010). Based on simultaneous measurements of methyl cyanide ($CH_3CN$) and model simulations, biomass burning in South and Southeast Asia and subsequent transport of the polluted air towards the Indian Ocean was identified as a major source of CO (Lelieveld et al., 2001). Over the open Indian Ocean, southward transport along with chemical processing, dilution, and surface deposition causes a strong north-south pollution gradient. In the boundary layer, the contrast between polluted NH and pristine Southern Hemisphere (SH) air results in a sharp gradient

1    across the ITCZ (Lawrence et al., 2003), while the upper troposphere was identified as a region
2    for interhemispheric exchange of these air masses (Williams et al., 2002).
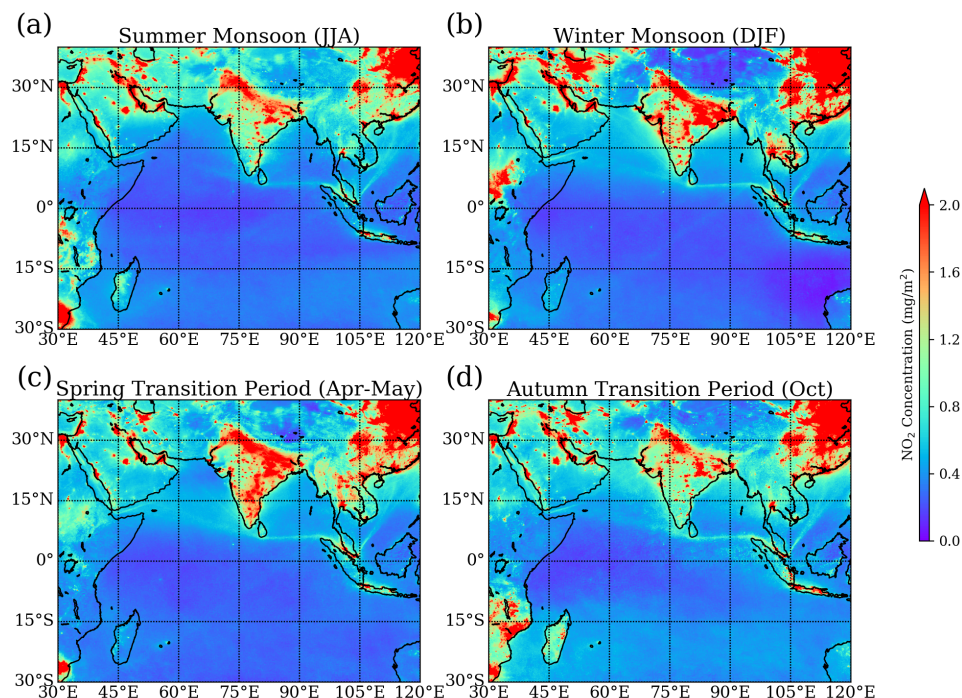


**Figure 13.** Tropospheric nitrogen dioxide (NO$_2$) column from TROPOMI for (a) summer monsoon
2019 (June - August), (b) winter monsoon 2018/2019 (December - February), (c) spring transition 2019
(April - May) and (d) autumn transition 2019 (October) periods.

8    Recent studies of atmospheric composition during the winter monsoon period have focused on
9    the Bay of Bengal where the ship-based measurements were conducted during the second part
10   of ICARB for December 2008–January 2009. Mixing ratios of NO$_2$ and CO show a distinct
11   spatial pattern with elevated values in the head and the south-east Bay of Bengal due to transport
12   from adjoining landmasses (Asatar and Nair, 2010; David et al., 2011). The in-situ
13   measurements reveal highest CO surface mixing ratios of 379±58 ppb over the south-east Bay
14   of Bengal, which exceed the MOPITT multiannual mean values (Fig. 12b). Similar to CO, the
15   NO$_2$ surface distribution exhibits prominent highs over the head and the south-east Bay of
16   Bengal, with lower values in the south (David et al., 2011). Analysis of back trajectories and
17   airflow patterns revealed that the high pollution over the head of the Bay of Bengal (15°N-
18   21°N) was advected from the Indo-Gangetic Plain, which is one of the major CO emission
19   centres (Fig. 3). The high pollution over the south-east Bay of Bengal, on the other hand, was
20   attributed to the effects of continental outflow from Southeast Asia, a transport pattern
21   discernible from the wind patterns in Fig. 12. Airborne measurements conducted during the
22   same campaign confirm the higher pollution over the northern and south-eastern part of the Bay
23   of Bengal (Srivastava et al., 2012b). Analyses of the acetylene/CO ratio suggested that air mass

1   samples taken over the northern Bay of Bengal were less chemically aged compared to samples
2   taken during the other flights.

3   Seasonal variations of $NO_x$ at a surface station in Trivandrum, situated on the south-west coast
4   of India, also show highest values during the winter monsoon season due to land-based
5   emissions and transport patterns (David and Nair, 2011). While the strongest $NO_x$ emissions
6   are located in East Asia, enhanced emissions also exist in southern India (Fig. 4) contributing
7   to the wintertime $NO_x$ maxima over the Indian coastline (see also Fig. 13). Ship based
8   observations of $NO_2$ show a strong decreasing gradient in concentrations from the sub-continent
9   towards the open ocean. Observations made on the IIOE-2 expedition observed peak values of
10  $854 \pm 223$ ppt close to Goa, but the values were below the detection limit of 120 ppt away from
11  the coast. A similar gradient is evident from the satellite retrieved tropospheric $NO_2$ with the
12  emissions of $NO_x$ over the sub-continent leading to higher values close to the coast (Fig. 13;
13  Mahajan et al., 2019a).

14  The impact of anthropogenic emissions during the winter monsoon is evident over large parts
15  of the Indian ocean, as demonstrated by surface measurements from the island of Mahé in the
16  western Indian Ocean just south of the equator. Seasonal variations of CO values peak in
17  January–February as a result of the long-range transport of anthropogenic emissions from India
18  during this time of year (Wai et al., 2014). Reunion Island around 19°S, on the other hand, is
19  much less impacted by the winter monsoon due to the ITCZ functioning as a transport barrier.
20  Seasonal variations of CO measurements at two stations on Reunion Island peak in September–
21  November, primarily driven by the emissions from biomass burning in Africa and South
22  America (Zhou et al., 2018). The seasonal variations of the CO distribution given by the
23  MOPITT satellite observations (Fig. 12) are consistent with the findings of the in-situ
24  measurement studies discussed above.

25  During the summer monsoon, CO mixing ratios over the Arabian Sea, Bay of Bengal and the
26  Indian Ocean drop mostly below 80 ppb, except for over coastal waters in the Bay of Bengal
27  with values of up to 150 ppb (Fig 12). As the ITCZ moves north over the Indian subcontinent,
28  the large-scale air flow is directed from the Indian Ocean towards the land, preventing the
29  spread of pollution in the maritime environment. The coastal regions of Bangladesh and eastern
30  India are exceptions, as they are impacted by strong westerlies transporting polluted air from
31  southern India and Sri Lanka resulting in elevated CO mixing ratios larger than 150 ppb (Fig.
32  12a). The elevated pollution along the eastern India coastline is in stark contrast to the western
33  India coastline, with very low CO mixing ratios of well below 100 ppb. The overall prevalence
34  of clean oceanic background air during the summer monsoon season was confirmed by the low
35  CO values detected over the equatorial Indian Ocean during the OMO campaign in July/August
36  2015 (Tomsche et al., 2019). Vertical profiles of CO were derived during flights over Gan
37  (Maldives), which is situated close to the equator and, thus, influenced by air from the southern
38  Indian Ocean. The CO profiles over Gan with values of ~60 ppb were found to be lower than
39  the NH background and the Asian monsoon CO profiles for all altitudes below 8 km (Fig. 2 in
40  Tomsche et al., 2019). During the AQABA ship campaign in summer 2017, low pollution levels
41  over the Arabian Sea were confirmed by measurements of relatively low $NO_x$ mixing ratios
42  (0.19 ppb, Tadic et al., 2019).

43  The transition periods during boreal spring and autumn are characterized by a large spatial and
44  temporal variability of the pollution distribution, which shifts between the clean summer regime
45  and the polluted winter regime. Mean CO mixing ratios in the Bay of Bengal and Arabian Sea
46  range between 100 and 200 ppb, while the equatorial and southern Indian Ocean are dominated
47  by clean oceanic air with CO values below 100 ppb (Fig 12c and d). ICARB measurements
48  during March-April 2006 show higher CO values in the Bay of Bengal compared to the Arabian
49  Sea and higher CO values towards the coast, as expected with continental pollution being the

1   main source of the observed values (Aneesh et al., 2008). Transport regimes start to shift in
2   March when the outflow from India into the Arabian Sea and from Southeast Asia into the Bay
3   of Bengal begins to weaken. This shift leads to slowly decreasing pollution, as observed during
4   ICARB where CO values over the northern Bay of Bengal were found to be around 234 ppb
5   during March (Srivastava et al., 2012a), thus being lower than the above discussed winter
6   monsoon values. In April, offshore flow from the Indian subcontinent or Southeast Asia has
7   weakened further leading to very little pollution transport towards the ocean. The southern Bay
8   of Bengal is dominated by south-westerly winds (see also Fig 12c) carrying cleaner marine air,
9   as evident from CO mixing ratios of 88 ppb obtained during ICARB April measurements
10  (Srivastava et al., 2012a).

11  The boreal autumn transition period, also referred to as post-summer monsoon, marks the onset
12  of the polluted winter regime after the withdrawal of the monsoon winds. During this period, a
13  sudden increase of pollutant levels can be expected, in particular in coastal regions and over the
14  Bay of Bengal. During the SK-277 ship campaign, a large spatial heterogeneity of pollution
15  was observed over the Bay of Bengal (Mallik et al., 2013) reflecting the direct impact of air
16  masses being advected from different source regions in South Asia. Highest CO levels were
17  found in air masses originating in Southeast Asia with signatures of biomass and biofuel
18  burning. Continental pollution sources for $NO_x$ were further enhanced by regional sources
19  possibly from ship emissions over the Bay of Bengal, which contains the international shipping
20  corridor connecting the southern tip of India and the Strait of Malaga.

21  **Sulfur dioxide ($SO_2$), mercury and ammonia**
22  In comparison to other pollutants, the $SO_2$ characterisation above the Indian Ocean is sparse.
23  Data available from the recent ICARB campaign in 2018, nonetheless, can be used to assess
24  the influence of anthropogenic $SO_2$ in the marine atmosphere over the Indian Ocean. Aswini et
25  al. (2020) show the presence of non-sea salt sulfate aerosol ($SO_4^{2+}$) in an intense pollution
26  plume over the Arabian Sea and the Indian Ocean during the winter monsoon. Meteorological
27  conditions during this season are favourable for $SO_2$ to $SO_4^{2+}$ conversion. This is proposed to
28  take place through photochemical oxidation of $SO_2$ by the OH radical in the gas phase and
29  through oxidation of $SO_2$ by $H_2O_2$ and $O_3$ in the aqueous phase (Seinfeld and Pandis, 2006).
30  About two-thirds of the total tropospheric $SO_4^{2+}$ formation is thought to occur through aqueous
31  phase reactions (e.g., Warneck, 1999).

32  $SO_2$ has both anthropogenic and natural sources (i.e. oxidation of DMS), but comparison with
33  previous research cruise studies conducted nearly two decades ago shows a more than two-fold
34  increase in the concentration of nss-sulphate aerosols over the continental outflow region in the
35  Arabian Sea that appears to be due to anthropogenic $SO_2$ (Aswini et al., 2020). Despite
36  decreasing $SO_2$ emissions in East Asia since 2010, emissions are rapidly increasing in South
37  Asia, by about 10% per year with the Indo-Gangetic Plains being a major source region
38  (Lelieveld et al., 2019, Sec. 4). In order to further explore the contribution of anthropogenic
39  $SO_2$ to nss-sulphate aerosol formation, the ratio of methanesulphonic acid (MSA), due solely
40  to DMS oxidation, to $SO_4^{2+}$ was computed. The average MSA/nss-$SO_4^{2+}$ ratio during the
41  ICARB campaign was $3.1 \times 10^3$. Over the more pristine sections of the cruise, the average ratio
42  was $4.7 \times 10^3$. In remote marine regions, ratios of 0.065 have been found (Savoie and Prospero,
43  1989). The lower MSA/nss-$SO_4^{2+}$ ratio implies that most of the nss-$SO_4^{2+}$ is from anthropogenic
44  sources (Aswini et al., 2020).

45  Under the framework of the Global Mercury Observation System (GMOS) project, a mercury
46  monitoring station was set up on Amsterdam Island, a remote and small island located in the
47  southern Indian Ocean (Sprovieri et al., 2016). Observations of gaseous elemental mercury
48  (GEM), reactive gaseous mercury (RGM) and particle-bound mercury (PBM) from this station
49  over several years were reported by Angot et al. (2014). GEM concentrations were found to be

1   remarkably steady, with an average hourly mean concentration of $1.03 \pm 0.08$ ng m$^{-3}$, and show
2   a small seasonal cycle. In comparison, the high altitude GMOS site in Kodaikanal located in
3   southern India shows significantly higher GEM concentrations of $1.54 \pm 0.20$ ng m$^{-3}$ in 2013,
4   possibly related to different long-range transport patterns and closer proximity of anthropogenic
5   sources (Sprovieri et al., 2016).

6   RGM and PBM concentrations at Amsterdam Island were also very low ($0.34$ pgm$^{-3}$ and $0.67$
7   pgm$^{-3}$, respectively), but displayed a strong seasonal variability (ranging between the detection
8   limit and $4.07$ pgm$^{-3}$ and $12.67$ pgm$^{-3}$, respectively). Analysis showed that, despite the
9   remoteness of the island, long-range transport from southern Africa contributed significantly to
10   the GEM and PBM budgets from July to September when biomass burning peaks in Africa
11   (Angot et al., 2014). During these periods, the higher GEM concentrations observed at
12   Amsterdam island were comparable to those recorded at other tropical stations distributed
13   around the globe. During periods of lower GEM concentrations, on the other hand, values of
14   less than 1 ng m$^{-3}$ were found to be characteristic for air masses from the southern Indian
15   Ocean and Antarctic continent (Sprovieri et al., 2016).

16   Observations of ambient ammonia ($NH_3$) are rare in the Indian Ocean region. Early
17   observations in 1980 by Ayers and Gras (1980) in the Southern Indian Ocean showed a range
18   between 2.2 and 4.4 nmol m$^{-3}$. Later observations in the same region of the ocean showed a
19   lower range of 0.3 to 2.1 nmol m$^{-3}$ (mean of 1.1 nmol m$^{-3}$) (Norman and Leck, 2005). In the
20   north west Arabian Sea, observations of $NH_3$ were first carried out in 1999 reporting higher
21   concentrations in the coastal environment 2.5 to 5.6 nmol m$^{-3}$ (mean 3.8 nmol m$^{-3}$) as compared
22   to the remote open ocean environment 0.4 to 1.8 nmol m$^{-3}$ (mean 1 nmol m$^{-3}$), showing the
23   importance of continental fluxes to the ambient marine $NH_3$ loading (Gibb and Mantouura,
24   1999a; 1999b). Similar to the Southern Indian Ocean, later observations by Norman and Leck
25   (2005) again reported a lower range between 0.05 and 0.2 nmol m$^{-3}$ (0.1 nmol m$^{-3}$). The reason
26   for this discrepancy between the two studies is not clear and was not discussed in the study by
27   Norman and Leck (2005).

28   Closer to the Indian coast, observations of $NH_3$ have been made in the Bay of Bengal over five
29   studies and show much higher concentrations as compared to the central or southern Indian
30   Ocean. Khemani et al. (1987) reported high concentrations of $NH_3$ in the coastal region in the
31   range between 117.6 and 211.8 nmol m$^{-3}$ (mean 158.8 nmol m$^{-3}$). Later, Carmichael et al. (2003)
32   also reported high $NH_3$ concentrations at two coastal sites (Bhubneswar: mean 288.2 nmol m$^{-3}$
33   and Berhampur: mean 329.4 nmol m$^{-3}$). These observations show a west-east positive gradient
34   close to the western coast of the Bay of Bengal, which is most likely driven by the local
35   transport of $NH_3$. Further to the northwest, Biswas et al. (2005) made observations of ambient
36   $NH_3$ close to the Sundarban mangrove forest which is one of the largest river deltas in the world.
37   They saw highly elevated levels, ranging from 105.2 to 675.0 nmol m$^{-3}$ (mean 265.2 nmol m$^{-3}$). The most recent reports in the literature were measurements done during the winter phase of
39   ICARB in the Bay of Bengal, which reported an average concentration of ranging between 11.7
40   and 441.2 nmol m$^{-3}$ (mean 281.2 nmol m$^{-3}$), with higher concentrations observed closer to the
41   coast and the lower concentrations observed in the open ocean environment (Sharma et al.,
42   2012). Unfortunately, no seasonal information is available due to the lack of continuous
43   observations through the entire year in the marine environment.

44   **Ozone**
45   Ozone distribution over the Indian Ocean is largely determined by the abundance of precursor
46   gases, transport patterns and chemical processing. During the winter monsoon, the southern
47   Asian outflow brings ozone precursors such as CO, $NO_x$ and VOCs from their source regions
48   in South and East Asia (Section 4) into the marine environment. Within the outflow, substantial

1   photochemical production of ozone occurs due to high pollution levels, strong tropical solar
2   radiation and frequently cloud-free conditions. As a result, relatively high ozone mixing ratios
3   of 60–70 nmol/mol have been observed off the coast of India and over the Bay of Bengal up to
4   a few hundred kilometres downwind (Lawrence and Lelieveld, 2010 and references therein).
5   Once produced, ozone can be transported to the remote marine environment, where local
6   dominant sources of ozone precursor gases are absent. As a result, the marine boundary layer
7   is considered as an ideal place to study the processes that drive ozone photochemistry (e.g.,
8   Monks et al., 1998). Tropospheric ozone is also influenced by downward transport from the
9   stratosphere (e.g., Ganguly and Tzanis, 2011) and deposition to surfaces (Graedel and Crutzen,
10  1992). Photo-dissociation of ozone leads to increasing OH levels particularly within the highly
11  humid marine boundary layer affecting the chemistry of the tropical marine environment and
12  highlighting the importance of continental outflow over cleaner oceanic regions.

13  A continuous dataset of $O_3$ vertical profiles at Ahmedabad, a city in western India, shows a
14  clear annual cycle dominated by the wind patterns (Lal et al., 2014). The lowest ozone (~20
15  ppb) was observed near the surface during September, which is at the end of the summer
16  monsoon. Clean air from the ocean and removal of precursors due to monsoon rains drive this
17  reduction. Model simulations showed that the lower tropospheric (<3 km) $O_3$ during the
18  summer monsoon was transported from the Indian Ocean via the east coast of Africa and the
19  Arabian Sea. Observations of mid-tropospheric ozone are highest (70–75 ppb) during April–
20  June and lowest (40–50 ppb) during winter due to the impact of long-range transport from North
21  Africa, North America and the stratosphere. Unfortunately, such continuous measurements are
22  not available at any site off the Indian subcontinent, but model simulations suggest that a similar
23  annual cycle can also be expected in the northern Indian Ocean environment (Lal et al., 2014).

24  During the winter monsoon, measurements of ozone in the Bay of Bengal have been carried
25  out as a part of the ICARB campaign (David et al., 2011). The marine boundary layer showed
26  large variations in the mixing ratios of ozone and its precursor gases with similar spatial patterns
27  (Fig. 14a) pointing to the same source regions, but different relative contributions. In the head
28  and south-east of the Bay of Bengal, mixing ratios of ozone (61 ± 7 ppb and 53 ± 6 ppb) and
29  precursors (discussed earlier) were found to be very high. Air mass back trajectories originated
30  from the Indo-Gangetic Plain and Southeast Asian countries, respectively, both characterized
31  by high tropospheric ozone and $NO_2$ values. In the south/south-western part of the Bay of
32  Bengal, the ozone mixing ratios were low, and the back trajectories originated from coastal
33  regions. Here, the longer transit times over the marine environment could have resulted in the
34  OH-driven destruction of ozone and precursors as well as in changes of surface level mixing
35  ratios due to updrafts and downdrafts (David et al., 2011). Three different ozone diurnal cycles
36  were observed, with most patterns showing maximum mixing ratios in the morning followed
37  by a decrease during the daytime and night-time increase. Over this oceanic region,
38  photochemical production involving $NO_2$ did not play a major role for the ozone production,
39  while the high water vapour acted as a sink.

40  Post-winter observations of near-surface ozone in the Bay of Bengal were carried out as part of
41  the first ICARB phase during March and April 2006 (Fig. 14b). Over the northern Bay of
42  Bengal, higher ozone mixing ratios (~30 ppb, Nair et al., 2011) were found to be well correlated
43  with precursor gases indicating their co-located sources (Srivastava et al., 2012a). Similar to
44  the winter monsoon conditions, north-westerly winds transported large amounts of
45  anthropogenic pollutants from the Indo-Gangetic Plain to the northern part of the Bay of Bengal
46  causing the elevated pollution levels. The middle and southern Bay of Bengal were more
47  influenced by the open ocean environment and showed lower ozone mixing ratios (~10-15 ppb,
48  Nair et al., 2011). For both regions, the surface ozone mixing ratios were anticorrelated with
49  the boundary layer height. Ozonesonde measurements taken during the same campaign
50  revealed an elevated plume between 1 and 3 km over the northern Bay of Bengal with very high

1   ozone mixing ratios of 60–90 ppb (Srivastava et al., 2011). The plume was also characterised
2   by higher temperature and lower specific humidity compared to the background marine air over
3   other regions. This elevated layer sandwiched between the marine boundary layer and the free
4   troposphere can be attributed to the advection of land air mass as a consequence of land-sea
5   breeze circulation near the coast or long-range transport.

6   Observations over the Arabian sea during the post-winter monsoon period revealed a
7   completely different picture. Ozone and pollutants showed significantly lower mixing ratios
8   when compared to the northern Bay of Bengal, suggesting the larger impact of cleaner marine
9   air (Srivastava et al., 2012a). This argument is further supported by the poor inter-correlations
10  of ozone and the various precursors. Latitudinal gradients of the gases were slightly negative
11  most likely due to some transport of polluted air from southern India over the southern Arabian
12  Sea and continuous dilution of pollution with time over this region. Such negative pollution
13  gradients over the Arabian sea during the transition periods were confirmed by the CO
14  distribution obtained from MOPITT (Srivastava et al., 2012a; Fig. 12c and d).
15
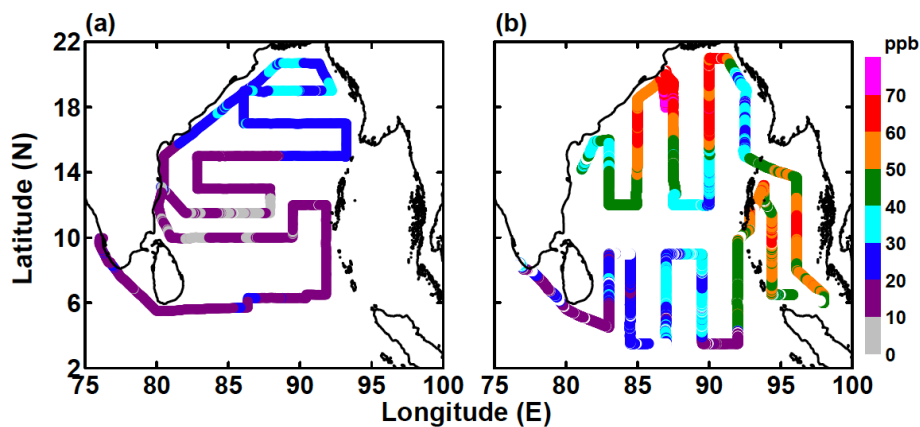


17  **Figure 14**. Surface ozone mixing ratios in the Bay of Bengal observed during a) boreal spring (March-
18  April 2006, ICARB) and b) winter monsoon (December-January 2009, ICARB). From David et al.,
19  2011, copyright 2011, reproduced with permission.

20  Similarly, simultaneous measurements of $O_3$ and precursors were made over the Bay of Bengal
21  during the post-summer monsoon season in October-November 2010. These measurements
22  revealed large variability in $O_3$ (11 to 60 ppb) with maximum values found in the northern Bay
23  of Bengal. Back trajectory analysis showed a similar conclusion to the above mentioned ICARB
24  study, with the influence of pollution plumes from the India-Bangladesh region and Southeast
25  Asia, and the influence of long-range transport of pristine marine air from the Indian Ocean
26  (Mallik et al., 2013).

27  During the summer monsoon period, ozone measurements in the Arabian Sea close to the
28  Arabian Peninsula are available from the AQABA ship campaign in 2017. Consistent with the
29  low pollution levels detected in this region, ozone mixing ratios were relatively low (22.5 ppb)
30  representing remote MBL conditions (Tadic et al., 2019). Net ozone production rates did not
31  significantly deviate from zero and indicate weak net ozone production of 5 ppb day$^{-1}$. In
32  contrast, measurements during the rest of the campaign in the Red Sea, Oman Gulf and Arabian
33  Gulf revealed strongly enhanced tropospheric ozone with larger ozone production rates of up
34  to 28 ppb day$^{-1}$. The sensitivity of ozone production to the prevailing conditions was assessed

Atmospheric
Chemistry
and Physics
Discussions

Open Access

EGU

1  by defining ozone production regimes in terms of the OH reactivities of VOCs and $NO_x$. Based
2  on this analysis, the relatively clean air of the Arabian Sea was found to be due to partially $NO_x$-
3  limited ozone production in this region (Pfannerstill et al., 2019).

4  In addition to the studies focusing on the Bay of Bengal and the Arabian Sea, observations of
5  $O_3$ were made along two ship tracks from the east and west of the Indian subcontinent and
6  heading towards the open oceans during December-March as a part of the ISOE 8 and IIOE-2
7  in 2014 and 2015. The ISOE 8 campaign started from Chennai on the east coast and headed
8  towards the Southern Ocean, while IIOE-2 started in Goa and went across the Arabian sea and
9  the north equatorial Indian Ocean towards Mauritius. Both of these campaigns show a strong
10 reduction in the ozone concentrations from ~50 ppb to ~5-10 ppb within a few degrees off the
11 Indian coast (Mahajan et al. 2019a; 2019b), demonstrating that continental emissions are the
12 main drivers behind the high ozone concentrations close to the Indian subcontinent.

13 **Table 4**. $O_3$ mean values [ppb] and latitudinal gradients reported for various campaigns in the Bay of
14 Bengal, Arabian Sea and Indian Ocean. Ozone maximum values are given in the marine boundary layer
15 (MBL) and in the elevated layer (EL), as available.

| Season | Year and campaign | Region | $O_3$ [ppb] | $O_3$ maxima [ppb] | Latitudinal $O_3$ gradient [ppb/°] | Reference |
|---|---|---|---|---|---|---|
| Winter monsoon | 1999 INDOEX | Indian Ocean Arabian Sea 15°S–20°N | 21.5 ± 3.5 43.9 ± 7.9 | 80 − 100 (EL) | 1.5 − 2 | Lelieveld et al. (2001) Lal et al. (2006) |
| | 2001 BOBEX I | Bay of Bengal 13°N–20°N | 42 ± 12 | 64 (MBL) | 1.5 | Lal et al. (2006) |
| | 2008/2009 ICARB | Bay of Bengal 8°N–21°N | 48 ± 8 | 65 (MBL) | 2.1 | David et al. (2011) |
| | 2003 BOBEX I | Bay of Bengal 4°N–19°N | 34 ± 6 | 50 (MBL) | 1.4 | Lal et al. (2007) |
| | 2014 ISOE-8 | Bay of Bengal Indian Ocean 11.5°N–55°S | range: 5 − 53 | 53 (MBL) | | Mahajan et al. (2019b) |
| | 2015 IIOE-2 | Arabian Sea Indian Ocean 11.5°N–20°S | range: 10 − 52 | 52 (MBL) | | Mahajan et al. (2019a) |
| | | Bay of Bengal 6°N–21°N | 18 | 30 (MBL) | 1.3 ± 0.1 | Nair et al. (2011) |
| | 2006 | Bay of Bengal 6°N–21°N | 28.3 ± 14.4 | 55 (MBL) 80 (EL) | 5.4 ± 0.9 (>12°N) | Srivastava et al. (2012a) |

| Post-winter monsoon | ICARB | Arabian Sea 9°N–22°N | 19.8 ± 4.1 | 26 (MBL) 60 (EL) | -0.4 ± 0.2 | Srivastava et al. (2012a) |
|---|---|---|---|---|---|---|
| Summer and post-summer monsoon | 2002 BOBPS | Bay of Bengal 7°N–20°N | 27 ± 6 | 43 (MBL) | 1.3 | Sahu et al. (2006) |
| Summer monsoon | 2017 AQABA | Arabian Sea 12°N–23°N | 22.5 | 35 (MBL) | | Tadic et al., 2019 |
| Post-summer monsoon | 2010 | Bay of Bengal 8°N–18°N | 41 ± 9 | 60 | 3.95 | Mallik et al. (2013) |

1

2    Available ozone measurements from campaigns conducted in the Bay of Bengal, Arabian Sea
3    and Indian Ocean over the last decades have been summarized in Table 4. The measurements
4    reveal some clear spatial and seasonal patterns with highest ozone mixing ratios during the
5    winter monsoon, in particular in the Bay of Bengal and Arabian Sea. On average, ozone
6    abundances decrease during the post-winter transition period and increase again after the
7    summer monsoon. Nearly all campaigns detected highest ozone values close to the northern
8    continental landmasses, reflecting direct impact of air masses originating from different
9    pollution source regions in South Asia and the Indo-Gangetic Plain. However, the situation can
10    also be reversed, with higher levels of ozone observed over the central Bay of Bengal, not near
11    the coastal regions (Lal et al., 2006), due to different types of wind patterns and possible
12    titration by fresh emissions of NO. Sharp latitudinal gradients ranging from 1.3 to 5.4 ppb $O_3$/°
13    with increasing ozone towards northern landmasses were identified during all campaigns except
14    for ICARB measurements in the Arabian Sea during the post-winter transition period. The
15    strength of the gradients depends on the season, with sharper gradients during the winter and
16    sometimes transition periods, and on the latitudinal extent, with sharper gradients closer to the
17    coastlines. Air-sea breeze triggered transport of polluted air masses in the elevated layer can
18    lead to substantially higher ozone values above the MBL, as demonstrated during the
19    campaigns where ozonesonde measurements were available. Direct comparisons of ozone
20    values in the Bay of Bengal and the Arabian Sea are in most cases not possible, except for the
21    ICARB post winter campaign during which ozone peaked in the Bay of Bengal.

22    **5.2 Greenhouse gases**

23    Greenhouse gases are largely emitted from anthropogenic activities over the continents, as are
24    most of the atmospheric pollutants discussed above (Section 4). Therefore, both greenhouse
25    gases and pollution show a similar spatial distribution with higher values towards the coast and
26    lower values over the open ocean. However, greenhouse gases have in general longer lifetimes
27    resulting in overall smaller spatial gradients. In addition, they often have large sources from the
28    terrestrial biosphere of the NH midlatitudes, which can impact their seasonal cycle over coastal
29    and open ocean regions. In the following section, we discuss the distribution and variability of
30    the greenhouse gases $CH_4$, $N_2O$, $CO_2$ and COS.
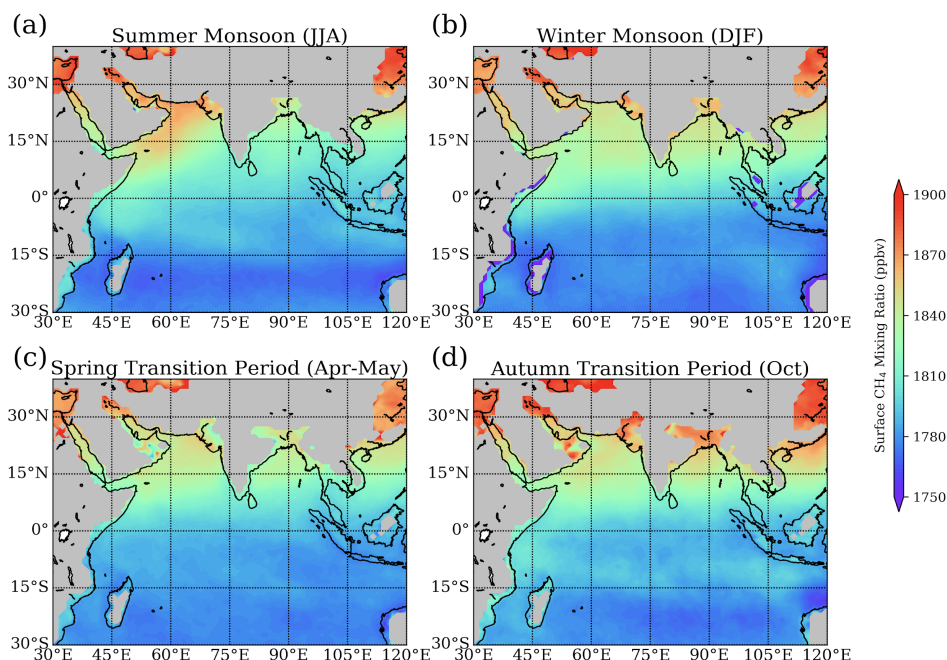
31    **Methane ($CH_4$)**

1    The three-dimensional distribution of $CH_4$ over the Arabian Sea, Bay of Bengal and Indian
2    Ocean can be investigated based on AIRS satellite measurements (Fig. 15; Kavitha and Nair,
3    2019). In the boundary layer, $CH_4$ is higher towards the coast and lower over the open ocean
4    due to the proximity of the source rich land regions. In particular, the fossil fuel mining areas
5    in the Arab region are believed to contribute to enhanced $CH_4$ over the northern Arabian Sea
6    (Kavitha and Nair, 2019). In-situ observations revealed near-surface $CH_4$ mixing ratios of 1830
7    ± 140 ppb over the northern Bay of Bengal during summer monsoon months in 2009 (Girach
8    et al., 2017) in agreement with the satellite observations (Fig. 15a). Back trajectory simulations
9    linked the enhanced values over the Bay of Bengal to emissions from central and northern India.
10   Overall, latitudinal $CH_4$ variations between 20°N and 30°S of up to 6% are much smaller than
11   latitudinal variations of CO over the same region of up to 150%.

12   Maximum $CH_4$ mixing ratios of around 1870 ppb are found over the northern and western
13   Arabian Sea during the summer monsoon (Fig. 15a) together with the strongest latitudinal
14   gradients. Mixing ratios over this region are weaker during the rest of the year resulting in a
15   seasonal cycle quite different to the one observed over other parts of the Indian Ocean. The
16   elevated mixing ratios over the northern Arabian Sea during the summer monsoon are
17   somewhat surprising given that during this time of year south-westerlies bring pristine oceanic
18   air masses and transport from land regions is limited. One possible explanation of this feature
19   could be elevated oceanic $CH_4$ emissions from the coastal upwelling. Such upwelling centres
20   are found along the coast of the Arabian Peninsula and Somalia during the summer monsoon
21   (Section 2.2) and can trigger significant $CH_4$ release to the atmosphere (Section 4.2; Bange et
22   al., 1998).

23   $CH_4$ over the eastern Arabian Sea and Bay of Bengal shows a different seasonal cycle, with
24   surface values peaking during the post-summer and winter monsoon seasons. During the post-
25   summer season, $CH_4$ production from Asian rice cultivation maximises as the plants are fully
26   grown (Section 4.2). At the same time, the onset of the winter regime starts to allow for air
27   mass transport from continental regions with significant anthropogenic influence. During the
28   winter monsoon, these transport patterns intensify bringing air masses with elevated $CH_4$ over
29   the Indian Ocean.

30   The overall spatial distribution does not change much with height and at all altitudes between
31   850 hPa - 200 hPa highest $CH_4$ values are found over the northern Arabian Sea and northern
32   Bay of Bengal (Kavitha and Nair, 2019). However, the distinct seasonal cycle observed over
33   the northern and western Arabian Sea changes with height to maximum mixing ratios during
34   the post-monsoon season, further supporting the hypothesis that oceanic sources cause the
35   surface $CH_4$ maxima during the summer. The monthly variation of $CH_4$ mixing ratio over all
36   other oceanic regions remains more or less similar at all altitudes with a peak during the post-
37   monsoon season.

Atmospheric
Chemistry
and Physics
Discussions



**Figure 15.** Surface methane ($CH_4$) mixing ratios from AIRS for (a) summer monsoon 2011 - 2015 (June - August), (b) winter monsoon 2011/2012 - 2015/2016 (December - February), (c) spring transition 2011 - 2015 (April - May) and (d) autumn transition 2011 - 2015 (October) periods.

Over the equatorial Indian Ocean, $CH_4$ values are relatively low during all seasons with values mostly below 1800 ppb (Fig. 15). The OMO campaign in July/August 2015 confirmed the low $CH_4$ values detected by the satellite. Observations over Gan (Maldives) show average $CH_4$ mixing ratios of 1778.3±19.5 ppb during the monsoon period being significantly lower than in the NH background or the Asian monsoon profiles (Tomsche et al., 2019). $CH_4$ mixing ratios increase with height due to inter-hemispheric transport mixing NH air masses into the SH at higher altitudes. As the NH air masses have experienced convective uplift from the boundary layer, they advect higher $CH_4$ mixing ratios into the SH (Bergamaschi et al., 2013).

The SH Indian Ocean has been found to be much less impacted by the winter monsoon compared to the NH Indian Ocean due to the ITCZ functioning as a transport barrier. In situ measurements from Reunion Island around 19°S, suggest the opposite seasonal cycle with lowest $CH_4$ values in December–February and highest $CH_4$ values in August–September (Zhou et al., 2018). Here, the $CH_4$ variability is not dominated by nearby land sources, but rather seasonal variations of OH radicals drive the seasonal cycle of $CH_4$.

**Nitrous oxide ($N_2O$)**
Measurements of $N_2O$ over the Indian Ocean are sparse. The distribution of $N_2O$ derived during a ship campaign in the Arabian Sea, equatorial Indian Ocean and southwest part of the Bay of Bengal during the post-summer monsoon period (October–November 2004) reveals clear latitudinal gradients (Mandal et al., 2006). Near the coast, $N_2O$ values of 312 ppb were found and they increased towards the open ocean, with a maximum of 432 ppb at the equator. In the equatorial SH, $N_2O$ decreased sharply to 312 ppb and did not change substantially during the

1   rest of the cruise along the equator and in the southwest part of the Bay of Bengal. Given the
2   sparse data it is difficult to determine if the peak values around the equator are caused by local
3   oceanic emissions or are related to long-range transport from other sources.

4   **Carbon dioxide ($CO_2$)**
5   $CO_2$ satellite-based observations over the Indian Ocean reveal strong seasonal and latitudinal
6   gradients (Nalini et al., 2018; Nayak et al., 2011). During most seasons, larger $CO_2$ values over
7   the south and south-east Asian land masses are accompanied by pronounced latitudinal
8   gradients over the coastal regions and lower $CO_2$ values over the ocean. This distribution has
9   been confirmed by ship-based observations during the summer monsoon season (Kumar et al.,
10  2014) and during the post-summer monsoon season (Mandal et al., 2006). The measurements
11  showed elevated $CO_2$ with large variability near the coastal region and relatively low $CO_2$ with
12  correspondingly lower variability over the open ocean.

13  $CO_2$ over the Bay of Bengal and Arabian Sea is characterized by a pronounced seasonal cycle,
14  with highest values in boreal spring and lowest values in autumn (Nalini et al., 2018). Satellite
15  observations show that during winter, a band of relatively low $CO_2$ mixing ratios (376-378
16  ppm) extends over the northern Indian Ocean between 0°-25°N in the west-east direction, where
17  the smallest values exist over the western Arabian Sea (Nayak et al., 2011). During boreal
18  spring, the $CO_2$ in this region increases, in particular over the Bay of Bengal. Seasonality over
19  the southern Indian Ocean shows a different pattern. Similarly, to the northern part, a belt of
20  low $CO_2$ is found during boreal winter between 10°S and 25°S. During boreal spring, however,
21  this band of relatively low $CO_2$ values remains prominent (Nayak et al., 2011), highlighting the
22  potential role of this region as an oceanic $CO_2$ sink (Section 4.2).

23  Lagrangian transport simulations, carried out to analyse the seasonal cycle at two Indian coastal
24  stations, suggest that the seasonality of the $CO_2$ distribution over the Indian Ocean is driven by
25  atmospheric circulation changes combined with the seasonal cycle of $CO_2$ over land regions
26  (Nalini et al., 2018). While dominant marine contributions during the summer monsoon result
27  in slowly decaying values, the winter and spring monsoon season is characterized by sources
28  from the eastern continental land masses, leading to maximum values over the coastal stations
29  during spring. The equatorial Indian Ocean, on the other hand, shows only a weak seasonal
30  cycle when compared to Indian coastal locations, the Bay of Bengal and the Arabian Sea. Here,
31  contributions from oceanic regions dominate during all seasons with smaller continental
32  contributions during the winter period. Overall, the anthropogenic emissions over the
33  continental land masses appear not to be a large source for $CO_2$ in the open Indian Ocean
34  environment.

35  **Carbonyl sulfide (COS)**
36  There are only three published datasets of ship or land-based observations of COS mixing ratios
37  over the Indian Ocean. The measurements were made over the course of a year at Amsterdam
38  Island (Mihalopoulos et al., 1991), on a research cruise in the eastern and southern Indian Ocean
39  in November (Inomata et al., 2006), and on the OASIS research cruise in the western tropical
40  Indian Ocean in July (Lennartz et al., 2017, see section 3). All measured COS values are either
41  at or below the global mean COS atmospheric mixing ratio of ~549 ppt and exhibit no clear
42  seasonal or latitudinal pattern (Lennartz et al., 2020). Satellite measurements and inverse
43  modelling studies show elevated values of the atmospheric COS mixing ratio over the Indian
44  Ocean, but the values are not as high as those over the Pacific Ocean and Maritime Continent
45  at similar latitudes (Glatthor et al., 2015; Kuai et al., 2015). The elevated values have led to the
46  hypothesis that the northern Indian Ocean is one of the missing source regions (Kuai et al.,
47  2015). Given the lack of compelling evidence from surface ocean measurements, however, it

Atmospheric
Chemistry
and Physics
Discussions
Open Access
EGU

1  does not appear that the Indian Ocean is the location of the missing source. Instead,
2  anthropogenic sources around Southeast Asia could be responsible, as discussed in section 4.
3
4  **5.3 Short-lived gases DMS, isoprene and halogens**

5  **DMS and isoprene**
6  DMS in the Arabian Sea is projected to act as a relatively large oceanic source of sulfur to the
7  atmosphere during the Asian summer monsoon season (Lana et al., 2011). These high emissions
8  have been confirmed by recent ship-based measurements during the AQABA campaign,
9  identifying elevated DMS values in the atmosphere ranging from 100 to 500 ppt (Edtbauer et
10  al., 2020). Given the low atmospheric background pollution and the elevated DMS mixing
11  ratios, the latter was found among the ten most important OH sinks with a reactivity of 0.02 s[1]
12  (Pfannerstill et al., 2019). During the OASIS campaign, similar atmospheric mixing ratios of
13  approximately 20-300 ppt were measured over the western tropical Indian Ocean. The
14  atmospheric distribution patterns in time and space during OASIS generally matched measured
15  fluxes (Zavarsky et al., 2018b). During this study, the directly measured DMS fluxes, as well
16  as calculated isoprene fluxes and sea spray fluxes, were correlated with satellite-derived aerosol
17  products over the region. Many of the correlations, which took into account the influence of
18  regional transport as computed FLEXPART trajectories, were statistically significant. The
19  aerosol product distribution more closely resembled the trace gas fluxes than the sea spray flux
20  distributions. Thus, sea spray appears to be more of a minor precursor than the trace gases. This
21  is supported by Quinn et al. (2017) who found a 30% contribution of sea spray to cloud
22  condensation nuclei in the tropics. These results illustrate the importance of the regional
23  coupling between marine-derived gaseous precursors and aerosol products in the remote MBL,
24  which can give rise to local feedback processes (Zavarsky et al., 2018b).

25  The longest continuous observations of atmospheric DMS in the Indian Ocean were obtained
26  at the Amsterdam Islands (37.8°S, 77.5°E) in the southern Indian Ocean (Scaire et al., 2000).
27  Measurements from 1990 to 1999 revealed atmospheric DMS ranging from 5 to 1900 ppt with
28  a clear seasonal cycle. Maximum DMS values in January were on average 20 times higher than
29  minimum values in July-August. These strong seasonal variations are not caused by
30  atmospheric transport patterns but are linked to a similar cycle in DMS concentration in
31  seawater induced by enhanced phytoplanktonic activity during the boreal summer. Model runs
32  using the Lana et al. (2011) climatology show a good match with these observations confirming
33  the dominant impact of oceanic processes on atmospheric DMS concentrations over the open
34  Indian Ocean (Mahajan et al., 2015b).

35  Atmospheric mixing ratios of isoprene were also measured during the OASIS campaign. The
36  mean measured mixing ratio was $2.5 \pm 1.5$ ppt (Booge et al., 2016), which is in agreement with
37  atmospheric measurements in other remote open ocean regions (Shaw et al., 2003). Booge et
38  al. (2016) used a top-down approach to calculate isoprene emissions in order to compare with
39  the bottom-up flux estimates using a box model, in which the only source of isoprene for the
40  air was assumed to be the sea-to-air flux (emission), the atmospheric lifetime was assumed to
41  be determined by reaction with OH (chemical loss, 1 h) and assuming air values to be zero at
42  the start. Computed atmospheric mixing ratios were 45 times lower than measured. In order to
43  calculate values consistent with measured mixing ratios, isoprene emissions must be more than
44  one order of magnitude greater than those computed using the bottom-up estimate based on
45  measured oceanic isoprene levels (section 4). This result agrees with isoprene emissions
46  computed with a numerical model by Luo and Yu (2010). One possible explanation could be
47  that production in the surface microlayer (SML) is not taken into account with the bottom-up
48  approach. Ciuraru et al. (2015) showed that isoprene can be produced photochemically by
49  surfactants in an organic monolayer directly at the air–sea interface. SML surfactant enrichment

1   has been observed (Wurl et al., 2011), which could result in about two orders of magnitude
2   larger isoprene fluxes than the highest fluxes calculated during the OASIS campaign. Further
3   field measurements targeting isoprene production in the SML could be a step forward in
4   reconciling the ocean source of isoprene to the atmosphere.

5   **Halogens**
6   The Indian Ocean is an important source region for halogenated VSLS such as $CHBr_3$, $CH_2Br_2$
7   and $CH_3I$. During the OASIS ship campaign in summer 2014 in the west Indian Ocean, high
8   VSLS emissions with pronounced hotspots were detected (Fiehn et al., 2017). The prevailing
9   atmospheric mixing ratios, however, were generally low. The atmospheric mixing ratios of
10   $CHBr_3$ showed an overall mean of 1-1.5 ppt. Elevated mixing ratios larger than 1.5 ppt were
11   found in the equatorial region coinciding with lower wind speeds and maximum values larger
12   than 2 ppt were detected close to islands, where coastal sources appear to influence the
13   atmosphere. Atmospheric mixing ratios of $CH_2Br_2$ varied little around the mean value of 0.9
14   ppt and showed a similar pattern to the $CHBr_3$ mixing ratios. The $CH_3I$ mixing ratios showed
15   relatively large variations with a mean of 0.8 ppt (Fiehn et al., 2017).

16   Reactive halogen species, such as iodine oxide (IO) and bromine oxide (BrO), that result from
17   VSLS and other sources (Section 4.3), were found to be below the detection limit or very low
18   over the Indian Ocean. In December 2000, measurements in the southern Indian Ocean were
19   carried out as preparative study for an intensive field campaign within the ELCID4 project with
20   ship track between Reunion Islands, Amsterdam Islands, Corzet Islands and Kerguelen Islands.
21   IO and BrO were both below the detection limit of the instrument, and hence upper limits of 4
22   ppt were reported for both species in the Indian Ocean (Hönninger, 2002). A field campaign in
23   the Maldives also reported upper limits for the BrO vertical columns ($3 \times 10^{14}$ molecules $cm^{-2}$)
24   (Ladstätter-Weißenmayer et al., 2007). Observations on the ISOE and IIOE-2 cruises
25   reconfirmed that BrO was below the detection limit, with a lower upper limit of 2 ppt on cruises
26   starting from both the east and west of the Indian subcontinent (unpublished data). However,
27   ship-based observations have confirmed the presence of iodine oxide in the marine atmosphere,
28   although at low levels (<1 ppt). At these levels, the effect of halogen chemistry on ozone
29   destruction in the Indian Ocean MBL is significantly smaller than the Atlantic MBL, where
30   reactive halogen species can result in as much as 45% of the total ozone loss (Read et al., 2008).
31   Additionally, the outflow of $NO_x$ from the Indian sub-continent can titrate iodine chemistry
32   through the formation of $IONO_2$, which further reduces the impact of iodine on atmospheric
33   chemistry (Mahajan et al., 2019a, 2019b). Another land-based campaign observed between 2.4-
34   3.1 ppt of IO at the Maldives (Oetjen, 2009). These results suggest that, although the reactive
35   species are low, they could contribute to local oxidative chemistry, considering that they are
36   higher than levels observed in the Atlantic MBL where they contribute towards significant
37   surface ozone loss (Mahajan et al., 2010).
38

39   **6 Synthesis and discussion**

40   Over the last decade, new knowledge of the atmospheric composition and related processes
41   over the Indian Ocean has been derived from intensive ship and aircraft campaigns, coastal
42   station measurements and satellite data. Here, we discuss how our understanding of the
43   atmospheric composition improved since 2010 and present new insights into long-term changes
44   and their impact on other Earth system components such as ocean biogeochemistry.

45   In Section 6.1, we provide a synthesis of the scientific progress made after 2010 taking into
46   account measurement data, updated emission inventories and insights from modelling studies
47   presented in Sections 3, 4 and 5. In section 6.2, we discuss how long-term changes of
48   atmospheric dynamics, oceanic processes and anthropogenic emissions impact the atmospheric

1    composition over the Indian Ocean. We highlight trends of air pollutants such as CO and $NO_2$
2    as well as greenhouse gases such as $CH_4$ estimated from satellite measurements. Quantifying
3    long-term changes of ozone or short-lived marine traces gases, however, is an ongoing
4    challenge given their high variability and the scarcity of long-term measurement stations, so
5    that currently reliable trend estimates are not available.

6    The changing atmospheric composition over the Indian Ocean influences radiative forcing, air
7    quality and weather on a regional scale and plays a role for remote regions like the stratosphere
8    via convective transport pathways (section 6.3). It can also interact with the ocean by impacting
9    biogeochemical cycles and marine ecosystems which can, in turn, feedback on the overlying
10   atmosphere. However, as discussed in section 6.4, the impacts of atmospheric pollution and
11   dust on the Indian Ocean's biogeochemistry, as well potential climate feedbacks, are severely
12   understudied.

13

14   **6.1 Synthesis of scientific progress after 2010**

15   **Pollution and $O_3$**

16   Over the last decade, campaign and station measurements in the Bay of Bengal, Arabian Sea
17   and Indian Ocean have revealed new findings of the detailed distribution of pollution and ozone
18   with some clear spatial and seasonal patterns. Particular progress has been made in the Bay of
19   Bengal, where strongly elevated pollution and ozone abundances in the head and the south-
20   eastern part were detected during winter and attributed to advection from the Indo-Gangetic
21   Plain and continental outflow from Southeast Asia, respectively. Post-winter observations show
22   similar maxima in the head, but significantly lower values in middle and southern Bay of
23   Bengal due to open ocean influence. A completely different picture was found over the Arabian
24   sea, where during post-winter monsoon clean marine air results in significantly lower pollution
25   when compared to the northern Bay of Bengal. For the post-summer season, new findings
26   revealed a particularly large spatial heterogeneity of pollution and ozone. Enhanced NOx in
27   Indian Ocean air masses in contrast to the typical latitudinal gradients was suggested to be
28   linked to emissions from international shipping lanes. During the summer monsoon period, zero
29   net ozone production was found in the Arabian Sea connected to low pollution levels.

30   Recent scientific progress has also been made in better understanding the large-scale
31   distribution of pollution and assessing long-term changes. Comparisons of current observations
32   and previous data obtained two decades earlier have demonstrated the growing influence of
33   anthropogenic SO2 on the marine atmosphere over the Indian Ocean and Arabian Sea. This
34   pronounced increase has occurred despite the decreasing $SO_2$ emissions in East Asia and is
35   most likely related to rapidly increasing emissions in South Asia. Recent studies have also
36   revealed how far the impact of anthropogenic pollution can extend over the Indian Ocean.
37   Remote locations such as the island of Mahé just south of the equator show CO maxima during
38   winter that result from the long-range transport of anthropogenic emissions from India.
39   Pollution levels further south, on the other hand, such as over Reunion Island are driven by the
40   emissions from biomass burning in Africa and South America. In the case of $NH_3$, trends have
41   yet to be identified due to the lack of continuous observations, with just a few campaigns
42   showing the difference between the coastal and open ocean environments.

43   As discussed above, scientific studies conducted over the last 10 years have added many details
44   to our picture of the spatial distribution and sharp latitudinal gradients in pollution and,
45   particularly, in ozone. However, our understanding of seasonal, vertical and long-term changes
46   in ozone is still limited. A coastal ozone profile data set has revealed that the seasonal cycle of

Atmospheric
Chemistry
and Physics
Discussions
Open Access
EGU

1 ozone changes with altitude with surface maxima during September and mid-tropospheric
2 maxima during April–June, prompting the need for further continuous measurement stations at
3 different locations.

4 **Greenhouse gases**

5 By using the most recent EDGAR emissions database, we observe steady increases in emissions
6 over the last decade for $CH_4$, $N_2O$, and $CO_2$ in the regions surrounding the Indian Ocean. This
7 is true not only for southern Asia, but also for East Asia, the Middle East, and East Africa, with
8 East Asia often being the largest emitter. This is especially significant for $CO_2$ emissions from
9 China despite the promises of the Paris Climate Accord. An important recent finding is that
10 especially high, and increasing, $CH_4$ emissions are observed from east African wetlands. As
11 these land-based emissions influence the atmosphere over the Indian Ocean, especially during
12 the winter monsoon season, it is necessary to periodically assess current levels and updated
13 long-term trends.

14 Another major advance in this review compared to previous work has been the explicit
15 inclusion of ocean sources and sinks of greenhouse gases in the region. The ocean is an
16 important source/sink, especially for N2O (source), CO2 (sink), and OCS (source), and its role
17 in regulating atmospheric budgets must be understood. Although CH4 emissions from the ocean
18 are low compared to other sources, a recent remote sensing study reveals elevated mixing ratios
19 over the northern Arabian Sea during the summer monsoon that are somewhat unexpected and
20 may be due to elevated oceanic $CH_4$ emissions from coastal upwelling. In addition, the distinct
21 seasonal cycle over the northern and western Arabian Sea changes with altitude showing
22 maximum mixing ratios during the post-monsoon season, which supports the idea that surface
23 $CH_4$ maxima during the summer are due to oceanic sources. We also report a drastic decrease
24 in oceanic $CO_2$ observations over the last decades that must be rectified. Nonetheless, we report
25 an important finding that the CO2 sink in the southern Indian Ocean appears to be weakening,
26 as observed by comparing data from campaigns that did occur from 1999-2000 to those from
27 2004-2005. This has been supported by a recent modelling study. Please note that all
28 information presented here for $N_2O$ and OCS is primarily new, as it was either not included in
29 Lawrence and Leliveld (2010) at all or only very sparsely.

30 Recent important progress has been made in understanding the interplay of greenhouse gases
31 and aerosols in driving physical trends in the region. As of the publishing of Lawrence and
32 Leliveld (2010) it was thought that the suppression of summer precipitation may be a combined
33 consequence of aerosols and greenhouse gases, but the use of modeling tools to understand
34 anthropogenic drivers of trends in the monsoon and extreme weather was just beginning. We
35 now report that many studies have taken place since, focusing on monsoon rainfall trends,
36 extreme weather and forcing mechanisms. It is clear that the Indian Ocean continues to warm
37 due to greenhouse warming and this has serious consequences for both the monsoon and
38 extreme weather. This warming has been shown to be dampened by anthropogenic aerosols.
39 The recent hiatus period at the beginning of the 21st century highlighted the importance of the
40 Indian Ocean for the global heat budget. The warming is expected to increase throughout the
41 21st century in response to continuing greenhouse gas emissions, with the strongest warming
42 in the Arabian Sea and western equatorial Indian Ocean consistently projected in CMIP models.

43

44 **Short-lived gases DMS, isoprene and halogens**

45 Before 2010, short lived trace gases such as DMS, isoprene and halogens were some of the least
46 sampled compounds in the Indian Ocean. This review shows that over the last 10 years
47 significant improvements have been made in order to address the lack of data through multiple
48 campaigns by groups from all over the world. For DMS, the number of datapoints available in

Atmospheric
Chemistry
and Physics
Discussions

1    the Indian Ocean in 2010 was 1313, since when the latest available dataset shows an increase
2    of ~40%. A similar increase is also observed in the Indian sector of the Southern Ocean, where
3    new campaigns have resulted in an increase of ~32% (NOAA-PMEL, 2020). These
4    observations are critical in improving the DMS emission estimates in the Indian Ocean region,
5    which were a major uncertainty in the currently available emission climatology (Lana et al.,
6    2011). Unfortunately, these observations are still not enough to identify a trend in DMS,
7    although new proxy-based estimations suggest an increase in oceanic DMS concentrations in
8    the global oceans, including the Indian Ocean (Galí et al., 2018).

9    In case of isoprene, there was also a lack of observations in the Indian Ocean until 2010, with
10   just a few campaigns reporting data. The OASIS campaign in 2014 (Booge et al., 2016, 2018)
11   along with other campaigns in the northern Indian Ocean and the Indian sector of the Southern
12   Ocean (Tripathi et al., 2020; Rodríguez-Ros et al., 2020) have increased our understanding of
13   isoprene emissions, highlighting important aspects such as the Arabian Sea isoprene emissions
14   peak in the oxygen minimum zone. An important correlation that has been reported over the
15   last few years is that the fluxes of DMS and isoprene show a significant positive correlation
16   with aerosol, suggesting a regional influence of marine emissions (Zavarsky et al., 2018b).

17   For the reactive halogen species, there has been a drastic improvement in the available dataset
18   in the Indian Ocean, with only one study showing the presence of reactive halogens in the Indian
19   Ocean pre-2010. New observations since 2014 have confirmed the ubiquitous presence of
20   reactive iodine and bromine species in the Indian Ocean, which interact with air pollutants from
21   the Indian subcontinent and need to be considered for regional air quality modelling. Iodine
22   chemistry by itself can be responsible for as much as 25% ozone destruction in the northern
23   Indian Ocean marine boundary layer. Thus, observations over the last 10 years have not only
24   increased the data available for the short-lived species, but also increased our understanding on
25   the importance of these species on the regional atmosphere.

26

27   **6.2   Long-term changes**

28   The growth of traffic and industries can be expected to lead directly to increasing air pollution,
29   which can be detected by analysing variations of the mean total columnar amount of
30   tropospheric trace gases. Srivastava et al. (2012a), using monthly mean CO at 900 mb obtained
31   from MOPITT, have observed lower offshore pollution during the transition periods than
32   expected through modelling studies using the MOZART model. They suggest that temporal
33   dilution of pollutants is the main reason for this mismatch. A study focusing on regions further
34   south in the Indian Ocean indicates that CO was decreasing (1.8% per year over Madagascar
35   and 1.7% per year over Reunion Island) over the years 2005 to 2009. The main drivers behind
36   this decrease were identified as the La Niña between 2006 and 2008 and the reduction in
37   biomass burning emissions in southern Africa (Toihir et al., 2015). However, as demonstrated
38   in section 4, CO emissions in most regions surrounding the Indian Ocean have increased, which
39   highlights the importance of dynamics for trace gas variability. In particular, CO emissions
40   along the Mekong River, north of the Persian Gulf, in Afghanistan and East Africa have shown
41   pronounced growth rates. Future studies of the CO trends over the Indian Ocean over longer
42   time periods are needed in order to understand how these changing emissions, together with
43   changing atmospheric dynamics, impact the CO concentrations in the marine atmosphere.

44   The variation of the mean total columnar amount of tropospheric $NO_2$ has been studied in detail
45   over the Indian subcontinent. Mahajan et al. (2015a) have reported an average increase of 2.20
46   $\pm$ 073 % $yr^{-1}$ using four different satellites across India. For OMI, this rate of increase from
47   2004-2013 was 2.79 $\pm$ 0.23 % $yr^{-1}$. This compares well to the rate of 2.9 $\pm$ 1.9 % $yr^{-1}$ reported
48   by Ghude et al. (2013), even though their study focused on urban locations. Studies focusing

1  on the atmosphere over the Indian Ocean are relatively scarce, but a study by Tournadre (2014)
2  reported a 50% increase along the Sri Lanka-Sumatra-China shipping lane. The OMI
3  tropospheric column data from 2003-2020 shows an increasing trend in the Arabian sea, close
4  to the Indian coast ($0.83 \pm 0.24$ % yr$^{-1}$; $t_B$=3.41), but along the eastern coast in the Bay of Bengal
5  the trend is not significant ($0.44 \pm 0.29$ % yr$^{-1}$; $t_B$=1.53). In the remote Indian ocean, OMI
6  observations show an increasing trend ranging between 0.76-1.87 % yr$^{-1}$, although the open
7  ocean trends might not be accurate considering the low columnar densities close to or below
8  the detection limit of the satellite instruments (unpublished data).

9  Based on OMI satellite data, a positive long-term trend in annual mean ozone over the Arabian
10 Sea and northern Bay of Bengal was detected for the ten-year period from 2000 to 2009 (David
11 and Nair, 2013). The southern Bay of Bengal is an exception to this and shows a negative long-
12 term change for annual mean ozone and the annual minimum with the latter representing
13 background conditions.

14 Long-term changes of $CH_4$ have been estimated from AIRS satellite measurements over the
15 2003-2015 time period (Kavitha and Nair, 2019). Over the Arabian Sea and Bay of Bengal, a
16 consistent positive trend ranging from 2 ppb year$^{-1}$ to 6 ppb year$^{-1}$ was found at all pressure
17 levels comparable to trends over Indian land regions. Interestingly, the trend was larger at
18 higher altitudes (<500 hPa) and maximized at the 300 hPa–150 hPa level. The authors attributed
19 the changes of the growth rate with altitude to increased convective activity uplifting $CH_4$,
20 leading to a smaller growth rate at the lower levels and higher growth at the upper levels.

21 Observations of reactive halogen species over the Indian Ocean do not display any significant
22 long-term trends, with BrO values below the stated upper limits of 2 ppt across observations
23 made over two decades. In the case of IO, annual observations since 2014 during the ISOE ship
24 campaigns have also not identified a significant difference, although the time period is less than
25 one decade and hence changes would not be expected beyond instrumental accuracy and natural
26 variation. Laboratory studies indicate a strong link between ozone concentrations in the MBL
27 and emissions of iodine species from the ocean surface (Carpenter et al., 2013, section 6.3).
28 Modelling studies suggest that ocean emissions of iodine species have increased on a global
29 scale over the last few decades driven by an increase in ozone concentrations due to
30 anthropogenic emissions (Saiz-Lopez et al., 2014, 2015). This increase has been observed
31 indirectly through an increase in the concentrations of iodine species in ice cores in the Alps
32 and in the Arctic (Cuevas et al., 2018; Legrand et al., 2018). However, in the absence of long-
33 term ozone observations or iodine fluxes in the Indian Ocean region, it is difficult to quantify
34 the change in iodine emissions.

35 The examples listed above make clear that not only the increasing anthropogenic emissions,
36 but also atmospheric dynamics and ocean-atmosphere interactions, are important for the long-
37 term changes of the atmospheric composition over the Indian Ocean. In particular changes of
38 transport patterns and convective uplifting can amplify or dampen the emission-driven changes
39 of greenhouse gases and pollution. Furthermore, modes of interannual variability such as IOD
40 or ENSO can mask long-term changes of atmospheric composition if the analysed period is
41 relatively short. Long-term changes of the frequency of such modes will likely also impact
42 long-term changes of the trace gas fields. In addition, physical, chemical and biological
43 processes in the Indian Ocean, as well as dynamically driven changes of the air-sea gas
44 exchange, can be expected to impact the long-term trends of atmospheric composition.

45  **6.3  Impact on the stratosphere**

46 Marine trace gases emitted from the Indian Ocean can be transported into the stratosphere via
47 convection directly above the Indian Ocean or via the summer monsoon convection and
48 anticyclone. Recent studies have highlighted the role of the Indian Ocean as a source region for

1  stratospheric VSLS entrainment and similar mechanisms could also apply to other marine traces
2  gases.

3  Based on the OASIS campaign data and atmospheric modelling, Fiehn et al. (2017) have shown
4  that, from the west Indian Ocean boundary layer, VSLS can be transported into the tropical
5  tropopause layer and eventually into the stratosphere. The importance of the Indian Ocean
6  sources for the stratospheric halogen budget depends on the regional strength of emissions and
7  the transit time in preferred transport regimes. On very short timescales, convection above the
8  Indian Ocean lifts oceanic trace gases towards the tropopause. On longer timescales, the
9  summer monsoon circulation transports the oceanic VSLS towards India and the Bay of Bengal.
10 From there the VSLS are lifted with the monsoon convection and reach stratospheric levels in
11 the south-eastern part of the Asian monsoon anticyclone, which is generally the preferred
12 transport regime during the boreal summer. The stratospheric bromine injection from the
13 tropical Indian Ocean and west Pacific depends critically on the seasonality and spatial
14 distribution of the VSLS emissions (Fiehn et al., 2018). The main oceanic source regions for
15 the stratosphere include the Arabian Sea and Bay of Bengal in boreal summer and the tropical
16 west Pacific Ocean in boreal winter. For the OASIS case study in the western tropical Indian
17 Ocean, the projected $CH_2Br_2$ entrainment was very high due to high surface emissions, while
18 the entrainment of $CHBr_3$ and $CH_3I$ was found to be relatively small compared to case studies
19 in the tropical west Pacific Ocean (Fiehn et al., 2017; Tegtmeier et al., 2012). Overall, the Indian
20 Ocean is a strong source of VSLS for the stratosphere and modelled $CHBr_3$ shows a global
21 maximum over India, the Bay of Bengal, and the Arabian Sea (Tegtmeier et al., 2020)

22 Besides contributing to stratospheric halocarbons, during the summer monsoon, the Indian
23 Ocean and surrounding areas are potentially important source regions for stratospheric
24 entrainment of other naturally produced gases such as $N_2O$ and COS (Ma et al., 2018; Lennartz
25 et al., 2017). The open Indian Ocean is in general a rather weak, but likely perennial and far-
26 reaching (in terms of atmospheric transport) source of several trace gases to the atmosphere.
27 However, it is unclear to what extent the atmospheric mixing ratios at a given location in the
28 north Indian Ocean might actually correspond to air masses transported from the southwest
29 Indian Ocean, where they have been enriched in oceanic trace gases (Ma et al., 2018). Such
30 knowledge is necessary for quantifying the total contribution of the Indian Ocean emissions to
31 the stratosphere and should be addressed in future studies. Potentially important feedback may
32 occur if, for example, more $N_2O$ is emitted to the atmosphere as a result of over fertilization
33 (see section 6.3) and subsequently makes its way to the stratosphere. As $N_2O$ contributes to
34 stratospheric ozone depletion, resulting radiation changes at the ocean surface could feed back
35 on biological and chemical processes.

36 **6.4   Impact on the ocean**

37 Changes of the atmospheric composition over the Indian Ocean, together with changing
38 transport patterns and river inputs, affect oceanic production and biogeochemical trace gas
39 cycling, which in turn feedback on the overlying atmosphere. Satellite-derived time-series
40 measurements indicate that the gaseous atmospheric pollution and annual aerosol load,
41 including ship emissions, are increasing over the northern Indian Ocean and especially over the
42 Bay of Bengal (Hsu et al., 2012, Tournadre, 2014). River inputs lead to low salinities in the
43 surface mixed layer, resulting in strong stratification that dampens coastal upwelling and traps
44 nutrients in the subsurface (Prasanna Kumar et al., 2002, Rixen et al., 2006). Another concern
45 is how potentially changing monsoon intensity will affect air mass trajectories (Goes et al.,
46 2005), which influence deposition to the sea surface over the Indian Ocean.

47 While it is clear that the changing atmosphere and river input lead to an additional supply of
48 nutrients, trace metals, and potentially toxic substances, it is not known how this additional

Atmospheric
Chemistry
and Physics
Discussions
Open Access
EGU

1  supply will impact ocean biogeochemistry and in particular the OMZs. The impact of
2  atmospheric deposition on biota has been reported for many different types of oceanic areas
3  (Guieu et al., 2014). In both field and laboratory experiments, it has been shown that the
4  deposited material can have both favourable (nutrifying, e.g., Rahav et al., 2018) and non-
5  favourable effects (toxic, e.g., Paytan et al., 2009, Jordi et al., 2012, Wang et al., 2015) on
6  biological processes. Further, it has been shown that mixing natural and anthropogenic sources
7  of gases and aerosols may alter the properties and subsequent functionality of deposited
8  materials (increased bioavailability, e.g., Herut et al., 2016, Krom et al., 2016, Jickells et al.,
9  2017, Mahowald et al., 2018). There is evidence that atmospheric deposition alters the DOM
10  concentrations and characteristics in the surface ocean, with differing effects from natural vs.
11  anthropogenic or mixed sources (Sánchez-Pérez et al., 2016). The impacts of atmospheric
12  deposition include changing biomass standing stocks, primary and bacterial production, and $N_2$
13  fixation. However, predicting the impacts of atmospheric deposition to marine ecosystems is
14  restricted by limited knowledge of the specific sources, constituents, and transport pathways of
15  the atmospheric material delivered to oceanic regions, as well as the effect of steady vs. episodic
16  deposition. Any changes to biological processes have the potential to alter trace gas cycling in
17  the surface ocean. For example, when species such as *Trichodesmium* (e.g., Guieu et al., 2019)
18  or *Emiliania huxleyi* (coccolithophorid, e.g. Guerreiro et al., 2017) are affected, isoprene and
19  DMS, respectively, can be impacted. In addition, biogeochemical changes due to atmospheric
20  deposition in the SML could be important for trace gas cycling and air-sea exchange, for
21  example through reactions with deposited ozone (Zhou et al. 2014, Chiu et al. 2017, Mungall
22  et al. 2017, see below) or changes to the heterotrophic community (Astrahan et al. 2016).

23  To date, evidence of the influence of anthropogenic input, especially atmospheric deposition,
24  on the Indian Ocean appears to be mixed. There is an indication that the anthropogenically-
25  derived nitrogen input to the northern Indian Ocean, supplied by both atmospheric deposition
26  and riverine fluxes (Jickells et al., 2017), has significantly increased in recent decades. This
27  external nutrient source has the potential to affect the vulnerable biogeochemical systems of the
28  Arabian Sea and Bay of Bengal. The overfertilization of the surface waters increases primary
29  productivity and therewith remineralization in the water column, which contributes to enhanced
30  ocean deoxygenation and thus $N_2O$ production via denitrification and nitrification cycles. As a
31  consequence, the air-sea flux of $N_2O$ increases and can be expected to continue to do so in the
32  future via this feedback cycle (Suntharalingam et al., 2019). Furthermore, some modelling
33  studies show that atmospheric deposition will lead to less $CO_2$ uptake and less ocean
34  acidification (GESAMP 2012). Guieu et al. (2019), on the other hand, modelled that iron
35  deposition doubles primary production and is most important for non-$N_2$ fixing microbes.
36  Future changes in wind, temperature, and dust sources could influence primary productivity in
37  the region (GESAMP 2012). The increase of atmospheric $CO_2$ and its uptake by the ocean
38  enhances ocean acidification, which in turn can impact oceanic biogeochemical cycles and trace
39  gas emission to the atmosphere in multiple ways. One example is the oceanic sulfur cycle which
40  is linked to marine emissions of DMS. The DMS air-sea flux increased in short- term
41  experiments (96 h) with a concurrent decline of the oceanic precursor (Hopkins and Archer,
42  2014) and decreased in longer-term experiments (5 weeks) in response to a shift in the
43  phytoplankton community (Hopkins et al., 2010). Overall, the data suggest an increase in
44  biological stress-induced processes and shows that a marine trace-gas system can change in
45  response to anthropogenic perturbation.

46  As mentioned above, another example for the complex interaction between natural and
47  anthropogenic processes in marine surface water and atmosphere is the deposition of
48  tropospheric ozone, an important secondary pollutant from anthropogenic precursor gases, on
49  the ocean. Its deposition and reaction with marine iodide, which is linked to biological
50  productivity, increases the input of inorganic iodine to the atmosphere (Carpenter et al., 2013).

1  This major source of reactive iodine species in the marine atmosphere, in turn, forms a
2  significant sink for atmospheric ozone through catalytic destruction. In polluted regions,
3  however, anthropogenic $NO_x$ inactivates the reactive species to reservoir species (Mahajan,
4  2019b). As highest ozone values are generally detected closer to the northern continental
5  landmasses with sharp gradients at the coastlines and towards lower latitudes, these processes
6  may increase the gradients. The atmospheric deposition of ozone on marine surface water and
7  subsequent reaction with dissolved organic matter can also form volatile organoiodine
8  compounds (Martino et al., 2009) or organobromine compounds (Kornmüller, 2007).
9  Especially in polluted coastal regions, their formation from this process is expected in addition
10 to the release of organohalogens formed during industrial disinfection processes (Maas et al.,
11 2020). Measurement-based modelling showed that an unexpected formation of ozone from
12 reactive bromine and iodine species can occur in the marine boundary layer near coastlines and
13 ship plumes under VOC-limited conditions associated with high nitrogen oxide concentrations
14 (Shechner and Tas, 2017). Similar to the mechanism above, this could lead to higher ozone
15 gradients from the polluted coast towards the pristine ocean illustrating the complex
16 interactions of the chemical ocean-atmosphere interactions.

17 Evidence is mounting that anthropogenically influenced ocean-atmosphere interactions impact
18 higher trophic levels. The bioaccumulation of persistent organic pollutants and mercury in fish
19 are of prevailing concern for fish stocks and human health (Brooks et al., 2019). In turn, marine-
20 derived volatile forms of iodine, sulfur, and selenium are essential to recycle the elements onto
21 the land and can be important for human health (Rayman, 2000; Fuge and Johnson, 2015).

22
23 **7 Summary and current knowledge gaps**
24
25 The atmospheric composition over the Indian Ocean is determined by a complex array of
26 atmospheric transport patterns, anthropogenic emissions and atmosphere-ocean interactions.
27 Emissions of pollutants and greenhouse gases in the regions surrounding the Indian Ocean
28 generally correspond to population densities and economic activities with emission centres in
29 the Indo-Gangetic Plain, northern China and Java. The distribution of all major pollutants and
30 greenhouse gases show pronounced differences between the landmass source regions and the
31 Indian Ocean, with strong gradients over the coastal areas. During the winter monsoon, the
32 north-south pollution gradients continue over the open Indian Ocean driven by southward
33 transport along with chemical processing, dilution, and surface deposition. In the boundary
34 layer, the contrast between polluted NH and pristine SH air results in a sharp gradient across
35 the ITCZ, where interhemispheric exchange of these air masses occurs in the upper troposphere.
36 During the summer monsoon, clean air dominates the atmospheric composition over the Indian
37 Ocean, leading to a different chemical regime with low atmospheric pollutant levels.

38 Satellite measurements of CO and $NO_2$ have revealed highest surface pollution during the
39 winter monsoon over the Bay of Bengal and the Arabian Sea coastal waters. During this time,
40 most parts of the NH Indian Ocean fall into the category of polluted continental air. Based on
41 recent ship campaign data, pollution maxima over the head and the south-east Bay of Bengal
42 driven by air mass advection from the Indo-Gangetic Plain and Southeast Asia have been
43 identified. One clear difference in the CO and $NO_2$ distribution is the appearance of enhanced
44 $NO_2$ columns along the major shipping lanes. The region south of 5°S can be considered as part
45 of the pristine oceanic regime all year around with minimum values of pollution over the
46 equatorial western Indian Ocean. Long-term changes of pollution in the Indian Ocean MBL
47 and in particular how they are driven by changing emissions and transport patterns require
48 further investigation in the future.

49 Ozone measurements from multiple ship campaigns revealed spatial and seasonal patterns very
50 similar to the pollution fields. Nearly all campaigns detected highest ozone values close to the

1    northern continental landmasses reflecting direct impact of pollution source regions. The sharp
2    latitudinal ozone gradients maximise close to the coastlines during the transition periods due to
3    changing transport regimes. Vertical profiles can show substantially higher ozone values above
4    the MBL due to air-sea breeze triggered transport of polluted air masses in the elevated layer.
5    It has been noted that unusual types of wind patterns can lead to pronounced deviations of the
6    ozone distribution shifting maxima to different regions. A complete picture of the seasonal,
7    latitudinal and vertical ozone variations is not available from current measurements and, thus,
8    the chemical production and loss processes driving ozone distributions are not well known.

9    The distribution of greenhouse gases over the Indian Ocean shows many similarities when
10   compared to the pollution fields, presenting higher values towards the coast due to the proximity
11   of the source rich land regions. However, longer atmospheric lifetimes and active air-sea
12   exchange also lead to some clear differences, such as the latitudinal variations of greenhouse
13   gases being much smaller than the latitudinal variations of the shorter-lived pollutants. In
14   addition, greenhouse gas emissions are characterized by pronounced seasonal variations as a
15   result of their biogenic and agricultural sources. The seasonal cycle of $CO_2$ over the Bay of
16   Bengal and Arabian Sea shows highest values in boreal spring and lowest values in autumn
17   similar to the seasonal cycle of $CO_2$ over land. $CH_4$ over the northern Arabian Sea shows a
18   unique seasonal cycle with maximum values during the summer monsoon, which might be
19   linked to enhanced oceanic emissions during this time. While the large-scale distribution of
20   $CO_2$ and $CH_4$ is well known from satellite measurements, the relative contributions of
21   anthropogenic and oceanic sources and how they impact seasonal cycles and long-term changes
22   remains an open research topic.

23   For marine short-lived gases such as DMS and halogenated VSLS, the Indian Ocean is a hotspot
24   emission region. Ship campaign data suggest that oceanic sulfur fluxes in the form of DMS
25   emissions are the major precursor of aerosols in the summer monsoon remote MBL, with the
26   possibility to significantly contribute to cloud condensation nuclei in the tropical Indian Ocean.
27   Furthermore, halogenated VSLS emitted from the Indian Ocean can be transported into the
28   stratosphere via convection directly above the Indian Ocean or via the summer monsoon
29   convection and anticyclone. Similar mechanisms could also apply to other marine traces gases
30   and should be investigated in the future.

31   Long-term changes of the atmospheric composition over the Indian Ocean are driven by
32   increasing anthropogenic emissions, but also by atmospheric dynamics such as changes of
33   transport patterns and convection. Furthermore, physical, chemical and biological processes in
34   the Indian Ocean can be expected to play a role for the long-term trends of atmospheric
35   composition. Possible changes in stratification, mixing, microbial speciation, and primary
36   productivity will influence trace gases in the atmosphere via modified oceanic emissions.
37   Similarly, ocean acidification can impact biogenic trace gas production and exchange. In
38   addition to changes of oceanic trace gas production, most of the observed and predicted
39   atmospheric long-term changes can influence air-sea gas exchange. For example, more rainfall
40   and intensified cyclone activities could lead to more turbulence at the sea surface and higher
41   fluxes of gases. In most cases, the direction and magnitude of such changes are currently unclear
42   and future studies are required in order to link oceanic changes to observed changes of
43   atmospheric composition.

44   Our current understanding of the Indian Ocean is mostly based on sporadic ship campaigns and
45   remote sensing data. Details of the large-scale features such as the seasonal cycles over the
46   individual ocean basins, variations of the latitudinal gradients, the vertical distributions and
47   long-term changes for several trace gases are not well known, and nor are all the processes well
48   understood. Large uncertainties remain in the current emission inventories that are used in
49   models and data for validation of model simulations is sparse. Dedicated long-term

1  measurement stations, such as they exist in the Atlantic (e.g., Cape Verde Atmospheric
2  Observatory), Pacific (e.g. Mauna Loa Observatory) or the Southern Ocean (e.g. Pointe
3  Bénédicte station), are required in order to link the distribution of trace gases over the Indian
4  Ocean to transport patterns and chemical regimes and to investigate feedback and forcing
5  mechanisms. In addition to long term stations, it is imperative to maintain a repository of the
6  past and future observations made in the Indian Ocean. Identifying long term trends, which are
7  crucial to understanding the processes and impacts of climate change, are hindered by the lack
8  of a consolidated database.

9  Interactions between the Indian Ocean and the atmosphere are bidirectional, and it has become
10  clear that the changing atmospheric composition can impact many oceanic processes, leading
11  to feedback mechanisms. Severe atmospheric pollution, known as the 'South Asian Brown
12  Cloud' transports high levels of gaseous pollutants and aerosols (including dust) containing
13  various nutrients and toxic substances to the Indian Ocean. This review only covers gas-phase
14  composition over the Indian Ocean, however, the complex interactions between anthropogenic
15  and marine trace gases and aerosols are also highly important for atmosphere-ocean feedback
16  mechanisms and climate impacts. Interactions between aerosols and trace gases can form new
17  particles, thus contributing to cloud formation, and wet deposition in the clear marine
18  atmosphere, as well as influence storm patterns and tropical cyclones. Such dynamical effects
19  together with the additional supply of pollution and aerosols will impact biogeochemical and
20  biological processes in the Indian Ocean. The connection between ocean biogeochemistry and
21  atmospheric deposition involves several issues of importance for society, including global and
22  regional pollution, the health of the ocean, fisheries, ocean fertilization, and carbon
23  sequestration, all related to the UN Sustainable Development Goals. However, the impacts of
24  atmospheric pollution and dust on the Indian Ocean's biogeochemistry, trace gas cycling, and
25  potential climate feedbacks, are severely understudied. Further research is needed to understand
26  how sources, transport, reactivity and the atmosphere-ocean feedback mechanisms interact.
27  Such understanding is required in order to predict future changes, to assess if such changes can
28  have harmful effects on the environment and to find pathways which strengthen atmosphere,
29  ocean and community resilience in the Indian ocean region and globally.

30
31  **Appendix A: Major abbreviations and terms**
32
33  AQABA      Air Quality and climate change in the Arabian Basin
34  AIRS       Atmospheric Infrared Sounder
35  BOB        Bay of Bengal
36  BOBEX      Bay of Bengal Experiment
37  BOBPS      Bay of Bengal Processes Studies
38  CMIP       Coupled Model Intercomparison Project
39  EACC       East African Coastal Current
40  EDGAR      Emissions Database for Global Atmospheric Research
41  EMC        East Madagascar Current
42  ENSO       El Niño–Southern Oscillation
43  GMOS       Global Mercury Observation System
44  GOME       Global Ozone Monitoring Experiment
45  GOSAT      Greenhouse Gases Observing Satellite
46  ICARB      Integrated Campaign for Aerosols, gases and Radiation Budget
47  IGP        Indo-Gangetic Plains
48  IIOE-2     2nd International Indian Ocean Expedition program
49  INDOEX     Indian Ocean Experiment
50  IO         Indian Ocean

| 1 | IOD | Indian Ocean Dipole |
| 2 | ISOE | Indian Southern Ocean Expedition |
| 3 | ITF | Indonesian Throughflow |
| 4 | ITZC | Intertropical Convergence Zone |
| 5 | MBL | Marine Boundary Layer |
| 6 | MJO | Madden-Julian Oscillation |
| 7 | MSLP | Mean surface level pressure |
| 8 | MOPITT | Measurements of Pollution in the Troposphere |
| 9 | NH | Northern Hemisphere |
| 10 | NMHC | Non-Methane Hydrocarbon |
| 11 | NMVOC | Non-Methane Volatile Organic Compound |
| 12 | OASIS | Organic VSLS and their air sea exchange from the Indian Ocean to the |
| 13 | | Stratosphere |
| 14 | OMI | Ozone Monitoring Instrument |
| 15 | OMO | Oxidation Mechanism Observations |
| 16 | OMZ | Oxygen Minimum Zone |
| 17 | OVOC | Oxidized Volatile Organic Compound |
| 18 | PESO | Pilot Expedition to the Southern Ocean |
| 19 | SCIAMACHY | Scanning Imaging Absorption Spectrometer for Atmospheric Chartography |
| 20 | SEC | South Equatorial Current |
| 21 | SECC | South Equatorial Countercurrent |
| 22 | SH | Southern Hemisphere |
| 23 | SICC | South Indian Countercurrent |
| 24 | SML | Surface Microlayer |
| 25 | SOA | Secondary Organic Aerosols |
| 26 | SST | Sea Surface Temperature |
| 27 | TROPOMI | TROPOspheric Monitoring Instrument |
| 28 | VOC | Volatile Organic Compound |
| 29 | VSLS | Very Short-Lived Substance |
| 30 | | |
| 31 | | |

Atmospheric
Chemistry
and Physics

Discussions

11  **References**

13  Alory, G., and Meyers, G.: Warming of the upper equatorial Indian Ocean and changes in the
14  heat budget (1960–99). J. Climate, 22 (1), 93–113. doi:10.1175/2008jcli2330.1, 2009.

16  Aneesh, V.R., Mohankumar, G. and Sampath, S.: Spatial distribution of atmospheric carbon
17  monoxide over Bay of Bengal and Arabian Sea: Measurements during pre-monsoon period of
18  2006. J Earth Syst Sci 117, 449–455, https://doi.org/10.1007/s12040-008-0044-8, 2008.

20  Angot, H., Barret, M., Magand, O., Ramonet, M., and Dommergue, A.: A 2-year record of
21  atmospheric mercury species at a background Southern Hemisphere station on Amsterdam
22  Island. Atmos. Chem. Phys., 14(20), 11461–11473. https://doi.org/10.5194/acp-14-11461-
23  2014, 2014.

25  Annamalai, H., Taguchi, B., McCreary J.P., Nagura, M., and Miyama T.: Systematic errors in
26  south Asian monsoon simulation: importance of Equatorial Indian Ocean processes. J. Climate,
27  30, 8159–817, 2017.

29  Arneth, A., Monson, R. K., Schurgers, G., Niinemets, Ü., and Palmer, P. I.: Why are estimates
30  of global terrestrial isoprene emissions so similar (and why is this not so for monoterpenes)?,
31  Atmos. Chem. Phys., 8, 4605-4620, 10.5194/acp-8-4605-2008, 2008.

33  Arnold, S. R., Spracklen, D. V., Williams, J., Yassaa, N., Sciare, J., Bonsang, B., Gros, V.,
34  Peeken, I., Lewis, A. C., Alvain, S., and Moulin, C.: Evaluation of the global oceanic isoprene
35  source and its impacts on marine organic carbon aerosol, Atmos. Chem. Phys., 9, 1253-1262,
36  10.5194/acp-9-1253-2009, 2009.

38  Asatar, G. I. and Nair., P. R.: Spatial distribution of near-surface CO over Bay of Bengal during
39  winter:  role  of  transport,  J.  Atmos.  Sol.-Terr.  Phy.,  72,  1241–1250,
40  doi:10.1016/j.jastp.2010.07.025, 2010.

42  Asharaf, S., and Ahrens, B.: Indian summer monsoon rainfall processes in climate change
43  scenarios. J. Climate, 28(13), 5414–5429, 2015.

45  Astrahan P., Herut B., Paytan A., and Rahav E.: The Impact of Dry Atmospheric Deposition
46  on the Sea-Surface Microlayer in the SE Mediterranean Sea: An Experimental Approach,
47  Frontiers in Marine Science, 3, 222, doi=10.3389/fmars.2016.00222, 2016.

49  Aswini, A. R., Hegde, P., Aryasree, S., Girach, I. A., and Nair, P. R.: Continental outflow of
50  anthropogenic aerosols over Arabian Sea and Indian Ocean during wintertime: ICARB-2018

Atmospheric
Chemistry
and Physics
Discussions
Open Access

EGU

1    campaign, Sci. Total Environ., 712, 135214, https://doi.org/10.1016/j.scitotenv.2019.135214,
2    2020.
3
4    Ayers, G. P. and Gras, J. L.: Ammonia gas concentration over the Southern Ocean, Nature, 284,
5    539–540, 1980.
6
7    Bakker, D. C. et al.: A multi-decade record of high quality $fCO_2$ data in version 3 of the Surface
8    Ocean $CO_2$ Atlas (SOCAT). Earth Syst. Sci. Data, 8: 383-413. doi:10.5194/essd8-383-2016,
9    2016.
10
11   Bange, H. W., Ramesh, R., Rapsomanikis, S., and Andreae, M.: Methane in surface waters of
12   the Arabian Sea, Geophys. Res. Lett., 25, 3547–3550, 1998.
13
14   Bange, H. W.: New Directions: The importance of the oceanic nitrous oxide emissions, Atmos.
15   Environ., 40, 198–199, 2006.
16
17   Barnes, E. A., Fiore, A. M. and Horowitz, L. W.: Detection of trends in surface ozone in the
18   presence   of   climate   variability.   J.   Geophys.   Res.,   121:   6112–6129.   DOI:
19   10.1002/2015JD024397, 2016.
20
21   Bauer, S. E., Tsigaridis, K., and Miller, R.: Significant atmospheric aerosol pollution caused by
22   world     food     cultivation,     Geophys.     Res.     Lett.,     43,     5394-5400,
23   https://doi.org/10.1002/2016GL068354, 2016.
24
25   Behrenfeld, M. J., O'Malley, R. T., Siegel, D. A., McClain, C. R., Sarmiento, J. L., Feldman,
26   G. C., Milligan, A. J., Falkowski, P. G., Letelier, R. M., and Boss, E. S.: Climate-driven trends
27   in contemporary ocean productivity. Nature, 444(7120):752–755, 2006.
28
29   Bengtsson, L.: The global atmospheric water cycle, Environ. Res. Lett., 5, 025002.
30   http://dx.doi.org/10.1088/1748-9326/5/2/025002, 2010.
31
32   Bergamaschi, P., S. Houweling, A. Segers, M. Krol, C. Frankenberg, R. A. Scheepmaker, E.
33   Dlugokencky, S. C. Wofsy, E. A. Kort, C. Sweeney, T. Schuck, C. Brenninkmeijer, H. Chen,
34   V. Beck, C. Gerbig: Atmospheric $CH_4$ in the first decade of the 21st century: Inverse modeling
35   analysis using SCIAMACHY satellite retrievals and NOAA surface measurements, J. Geophys.
36   Res., 118, 7350– 7369, doi:10.1002/jgrd.50480, 2013.
37
38   Biswas, H., Chatterjee, A., Mukhopadhya, S. K., De, T. K., Sen, S., and Jana, T. K.: Estimation
39   of ammonia exchange at the land-ocean boundary condition of Sundarban mangrove northeast
40   coast of Bay of Bengal, India, Atmos. Environ., 39, 4489– 4499, 2005.
41
42   Blunden, J. and D. S. Arndt, Eds.: State of the Climate in 2018. Bull. Amer. Meteor. Soc., 100
43   (9), Si–S305, doi:10.1175/2019BAMSStateoftheClimate.1, 2019.
44
45   Boersma, K. F., Eskes, H. J., Richter, A., De Smedt, I., Lorente, A., Beirle, S., van Geffen, J.
46   H. G. M., Zara, M., Peters, E., Van Roozendael, M., Wagner, T., Maasakkers, J. D., van der A,
47   R. J., Nightingale, J., De Rudder, A., Irie, H., Pinardi, G., Lambert, J.-C., and Compernolle, S.
48   C.: Improving algorithms and uncertainty estimates for satellite NO2 retrievals: results from
49   the quality assurance for the essential climate variables (QA4ECV) project, Atmos. Meas.
50   Tech., 11, 6651–6678, https://doi.org/10.5194/amt-11-6651-2018, 2018.
51

1   Booge, D., Marandino, C. A., Schlundt, C., Palmer, P. I., Schlundt, M., Atlas, E. L., Bracher,
2   A., Saltzman, E. S., and Wallace, D. W. R.: Can simple models predict large-scale surface
3   ocean isoprene concentrations?, Atmos. Chem. Phys., 16, 11807-11821, 10.5194/acp-16-
4   11807-2016, 2016.
5
6   Booge, D., Schlundt, C., Bracher, A., Endres, S., Zäncker, B., and Marandino, C. A.: Marine
7   isoprene production and consumption in the mixed layer of the surface ocean – a field study
8   over two oceanic regions, Biogeosciences, 15, 649-667, 10.5194/bg-15-649-2018, 2018.
9
10  Bourtsoukidis, E., Ernle, L., Crowley, J. N., Lelieveld, J., Paris, J. D., Pozzer, A., Walter, D.,
11  and Williams, J.: Non-methane hydrocarbon (C2–C8) sources and sinks around the Arabian
12  Peninsula, Atmos. Chem. Phys., 19, 7209-7232, 10.5194/acp-19-7209-2019, 2019.
13
14  Bovensmann, H., Burrows, J. P., Buchwitz, M., Frerick, J., Noël, S., Rozanov, V. V., Chance,
15  K. V., and Goede, A. P. H.: SCIAMACHY: Mission Objectives and Measurement Modes, J.
16  Atmos. Sci., 56, 127-150, 10.1175/1520-0469(1999)056<0127:Smoamm>2.0.Co;2, 1999.
17
18  Bollasina, M. A., Ming, Y. and Ramaswamy, V., Anthropogenic Aerosols and the Weakening
19  of the South Asian Summer Monsoon, Science, 334, 6055, 502-505, 2011.
20
21  Brooks, S. D., T. D. Jickells, P. S. Liss, D. C. O. Thornton, and R. Zhang: Biogeochemical
22  Coupling between Ocean and Atmosphere—A Tribute to the Lifetime Contribution of Robert
23  A. Duce. J. Atmos. Sci., 76, 3289–3298, https://doi.org/10.1175/JAS-D-18-0305.1, 2019.
24
25  Brühl, C., Lelieveld, J., Crutzen, P. J., and Tost, H.: The role of carbonyl sulphide as a source
26  of stratospheric sulphate aerosol and its impact on climate, Atmos. Chem. Phys., 12, 1239-
27  1253, 10.5194/acp-12-1239-2012, 2012.
28
29  Butler, A.H., J.S. Daniel, R.W. Portmann, A.R. Ravishankara, P.J. Young, D.W. Fahey, and
30  K.H. Rosenlof: Diverse policy implications for future ozone and surface UV in a changing
31  climate. Environ. Res. Lett., 11: 064017, 2016.
32
33  Burrows, J. P., Weber, M., Buchwitz, M., Rozanov, V., Ladstätter-Weißenmayer, A., Richter,
34  A., DeBeek, R., Hoogen, R., Bramstedt, K., Eichmann, K.-U., Eisinger, M., and Perner, D.:
35  The Global Ozone Monitoring Experiment (GOME): Mission Concept and First Scientific
36  Results, J. Atmos. Sci., 56, 151-175, 10.1175/1520-0469(1999)056<0151:Tgomeg>2.0.Co;2,
37  1999.
38
39  Cai, W. et al.: Increased frequency of extreme Indian Ocean Dipole events due to greenhouse
40  warming. Nature 510, 254–258, 2014.
41
42  Cai, W., A. Sullivan, and T. Cowan: Climate change contributes to more frequent consecutive
43  positive Indian Ocean Dipole events. Geophys. Res. Lett., 36, L19783,
44  doi:10.1029/2009GL040163, 2009.
45
46  Campbell, J. E., Whelan, M. E., Seibt, U., Smith, S. J., Berry, J. A., and Hilton, T. W.:
47  Atmospheric carbonyl sulfide sources from anthropogenic activity: Implications for carbon
48  cycle constraints, Geophys. Res. Lett., 42, 3004-3010, 10.1002/2015gl063445, 2015.
49

Atmospheric
Chemistry
and Physics
Discussions

Carlton, A. G., Wiedinmyer, C., and Kroll, J. H.: A review of Secondary Organic Aerosol (SOA) formation from isoprene, Atmos. Chem. Phys., 9, 4987-5005, 10.5194/acp-9-4987-2009, 2009.

Carmichael, G. R., Ferm, M., Thongboonchoo, N., Woo, J. H., Chan, L. Y., Murano, K., Viet, P. H., Mossberg, C., Bala, R., Boonjawat, J., Upatum, P., Mohan, M., Adhikary, S. P., Shrestha, A. B., Pinaar, J. J., Brunke, E. B., Chen, T., Jie, T., Guoan, D., Peng, L. C., Dhiharto, S., Harjanto, H., Jose, A. M., Kimani, W., Kirouane, A., Lacaus, J.-P., Richard, S., Barturen, O., Cerda, J. C., Athayde, A., Tavares, T., Cotrina, J. S., and Bilici, E.: Measurements of sulfur dioxide, ozone and ammonia concentration in Asia, Africa and South America using passive samplers, Atmos. Environ., 37, 1293–1308, 2003.

Carpenter, L. J., and Liss, P. S.: On temperate sources of bromoform and other reactive organic bromine gases, J. Geophys. Res., 105( D16), 20539– 20547, doi:10.1029/2000JD900242, 2000.

Carpenter, L. J., MacDonald, S. M., Shaw, M. D., Kumar, R., Saunders, R. W., Parthipan, R., Wilson, J. and Plane, J. M. C.: Atmospheric iodine levels influenced by sea surface emissions of inorganic iodine, Nat. Geosci., 6(2), 108–111, doi:10.1038/ngeo1687, 2013.

Chang, J.-H.: The Indian Summer Monsoon, Geogr. Rev., vol. 57, no. 3, 373–396, 1967.

Charlson, R., Lovelock, J., Andreae, M., and Warren, S. G.: Oceanic phytoplankton, atmospheric sulphur, cloud albedo and climate. Nature 326, 655–661. https://doi.org/10.1038/326655a0, 1987.

Chen, L., Xu, S., Gao, Z., Chen, H., Zhang, Y., Zhan, J., and Li, W.: Estimation of monthly air-sea $CO_2$ flux in the southern Atlantic and Indian Ocean using in-situ and remotely sensed data, Remote Sens. Environ., 115, 1935-1941, https://doi.org/10.1016/j.rse.2011.03.016, 2011.

Chen, J., and Bordoni, S.: Early summer response of the East Asian summer monsoon to atmospheric CO2 forcing and subsequent sea surface warming, J. Climate. 295431–46, 2016.

Cheng, L., F. Zheng, and J. Zhu: Distinctive ocean interior changes during the recent warming slowdown. Sci. Rep., 5, 14346, https://doi.org/10.1038/srep14346, 2015.

Chin, M. and Davis, D. D.: Global sources and sinks of OCS and $CS_2$ and their distributions, Global Biogeochem. Cy., 7, 321–337, 1993.

Chiu, R., Tinel, L., Gonzalez, L., Ciuraru, R., Bernard, F., George, C., and Volkamer, R.: UV photochemistry of carboxylic acids at the air-sea boundary: A relevant source of glyoxal and other oxygenated VOC in the marine atmosphere, Geophys. Res. Lett., 44, 1079– 1087, doi:10.1002/2016GL071240, 2017.

Ciais, P., Dolman, A. J., Bombelli, A., Duren, R., Peregon, A., Rayner, P. J., Miller, C., Gobron, N., Kinderman, G., Marland, G., Gruber, N., Chevallier, F., Andres, R. J., Balsamo, G., Bopp, L., Bréon, F. M., Broquet, G., Dargaville, R., Battin, T. J., Borges, A., Bovensmann, H., Buchwitz, M., Butler, J., Canadell, J. G., Cook, R. B., DeFries, R., Engelen, R., Gurney, K. R., Heinze, C., Heimann, M., Held, A., Henry, M., Law, B., Luyssaert, S., Miller, J., Moriyama, T., Moulin, C., Myneni, R. B., Nussli, C., Obersteiner, M., Ojima, D., Pan, Y., Paris, J. D., Piao, S. L., Poulter, B., Plummer, S., Quegan, S., Raymond, P., Reichstein, M., Rivier, L., Sabine, C., Schimel, D., Tarasova, O., Valentini, R., Wang, R., van der Werf, G., Wickland, D.,

1  Williams, M., and Zehner, C.: Current systematic carbon-cycle observations and the need for
2  implementing a policy-relevant carbon observing system, Biogeosciences, 11, 3547-3602,
3  10.5194/bg-11-3547-2014, 2014.
4
5  Ciuraru, R., Fine, L., Pinxteren, M. V., D'Anna, B., Herrmann, H., and George, C.: Unravelling
6  New Processes at Interfaces: Photochemical Isoprene Production at the Sea Surface, Environ.
7  Sci. Technol., 49, 13199–13205, doi:10.1021/acs.est.5b02388, 2015.
8
9  Codispoti, L. A.: Interesting times for marine $N_2O$. Science, 327(5971), 1339–1340.
10 https://doi.org/10.1126/science.1184945, 2010.
11
12 Conte, L., Szopa, S., Séférian, R., and Bopp, L.: The oceanic cycle of carbon monoxide and its
13 emissions to the atmosphere, Biogeosciences, 16, 881–902, https://doi.org/10.5194/bg-16-881-
14 2019, 2019.
15
16 Crippa, M., Oreggioni, G., Guizzardi, D., Muntean, M., Schaaf, E., Lo Vullo, E., Solazzo, E.,
17 Monforti-Ferrario, F., Olivier, J.G.J., Vignati, E.: Fossil $CO_2$ and GHG emissions of all world
18 countries - 2019 Report, EUR 29849 EN, Publications Office of the European Union,
19 Luxembourg, ISBN 978-92-76-11100-9, doi:10.2760/687800, JRC117610, 2019.
20
21 Crippa, M., Solazzo, E., Huang, G., Guizzardi, D., Koffi, E., Muntean, M., Schieberle, C.,
22 Friedrich, R., and Janssens-Maenhout, G.: High resolution temporal profiles in the Emissions
23 Database for Global Atmospheric Research, Sci. Data, 7, 121, 10.1038/s41597-020-0462-2,
24 2020.
25
26 Cuevas, C. A., Maffezzoli, N., Corella, J. P., Spolaor, A., Vallelonga, P., Kjær, H. A.,
27 Simonsen, M., Winstrup, M., Vinther, B., Horvat, C., Fernandez, R. P., Kinnison, D.,
28 Lamarque, J.-F., Barbante, C. and Saiz-Lopez, A.: Rapid increase in atmospheric iodine levels
29 in the North Atlantic since the mid-20th century, Nat. Commun., 9(1), 1452,
30 doi:10.1038/s41467-018-03756-1, 2018.
31
32 Da-Allada, C.Y., Gaillard, F. and Kolodziejczyk, N.: Mixed-layer salinity budget in the tropical
33 Indian Ocean: seasonal cycle based only on observations. Ocean Dynam., 65, 845–857,
34 https://doi.org/10.1007/s10236-015-0837-7, 2015.
35
36 Daniel, J. S., and Solomon, S.: On the climate forcing of carbon monoxide, J. Geophys. Res.,
37 103(D11), 13249– 13260, doi:10.1029/98JD00822, 1998.
38
39 David, L. M., Girach, I. A., and Nair, P. R.: Distribution of ozone and its precursors over Bay
40 of Bengal during winter 2009: role of meteorology, Ann. Geophys., 29, 1613–1627,
41 https://doi.org/10.5194/angeo-29-1613-2011, 2011.
42
43 David, L. M., and Nair, P. R.: Diurnal and seasonal variability of surface ozone and $NO_x$ at a
44 tropical coastal site: Association with mesoscale and synoptic meteorological conditions, J.
45 Geophys. Res., 116, D10303, doi:10.1029/2010JD015076, 2011.
46
47 David, L. M. and Nair, P. R.: Tropospheric column $O_3$ and $NO_2$ over the Indian region observed
48 by Ozone Monitoring Instrument (OMI): Seasonal changes and long-term trends, Atmos.
49 Environ., 65, 25–39, https://doi.org/10.1016/j.atmosenv.2012.09.033, 2013.
50

Atmospheric
Chemistry
and Physics
Discussions

1    Davidson, E. A.: The contribution of manure and fertilizer nitrogen to atmospheric nitrous
2    oxide since 1860. Nat. Geosci., 2:659–662. https://doi.org/10.1038/NGEO608, 2009.
3
4    Deeter, M. N., Edwards, D. P., Francis, G. L., Gille, J. C., Mao, D., Martínez-Alonso, S.,
5    Worden, H. M., Ziskin, D., and Andreae, M. O.: Radiance-based retrieval bias mitigation for
6    the MOPITT instrument: the version 8 product, Atmos. Meas. Tech., 12, 4561-4580,
7    10.5194/amt-12-4561-2019, 2019.
8
9    DeVries, T., Le Quéré, C., Andrews, O., Berthet, S., Hauck, J., Ilyina, T., Landschützer, P.,
10   Lenton, A., Lima, I. D., Nowicki, M., Schwinger, J., and Séférian, R.: Decadal trends in the
11   ocean carbon sink, Proc. Natl. Acad. Sci. USA, 116, 11646-11651, 10.1073/pnas.1900371116,
12   2019.
13
14   Dixit, A., L, K., Bharti, R., and Mahanta, C.: Net Sea–Air $CO_2$ Fluxes and Modeled Partial
15   Pressure of $CO_2$ in Open Ocean of Bay of Bengal, IEEE J. Sel. Top. Appl., 12, 2462-2469,
16   10.1109/JSTARS.2019.2902253, 2019.
17
18   Dong L, Zhou T and B. Wu: Indian Ocean warming during 1958–2004 simulated by a climate
19   system model and its mechanism. Clim. Dynam., 42, 203–217, doi.org/10.1007/s00382-013-
20   1722-z (2014), 2014.
21
22   Dong, L. and T. Zhou: The Indian Ocean sea surface temperature warming simulated by CMIP5
23   models during the twentieth century: Competing forcing roles of GHGs and anthropogenic
24   aerosols. J. Clim. 27, 3348–3362, 2014.
25
26   Du, Y. and S. P. Xie: Role of atmospheric adjustments in the tropical Indian Ocean warming
27   during the 20th century in climate models. Geophys. Res. Lett., 35, L08712, 2008.
28
29   Du, Y., Zhang, Y., Feng, M., Wang, T., Zhang, N., and S.E. Wijffels: Decadal trends of the
30   upper ocean salinity in the tropical Indo–Pacific since mid-1990s. Sci. Rep., 5:16050.
31   doi.org/10.1038/srep1 6050, 2015.
32
33   Du, Q., Zhang, C., Mu, Y., Cheng, Y., Zhang, Y., Liu, C., Song, M., Tian, D., Liu, P., Liu, J.,
34   Xue, C., and Ye, C.: An important missing source of atmospheric carbonyl sulfide: Domestic
35   coal combustion, Geophys. Res. Lett., 43, 8720-8727, 10.1002/2016gl070075, 2016.
36
37   Edtbauer, A., Stönner, C., Pfannerstill, E. Y., Berasategui, M., Walter, D., Crowley, J. N.,
38   Lelieveld, J., and Williams, J.: A new marine biogenic emission: methane sulfonamide
39   (MSAM), DMS and $DMSO_2$ measured in air over the Arabian Sea, Atmos. Chem. Phys.
40   Discuss., https://doi.org/10.5194/acp-2019-1021, in review, 2020.
41
42   Engel, A., Rigby, M., Burkholder, J. B., Fernandez, R. P. Froidevaux, L., Hall, B. D., Hossaini,
43   R., Saito, T., Vollmer, M. K., Yao, B.: Update on ozone-depleting substances (ODSs) and other
44   gases of interest to the Montreal Protocol. In Scientific assessment of ozone depletion: 2018,
45   Doherty, S. J., Means, T., Stewart, B. C., McCarrick, A., Dailey-Fisher, D., Reiser, A. M., Eds.;
46   Global ozone research and monitoring project, Vol. 58; WMO (World Meteorological
47   Organization): Geneva; pp 1.1-1.87, 2019.
48
49   Ethe´, C., Basdevant, C., Sadourny, R., Appu, K. S., Harenduprakash, L., Sarode, P. R., and
50   Viswanathan, G.: Air mass motion, temperature, and humidity over the Arabian Sea and
51   western Indian Ocean during the INDOEX intensive phase, as obtained from a set of

superpressure drifting balloons, J. Geophys. Res., 107, 8023, doi:10.1029/2001JD001120, 2002.

Exton, D. A., Suggett, D. J., McGenity, T. J., and Steinke, M.: Chlorophyll-normalized isoprene production in laboratory cultures of marine microalgae and implications for global models, Limnol. Oceanogr., 58, 1301-1311, 10.4319/lo.2013.58.4.1301, 2013.

Fadnavis, S., Semeniuk, K., Schultz, M. G., Mahajan, A. S., Pozzoli, L., Sonbawane, S., and Kiefer, M.: Transport pathways of peroxyacetyl nitrate in the upper troposphere and lower stratosphere from different monsoon systems during the summer monsoon season. Atmos. Chem. Phys., 15(14), 11477–11499. https://doi.org/10.5194/acp-15-11477-2015, 2015.

Fiehn, A., Quack, B., Hepach, H., Fuhlbrügge, S., Tegtmeier, S., Toohey, M., et al.: Delivery of halogenated very short-lived substances from the west Indian Ocean to the stratosphere during the Asian summer monsoon. Atmos. Chem. Phys., 17(11), 6723–6741. https://doi.org/10.5194/acp-17-6723-2017, 2017.

Fiehn, A., Quack, B., Stemmler, I., Ziska, F., and Krüger, K.: Importance of seasonally resolved oceanic emissions for bromoform delivery from the tropical Indian Ocean and west Pacific to the stratosphere. Atmos. Chem. Phys., 18(16), 11,973–11,990. https://doi.org/10.5194/acp-18-11973-2018, 2018.

Fiore, A.M., West, J.J., Horowitz, L.W., Naik, V. and Schwarzkopf, M.D.: Characterizing the tropospheric ozone response to methane emission controls and the benefits to climate and air quality. J. Geophys. Res., 113(D08): 307. DOI: 10.1029/2007JD009162, 2008.

Franke, K., Richter, A., Bovensmann, H., Eyring, V., Jöckel, P., Hoor, P., and Burrows, J. P.: Ship emitted NO2 in the Indian Ocean: comparison of model results with satellite data, Atmos. Chem. Phys., 9, 7289–7301, https://doi.org/10.5194/acp-9-7289-2009, 2009.

Fuge, R., and C. C. Johnson: Iodine and human health, the role of environmental geochemistry and diet, a review. Appl. Geochem., 63, 282–302, 2015.

Galí, M., Levasseur, M., Devred, E., Simó, R., and Babin, M.: Sea-surface dimethylsulfide (DMS) concentration from satellite data at global and regional scales. Biogeosciences, 15(11), 3497–3519. https://doi.org/10.5194/bg-15-3497-2018, 2018.

Ganguly, N.D. and Tzanis, C.: Study of Stratosphere-troposphere exchange events of ozone in India and Greece using ozonesonde ascents. Met. Apps, 18: 467-474. doi:10.1002/met.241, 2011.

Gantt, B., Meskhidze, N., and Kamykowski, D.: A new physically-based quantification of marine isoprene and primary organic aerosol emissions, Atmos. Chem. Phys., 9, 4915-4927, 10.5194/acp-9-4915-2009, 2009.

GESAMP: Rep. Stud. GESAMP 84: 69, 2012.

Ghude, S. D., Beig, G., Kulkarni, P. S., Kanawade, V. P., Fadnavis, S., Remedios, J. J., and Kulkarni, S. H.: Regional CO pollution over the Indian-subcontinent and various transport pathways as observed by MOPITT, Int. J. Remote Sens., 32, 6133–6148, 2011.

Ghude, S.D., Kulkarni, S.H., Jena, C., Pfister, G.G., Beig, G., Fadnavis, S., van der A, R.J.: Application of satellite observations for identifying regions of dominant sources of nitrogen oxides over the Indian Subcontinent. J. Geophys. Res., 118, 1075e1089. http://dx.doi.org/10.1029/2012JD017811, 2013.

Gibb, S. W. and Mantoura, R. F. C.: Ocean-atmosphere exchange and atmospheric speciation of ammonia and methylamines in the region of the NW Arabian Sea, Global Biogeochem. Cycles, 13, 161–178, 1999a.

Gibb, S. W., Mantouura, R. F. C., and Liss, P. S.: Ocean-atmosphere exchange and speciation of ammonia and methylamines in the region of the NW Arbian Sea, Global Biogeochem. Cycles, 13, 161–178, 1999b.

Girach, I. A., Ojha, N., Nair, P. R., Pozzer, A., Tiwari, Y. K., Kumar, K. R., and Lelieveld, J.: Variations in $O_3$, CO, and $CH_4$ over the Bay of Bengal during the summer monsoon season: shipborne measurements and model simulations, Atmos. Chem. Phys., 17, 257–275, https://doi.org/10.5194/acp-17-257-2017, 2017.

Glatthor, N., Höpfner, M., Baker, I. T., Berry, J., Campbell, J. E., Kawa, S. R., Krysztofiak, G., Leyser, A., Sinnhuber, B.-M., Stiller, G. P., Stinecipher, J., von Clarmann, T.: Tropical sources and sinks of carbonyl sulfide observed from space, Geophys. Res. Lett., 42, 10,082–10,090, doi:10.1002/2015GL066293, 2015.

Goes, J.I., P.G. Thoppil, H. Gomes, and J.T. Fasullo: Warming of the Eurasian landmass is making the Arabian Sea more productive, Science, 308 (5721), 545-547, 10.1126/science.1106610, 2005.

Gopika, S., Izumo, T., Vialard, J., Lengaigne, M., Suresh, I. and M. R. R. Kumar: Aliasing of the Indian Ocean externally-forced warming spatial pattern by internal climate variability, Clim. Dynam., 54, 1-2, 1093-1111, 2020.

Graedel, T. E. and Crutzen, P. J.: Atmospheric Change: an Earth System Perspective, W. H. Freeman, New York, 1992.

Gregg, W. W., and Rousseaux, C. S.: Global ocean primary production trends in the modern ocean color satellite record (1998–2015). Environ. Res. Lett. 2019;14:1–9, 2019.

Gschwend, P. M., MacFarlane, J. K. and Newman, K. A.: Volatile halogenated organic compounds released to seawater from temperate marine macroalgae, Science 227, 1033–1035, 1985.

Guenther, A., Karl, T., Harley, P., Wiedinmyer, C., Palmer, P. I., and Geron, C.: Estimates of global terrestrial isoprene emissions using MEGAN (Model of Emissions of Gases and Aerosols from Nature), Atmos. Chem. Phys., 6, 3181-3210, 10.5194/acp-6-3181-2006, 2006.

Guenther, A. B., Jiang, X., Heald, C. L., Sakulyanontvittaya, T., Duhl, T., Emmons, L. K., and Wang, X.: The Model of Emissions of Gases and Aerosols from Nature version 2.1 (MEGAN2.1): an extended and updated framework for modeling biogenic emissions, Geosci. Model Dev., 5, 1471-1492, 10.5194/gmd-5-1471-2012, 2012.

1    Guerreiro, C. V., Baumann, K.-H., Brummer, G.-J. A., Fischer, G., Korte, L. F., Merkel, U.,
2    Sá, C., de Stigter, H., and Stuut, J.-B. W.: Coccolithophore fluxes in the open tropical North
3    Atlantic: influence of thermocline depth, Amazon water, and Saharan dust, Biogeosciences, 14,
4    4577–4599, https://doi.org/10.5194/bg-14-4577-2017, 2017.
5
6    Guieu, C., O. Aumont, A. Paytan, L. Bopp, C. S. Law, N. Mahowald, E. P. Achterberg, E.
7    Marañón, B. Salihoglu, A. Crise, T. Wagener, B. Herut, K. Desboeufs, M. Kanakidou, N.
8    Olgun, F. Peters, E. Pulido-Villena, A. Tovar-Sanchez and C. Völker: The significance of the
9    episodic nature of atmospheric deposition to Low Nutrient Low Chlorophyll regions, Global
10   Biogeochem. Cy., 28, 1179– 1198, doi:10.1002/2014GB004852, 2014.
11
12   Guieu, C., A., Azhar, M., Aumont, O., Mahowald, N., Levy, M., Ethé, C., and Lachkar, Z.:
13   Major impact of dust deposition on the productivity of the Arabian Sea. Geophys. Res. Lett.,
14   46, 6736– 6744. https://doi.org/10.1029/2019GL082770, 2019.
15
16   Han, W., and J. P. McCreary: Modelling salinity distributions in the Indian Ocean, J. Geophys.
17   Res., 106, 859 – 877, 2001.
18
19   Han, W. et al.: Indian Ocean decadal variability: a review. Bull. Am. Meteorol. Soc. 95, 1679–
20   1703, 2014.
21
22   Han, Z., Su, T., Zhang, Q., Wen. Q., and G. Feng: Thermodynamic and dynamic effects
23   of increased moisture sources over the Tropical Indian Ocean in recent decades, Clim. Dynam.,
24   53:7081–7096, 2019.
25
26   Hastenrath, S. and Polzin, D., Dynamics of the surface wind field over the equatorial Indian
27   Ocean. Q.J.R. Meteorol. Soc., 130: 503-517. doi:10.1256/qj.03.79, 2004.
28
29   Hastenrath, S., Zonal Circulations over the Equatorial Indian Ocean. J. Climate, 13, 2746–2756,
30   https://doi.org/10.1175/1520-0442(2000)013<2746:ZCOTEI>2.0.CO;2, 2000.
31
32   Hay, T., Kreher, K. and Riedel, K.: Bromine explosions and Antarctic ozone. Water and
33   Atmosphere, 15, pp. 12–13, 2007.
34
35   Henze, D. K., and Seinfeld, J. H.: Global secondary organic aerosol from isoprene oxidation,
36   Geophys. Res. Lett., 33, 10.1029/2006gl025976, 2006.
37
38   Hermes, J. C., Masumoto, Y., Beal, L. M., Roxy, M. K., Vialard, J., Andres, M., Annamalai,
39   H., Behera, S., D'Adamo, N., Doi, T., Feng, M., Han, W., Hardman-Mountford, N., Hendon,
40   H., Hood, R., Kido, S., Lee, C., Lee, T., Lengaigne, M., Li, J., Lumpkin, R., Navaneeth, K. N.,
41   Milligan, B., McPhaden, M. J., Ravichandran, M., Shinoda, T., Singh, A., Sloyan, B., Strutton,
42   P. G., Subramanian, A. C., Thurston, S., Tozuka, T., Ummenhofer, C. C., Unnikrishnan, A. S.,
43   Venkatesan, R., Wang, D., Wiggert, J., Yu, L., and Yu, W.: A Sustained Ocean Observing
44   System in the Indian Ocean for Climate Related Scientific Knowledge and Societal Needs,
45   Frontiers in Marine Science, 6, 10.3389/fmars.2019.00355, 2019.
46
47   Herut B., Rahav E., Tsagaraki T. M., Giannakourou A., Tsiola A., Psarra S., Lagaria A.,
48   Papageorgiou N., Mihalopoulos N., Theodosi C. N., Violaki K., Stathopoulou E., Scoullos M.,
49   Krom M. D., Stockdale A., Shi Z., Berman-Frank I., Meador T. B., Tanaka T., and Paraskevi
50   P.: The Potential Impact of Saharan Dust and Polluted Aerosols on Microbial Populations in

1  the East Mediterranean Sea, an Overview of a Mesocosm Experimental Approach, Frontiers in
2  Marine Science, 3, 226, doi=10.3389/fmars.2016.00226, 2016.
3
4  Hönninger, G.: Halogen Oxide Studies in the Boundary Layer by Multi Axis Differential
5  Optical Absorption Spectroscopy and Active Longpath-DOAS. University of Heidelberg, 2002.
6
7  Hood, R. R., Urban, E. R., McPhaden, M. J., Su, D., and Raes, E.: The 2nd International Indian
8  Ocean Expedition (IIOE-2): Motivating New Exploration in a Poorly Understood Basin,
9  Limnol. Oceanogr. Bulletin, 25, 117-124, 10.1002/lob.10149, 2016.
10
11  Hood R. R., Beckley, L. E. and Wiggert, J. D.: Biogeochemical and ecological impacts of
12  boundary currents in the Indian Ocean. Prog. Oceanogr., 156: 290–325, 2017.
13
14  Hopkins, F. E. and Archer, S. D.: Consistent increase in dimethyl sulfide (DMS) in response to
15  high $CO_2$ in five shipboard bio assays from contrasting NW European waters, Biogeosciences,
16  11, 4925–4940, https://doi.org/10.5194/bg-11-4925-2014, 2014.
17
18  Hopkins, F. E., Turner, S. M., Nightingale, P. D., Steinke, M., Bakker, D., and Liss, P. S.:
19  Ocean acidification and marine trace gas emissions, P. Natl. Acad. Sci. USA, 107, 760–765,
20  2010.
21
22  Hossaini, R., Mantle, H., Chipperfield, M. P., Montzka, S. A., Hamer, P., Ziska, F., Quack, B.,
23  Krüger, K., Tegtmeier, S., Atlas, E., Sala, S., Engel, A., Bönisch, H., Keber, T., Oram, D.,
24  Mills, G., Ordóñez, C., Saiz-Lopez, A., Warwick, N., Liang, Q., Feng, W., Moore, F., Miller,
25  B. R., Marécal, V., Richards, N. A. D., Dorf, M., and Pfeilsticker, K.: Evaluating global
26  emission inventories of biogenic bromocarbons, Atmos. Chem. Phys., 13, 11819-11838,
27  10.5194/acp-13-11819-2013, 2013.
28
29  Hsu, N. C., Gautam, R., Sayer, A. M., Bettenhausen, C., Li, C., Jeong, M. J., Tsay, S.-C., and
30  Holben, B. N.: Global and regional trends of aerosol optical depth over land and ocean using
31  SeaWiFS measurements from 1997 to 2010, Atmos. Chem. Phys., 12, 8037–8053,
32  https://doi.org/10.5194/acp-12-8037-2012, 2012.
33
34  Hu, Q. H., Xie, Z. Q., Wang, X. M., Kang, H., He, Q. F., and Zhang, P.: Secondary organic
35  aerosols over oceans via oxidation of isoprene and monoterpenes from Arctic to Antarctic, Sci
36  Rep, 3, 2280, 10.1038/srep02280, 2013.
37
38  Hu, S., and Sprintall, J.: Observed strengthening of interbasin exchange via the Indonesian seas
39  due to rainfall intensification. Geophys. Res. Lett. 44, 1448–1456. doi:
40  10.1002/2016GL072494, 2017.
41
42  Inamdar, S., Tinel, L., Chance, R., Carpenter, L. J., Sabu, P., Chacko, R., Tripathy, S. C.,
43  Kerkar, A. U., Sinha, A. K., Bhaskar, P. V., Sarkar, A., Roy, R., Sherwen, T., Cuevas, C., Saiz-
44  Lopez, A., Ram, K., and Mahajan, A. S.: Estimation of Reactive Inorganic Iodine Fluxes in the
45  Indian and Southern Ocean Marine Boundary Layer, Atmos. Chem. Phys. Discuss., 2020, 1-
46  57, 10.5194/acp-2019-1052, 2020.
47
48  Inomata, Y., Hayashi, M., Osada, K., and Iwasaka, Y.: Spatial distributions of volatile sulfur
49  compounds in surface seawater and overlying atmosphere in the northwestern Pacific Ocean,
50  Eastern Indian Ocean, and Southern Ocean, Global Biogeochem. Cy., 20, GB2022,
51  https://doi.org/10.1029/2005gb002518, 2006.

1
2   IPCC. Climate Change 2013: The Physical Science Basis. In: Stocker, TF, Qin, D, Plattner, G-
3   K, Tignor, M, Allen, SK, Boschung, J, Nauels, A, Xia, Y, Bex, V and Midgley, PM (eds.),
4   Contribution of Working Group I to the Fifth Assessment Report of the Intergovernmental
5   Panel on Climate Change, 1535. Cambridge University Press, Cambridge, United Kingdom and
6   New York, NY, USA, 2013.
7
8   Ito, A., Nishina, K., Ishijima, K. et al. Emissions of nitrous oxide ($N_2O$) from soil surfaces and
9   their historical changes in East Asia: a model-based assessment. Prog Earth Planet Sci 5, 55,
10  https://doi.org/10.1186/s40645-018-0215-4, 2018.
11
12  Iyengar, G. R., V. S. Prasad, and K. J. Ramesh, Circulation characteristic associated with Inter
13  Tropical Convergence Zone during northern winter, Curr. Sci., 76, 903–906, 1999.
14
15  Jensen, T. G.: Cross-equatorial pathways of salt and tracers from the northern Indian Ocean:
16  Modelling results, Deep Sea Res., Part II, 50, 2111 – 2128, 2003.
17
18  Jickells, T. D., E. Buitenhuis, K. Altieri, A. R. Baker, D. Capone, R. A. Duce, F. Dentener, K.
19  Fennel, M. Kanakidou, J. LaRoche, K. Lee, P. Liss, J. J. Middelburg, J. K. Moore, G. Okin, A.
20  Oschlies, M. Sarin, S. Seitzinger, J. Sharples, A. Singh, P. Suntharalingam, M. Uematsu, L. M.
21  Zamora: A reevaluation of the magnitude and impacts of anthropogenic atmospheric nitrogen
22  inputs   on   the   ocean.   Global   Biogeochem.   Cy.,   31,   289–305,   https://
23  doi.org/10.1002/2016GB005586, 2017.
24
25  Jordi, A., G. Basterretxea, A. Tovar-Sánchez, A. Alastuey, and X. Querol: Copper aerosols
26  inhibit phytoplankton growth, Proc. Natl. Acad. Sci. USA, 109 (52) 21246-21249; DOI:
27  10.1073/pnas.1207567110, 2012.
28
29  Kavitha, M. and P. R. Nair: Satellite-retrieved vertical profiles of methane over the Indian
30  region: impact of synoptic-scale meteorology, Int. J. Remote Sens., 40:14, 5585-5616, DOI:
31  10.1080/01431161.2019.1580791, 2019.
32
33  Khemani, L. T., Momin, G. A., and Singh, G.: Variation in trace gases concentrations in
34  different environments in India, PA- GEOPH., 125, 151–158, 1987.
35
36  Kitoh, A., Endo, H., Krishna Kumar, K., Cavalcanti, IFA, Goswami, P. and Zhou, T.: Monsoons
37  in a changing world: A regional perspective in a global context. J. Geophys. Res., 118(8):3053–
38  3065, 2013.
39
40  Kim, P. S., Jacob, D. J., Liu, X., Warner, J. X., Yang, K., Chance, K., Thouret, V., and Nedelec,
41  P.: Global ozone–CO correlations from OMI and AIRS: constraints on tropospheric ozone
42  sources, Atmos. Chem. Phys., 13, 9321–9335, https://doi.org/10.5194/acp-13-9321-2013,
43  2013.
44
45  Kornmüller, A.: Review of fundamentals and specific aspects of oxidation technologies in
46  marine waters. Water Sci Technol, 55 (12): 1–6. doi: https://doi.org/10.2166/wst.2007.379,
47  2007.
48
49  Kremser, S., Thomason, L. W., von Hobe, M., Hermann, M., Deshler, T., Timmreck, C.,
50  Toohey, M., Stenke, A., Schwarz, J. P., Weigel, R., Fueglistaler, S., Prata, F. J., Vernier, J.-P.,
51  Schlager, H., Barnes, J. E., Antuña-Marrero, J.-C., Fairlie, D., Palm, M., Mahieu, E., Notholt,

Atmospheric
Chemistry
and Physics
Discussions

Open Access

EGU

1  J., Rex, M., Bingen, C., Vanhellemont, F., Bourassa, A., Plane, J. M. C., Klocke, D., Carn, S.
2  A., Clarisse, L., Trickl, T., Neely, R., James, A. D., Rieger, L., Wilson, J. C., and Meland, B.:
3  Stratospheric aerosol—Observations, processes, and impact on climate, Rev. Geophys., 54,
4  278-335, 10.1002/2015rg000511, 2016.
5
6  Krishnamurti, T. N., Jha, B., Rasch, P. J., and Ramanathan, V.: A high resolution global
7  reanalysis highlighting the winter monsoon, Part I, Reanalysis fields, Met. Atmos. Phys., 64,
8  123–150, 1997a.
9
10 Krishnamurti, T. N., Jha, B., Rasch, P. J., and Ramanathan, V.: A high resolution global
11 reanalysis highlighting the winter monsoon, Part II, transients and passive tracer transports,
12 Met. At- mos. Phys., 64, 151–171, 1997b.
13
14 Krishnan, R. et al.: Assessment of Climate Change over the Indian Region, Springer Singapore,
15 DOI 10.1007/978-981-15-4327-2, 2020.
16
17 Krom M. D., Shi Z., Stockdale A., Berman-Frank I., Giannakourou A., Herut B., Lagaria A.,
18 Papageorgiou N., Pitta P., Psarra S., Rahav E., Scoullos M., Stathopoulou E., Tsiola A., and
19 Tsagaraki T. M.: Response of the Eastern Mediterranean Microbial Ecosystem to Dust and Dust
20 Affected by Acid Processing in the Atmosphere, Frontiers in Marine Science, 3, 133
21 doi=10.3389/fmars.2016.00133, 2016.
22
23 Krotkov, N. A., McLinden, C. A., Li, C., Lamsal, L. N., Celarier, E. A., Marchenko, S. V.,
24 Swartz, W. H., Bucsela, E. J., Joiner, J., Duncan, B. N., Boersma, K. F., Veefkind, J. P., Levelt,
25 P. F., Fioletov, V. E., Dickerson, R. R., He, H., Lu, Z., and Streets, D. G.: Aura OMI
26 observations of regional $SO_2$ and $NO_2$ pollution changes from 2005 to 2015, Atmos. Chem.
27 Phys., 16, 4605-4629, 10.5194/acp-16-4605-2016, 2016.
28
29 Kuai, L., Worden, J. R., Campbell, J. E., Kulawik, S. S., Li, K.-F., Lee, M., Weidner, R. J.,
30 Montzka, S. A., Moore, F. L., Berry, J. A., Baker, I., Denning, A. S., Bian, H., Bowman, K.
31 W., Liu, J., and Yung, Y. L.: Estimate of carbonyl sulfide tropical oceanic surface fluxes using
32 Aura Tropospheric Emission Spectrometer observations, J. Geophys. Res., 120, 11012–11023,
33 https://doi.org/10.1002/2015JD023493, 2015.
34
35 Kumar, K.R., Tiwari, Y.K., Valsala, V., and R. Murtugudde: On understanding the land–ocean
36 $CO_2$ contrast over the Bay of Bengal: A case study during 2009 summer monsoon. Environ Sci
37 Pollut Res 21, 5066–5075, https://doi.org/10.1007/s11356-013-2386-2, 2014.
38
39 Kunhikrishnan, T., Lawrence, M. G., von Kuhlmann, R., Richter, A., Ladstaetter, A., and
40 Burrows, J. P.: Analysis of tropospheric NOx over Asia using the Model of Atmospheric
41 Transport and Chemistry (MATCH-MPIC) and GOME-satellite observations, Atmos.
42 Environ., 38, 581–596, 2004.
43
44 Lachkar, Z., Levy, M. and Smith, S.: Intensification and deepening of the Arabian Sea oxygen
45 minimum zone in response to increase in Indian monsoon wind intensity. Biogeosciences 15,
46 159–186, 2018.
47
48 Ladstätter-Weißenmayer, A., Altmeyer, H., Bruns, M., Richter, A., Rozanov, A., Rozanov, V.,
49 Wittrock, F., and Burrows, J. P.: Measurements of $O_3$, $NO_2$ and BrO during the INDOEX
50 campaign using ground based DOAS and GOME satellite data, Atmos. Chem. Phys., 7, 283-
51 291, 2007.

1
2   Lago, V., Wijffels, S.E., Durack, P.J., Church, J.A., Bindoff, N.L., and Marsland, S.J.:
3   Simulating the role of surface forcing on observed multidecadal upper-ocean salinity changes.
4   J. Clim., 29:5575–5588. https ://doi.org/10.1175/JCLI-D-15-0519.1, 2016.
5
6   Lal, S., Chand, D., Sahu, L. K., Venkataramani, S., Brasseur, G., and Schultz, M. G.: High
7   levels of ozone and related gases over the Bay of Bengal during winter and early spring of 2001,
8   Atmos. Environ., 40, 1633–1644, 2006.
9
10  Lal, S., Sahu, L. K., and Venkataramani, S.: Impact of trans- port from the surrounding
11  continental regions on the distributions of ozone and related trace gases over the Bay of Ben-
12  gal during February 2003, J. Geophys. Res., 112, D14302, doi:10.1029/2006JD008023, 2007.
13
14  Lal, S., Venkataramani, S., Chandra, N., Cooper, O. R., Brioude, J., and Naja, M.: Transport
15  effects on the vertical distribution of tropospheric ozone over western India, J. Geophys. Res.,
16  119, 10012-10026, 10.1002/2014jd021854, 2014.
17
18  Lamb, P. J., and Hastenrath, S., Climatic Atlas of the Indian Ocean: Surface Climate and
19  Atmospheric Circulation. Madison: The University of Wisconsin Press, 1979.
20
21  Lana, A., Bell, T. G., Simó, R., Vallina, S. M., Ballabrera-Poy, J., Kettle, A. J., Dachs, J., Bopp,
22  L., Saltzman, E. S., Stefels, J., Johnson, J. E., and Liss, P. S.: An updated climatology of surface
23  dimethlysulfide concentrations and emission fluxes in the global ocean, Global Biogeochem.
24  Cy., 25, 10.1029/2010gb003850, 2011.
25
26  Latif, M. and T.P. Barnett: Interactions of the Tropical Oceans. J. Climate, 8, 952–964,
27  https://doi.org/10.1175/1520-0442(1995)008<0952:IOTTO>2.0.CO;2, 1995.
28
29  Launois, T., Belviso, S., Bopp, L., Fichot, C. G., and Peylin, P.: A new model for the global
30  biogeochemical cycle of carbonyl sulfide; Part 1: Assessment of direct marine emissions with
31  an oceanic general circulation and biogeochemistry model, Atmos. Chem. Phys., 15, 2295-
32  2312, 10.5194/acp-15-2295-2015, 2015.
33
34  Lawrence, M. G., Rasch, P. J., von Kuhlmann, R., Williams, J., Fischer, H., de Reus, M.,
35  Lelieveld, J., Crutzen, P. J., Schultz, M.,Stier, P., Huntrieser, H., Heland, J., Stohl, A., Forster,
36  C., Elbern, H., Jakobs, H., and Dickerson, R. R.: Global chemical weather forecasts for field
37  campaign planning: predictions and observations of large-scale features during MINOS,
38  CONTRACE, and INDOEX, Atmos. Chem. Phys., 3, 267–289, doi:10.5194/acp-3- 267-2003,
39  2003.
40
41  Lawrence, M.G., Export of Air Pollution from Southern Asia and its Large-Scale Effects. In:
42  Stohl A. (eds) Air Pollution. The Handbook of Environmental Chemistry, vol 4G. Springer,
43  Berlin, Heidelberg, 2004.
44
45  Lawrence and Lelieveld, Atmospheric pollutants outflow from southern Asia: a review, Atmos.
46  Chem. Phys., 10, pp. 11017-11096, 2010.
47
48  Le Quéré, C., Andrew, R. M., Friedlingstein, P., Sitch, S., Hauck, J., Pongratz, J., Pickers, P.
49  A., Korsbakken, J. I., Peters, G. P., Canadell, J. G., Arneth, A., Arora, V. K., Barbero, L.,
50  Bastos, A., Bopp, L., Chevallier, F., Chini, L. P., Ciais, P., Doney, S. C., Gkritzalis, T., Goll,
51  D. S., Harris, I., Haverd, V., Hoffman, F. M., Hoppema, M., Houghton, R. A., Hurtt, G., Ilyina,

T., Jain, A. K., Johannessen, T., Jones, C. D., Kato, E., Keeling, R. F., Goldewijk, K. K., Landschützer, P., Lefèvre, N., Lienert, S., Liu, Z., Lombardozzi, D., Metzl, N., Munro, D. R., Nabel, J. E. M. S., Nakaoka, S., Neill, C., Olsen, A., Ono, T., Patra, P., Peregon, A., Peters, W., Peylin, P., Pfeil, B., Pierrot, D., Poulter, B., Rehder, G., Resplandy, L., Robertson, E., Rocher, M., Rödenbeck, C., Schuster, U., Schwinger, J., Séférian, R., Skjelvan, I., Steinhoff, T., Sutton, A., Tans, P. P., Tian, H., Tilbrook, B., Tubiello, F. N., van der Laan-Luijkx, I. T., van der Werf, G. R., Viovy, N., Walker, A. P., Wiltshire, A. J., Wright, R., Zaehle, S., and Zheng, B.: Global Carbon Budget 2018, Earth Syst. Sci. Data, 10, 2141-2194, 10.5194/essd-10-2141-2018, 2018.

Lee, C.-L., and Brimblecombe, P.: Anthropogenic contributions to global carbonyl sulfide, carbon disulfide and organosulfides fluxes, Earth-Sci. Rev., 160, 1-18, https://doi.org/10.1016/j.earscirev.2016.06.005, 2016.

Lee, S.-K., W. Park, M. O. Baringer, A. L. Gordon, B. Huber, and Y. Liu: Pacific origin of the abrupt increase in Indian Ocean heat content during the warming hiatus, Nat. Geosci., 8, 445–449, https://doi.org/10.1038/ngeo2438, 2015.

Legrand, M., McConnell, J. R., Preunkert, S., Arienzo, M., Chellman, N., Gleason, K., Sherwen, T., Evans, M. J. and Carpenter, L. J.: Alpine ice evidence of a three-fold increase in atmospheric iodine deposition since 1950 in Europe due to increasing oceanic emissions, Proc. Natl. Acad. Sci., 115(48), 12136–12141, doi:10.1073/pnas.1809867115, 2018.

Lelieveld, J., Evans, J. S., Fnais, M., Giannadaki, D., and Pozzer, A.: The contribution of outdoor air pollution sources to premature mortality on a global scale, Nature, 525, 367-371, 10.1038/nature15371, 2015.

Lelieveld, J., Crutzen, P. J., Ramanathan, V., Andreae, M. O., Bren- ninkmeijer, C. A. M., Campos, T., Cass, G. R., Dickerson, R. R., Fischer, H., de Gouw, J. A., Hansel, A., Jefferson, A., Kley, D., de Laat, A. T. J., Lal, S., Lawrence, M. G., Lobert, J. M., Mayol- Bracero, O. L., Mitra, A. P., Novakov, T., Oltmans, S. J., Prather, K. A., Reiner, T., Rodhe, H., Scheeren, H. A., Sikka, D., and Williams, J.: The Indian Ocean experiment: Widespread air pollution from South and Southeast Asia, Science, 291, 1031–1036, 2001.

Lelieveld, J., Bourtsoukidis, E., Brühl, C., Fischer, H., Fuchs, H., Harder, H., Hofzumahaus, A., Holland, F., Marno, D., Neumaier, M.,Pozzer, A., Schlager, H., Williams, J., Zahn, A., and Ziereis, H.: The South Asian monsoon – Pollution pump and purifier, Science, 361, 270–273, https://doi.org/10.1126/science.aar2501, 2018.

Lelieveld, J., K. Klingmüller, A. Pozzer, R.T. Burnett, A. Haines and V. Ramanathan: Effects of fossil fuel and total anthropogenic emission removal on public health and climate. Proc. Natl. Acad. Sci. USA, 116 (15), 7192-7197, doi:www.pnas.org/cgi/doi/10.1073/pnas.1819989116, 2019.

Lennartz, S. T., Marandino, C. A., von Hobe, M., Cortes, P., Quack, B., Simo, R., Booge, D., Pozzer, A., Steinhoff, T., Arevalo-Martinez, D. L., Kloss, C., Bracher, A., Röttgers, R., Atlas, E., and Krüger, K.: Direct oceanic emissions unlikely to account for the missing source of atmospheric carbonyl sulfide, Atmos. Chem. Phys., 17, 385–402, https://doi.org/10.5194/acp-17-385-2017, 2017.

Lennartz, S. T., Marandino, C. A., von Hobe, M., Andreae, M. O., Aranami, K., Atlas, E., Berkelhammer, M., Bingemer, H., Booge, D., Cutter, G., Cortes, P., Kremser, S., Law, C. S.,

1   Marriner, A., Simó, R., Quack, B., Uher, G., Xie, H., and Xu, X.: Marine carbonyl sulfide
2   (OCS) and carbon disulfide ($CS_2$): a compilation of measurements in seawater and the marine
3   boundary layer, Earth Syst. Sci. Data, 12, 591–609, https://doi.org/10.5194/essd-12-591-2020,
4   2020.
5
6   Levelt, P. F., van den Oord, G. H. J., Dobber, M. R., Malkki, A., Huib, V., Johan de, V.,
7   Stammes, P., Lundell, J. O. V., and Saari, H.: The ozone monitoring instrument, IEEE T.
8   Geosci. Remote Sens., 44, 1093–1101, https://doi.org/10.1109/tgrs.2006.872333, 2006.
9
10  Li, Z., Lau, W.K., Ramanathan, V., Wu, G., Ding, Y., Manoj, M.G., Liu, J., Qian, Y., Li, J.,
11  Zhou, T., Fan., J., Rosenfeld, D., Ming, Y., Wang, Y., Huang, J., Wang, B., Xu, X., Lee, S.-S.,
12  Cribb, M., Zhang, F., Yang, X., Zhao, C., Takemura, T., Wang, K., Xia, X., Yin, Y., Zhang,
13  H., Guo, J., Zhao, P., Sugimoto, N., Babu, S. S., and Brasseur, G. P.: Aerosol and monsoon
14  climate interactions over Asia, Rev. Geophys., 54, 866–929, 2016.
15
16  Li, M., Zhang, Q., Kurokawa, J.-I., Woo, J.-H., He, K., Lu, Z., Ohara, T., Song, Y., Streets, D.
17  G., Carmichael, G. R., Cheng, Y., Hong, C., Huo, H., Jiang, X., Kang, S., Liu, F., Su, H., and
18  Zheng, B.: MIX: a mosaic Asian anthropogenic emission inventory under the international
19  collaboration framework of the MICS-Asia and HTAP, Atmos. Chem. Phys., 17, 935–963,
20  https://doi.org/10.5194/acp-17-935-2017, 2017.
21
22  Li, T., Wang, B., Chang, C.P., and Y. Zhang: A theory for the Indian Ocean dipole–zonal
23  mode. J. Atmos. Sci., 60(17):2119–2135, 2003.
24
25  Li, Y., Han W., A. Hu, G. A. Meehl, and F. Wang: Multidecadal changes of the upper Indian
26  Ocean    heat    content    during   1965–2016.   J.   Climate,   31,   7863–7884,
27  https://doi.org/10.1175/JCLID-18-0116.1, 2018.
28
29  Liang, Q., Stolarski, R. S., Kawa, S. R., Nielsen, J. E., Douglass, A.R., Rodriguez, J. M., Blake,
30  D. R., Atlas, E. L., and Ott, L. E.: Finding the missing stratospheric $Br_y$: a global modeling
31  study of $CHBr_3$ and $CH_2Br_2$, Atmos. Chem. Phys., 10, 2269–2286, https://doi.org/10.5194/acp-
32  10-2269-2010, 2010.
33
34  Liu, X., Bhartia, P. K., Chance, K., Spurr, R. J. D., and Kurosu, T. P.: Ozone profile retrievals
35  from the Ozone Monitoring Instrument, Atmos. Chem. Phys., 10, 2521–2537,
36  https://doi.org/10.5194/acp-10-2521-2010, 2010.
37
38  Llovel, W. and Lee, T.: Importance and origin of halosteric contribution to sea level change in
39  the southeast Indian Ocean during 2005–2013. Geophys. Res. Lett., 42, 1148–1157, 2015.
40
41  Lombardozzi, D, Levis, S, Bonan, G, Hess, P. G. and Sparks, J. P.: The influence of chronic
42  ozone exposure on global carbon and water cycles. J. Climate, 28: 292–305. DOI:
43  10.1175/JCLI-D-14-00223.1, 2015.
44
45  Lunt, M. F., Palmer, P. I., Feng, L., Taylor, C. M., Boesch, H., and Parker, R. J.: An increase
46  in methane emissions from tropical Africa between 2010 and 2016 inferred from satellite data,
47  Atmos. Chem. Phys., 19, 14721–14740, https://doi.org/10.5194/acp-19-14721-2019, 2019.
48
49  Luo, G. and Yu, F.: A numerical evaluation of global oceanic emissions of a-pinene and
50  isoprene, Atmos. Chem. Phys., 10, 2007–2015, doi:10.5194/acp-10-2007-2010, 2010.
51

Atmospheric
Chemistry
and Physics
Discussions

1   Ma, X., Bange, H. W., Eirund, G. K., and Arévalo-Martínez, D. L.: Nitrous oxide and
2   hydroxylamine measurements in the Southwest Indian Ocean. J. Marine Syst.,
3   https://doi.org/10.1016/j.jmarsys.2018.03.003, 2018.
4
5   Maas, J., Jia, Y., Quack, B., Durgadoo, J. V., Biastoch, A., and Tegtmeier, S.: Simulations of
6   anthropogenic bromoform indicate high emissions at the coast of East Asia, Atmos. Chem.
7   Phys. Discuss., 2020, 1-31, 10.5194/acp-2019-1004, 2020.
8
9   Madden, R.A. and P.R. Julian: Description of Global-Scale Circulation Cells in the Tropics
10  with a 40–50 Day Period. J. Atmos. Sci., 29, 1109–1123, https://doi.org/10.1175/1520-
11  0469(1972)029<1109:DOGSCC>2.0.CO;2, 1972.
12
13  Mahajan, A. S., Plane, J. M. C., Oetjen, H., Mendes, L., Saunders, R. W., Saiz-Lopez, A., Jones,
14  C. E., Carpenter, L. J., and McFiggans, G. B.: Measurement and modelling of tropospheric
15  reactive halogen species over the tropical Atlantic Ocean, Atmos. Chem. Phys., 10, 4611–4624,
16  https://doi.org/10.5194/acp-10-4611-2010, 2010.
17
18  Mahajan, A. S., Tinel, L., Hulswar, S., Cuevas, C. A., Wang, S., Ghude, S., et al.: Observations
19  of iodine oxide in the Indian Ocean Marine Boundary Layer: a transect from the tropics to the
20  high latitudes, Atmos. Environ.: X. https://doi.org/10.1016/j.aeaoa.2019.100016, 2019a.
21
22  Mahajan, A. S., Tinel, L., Sarkar, A., Chance, R., Carpenter, L. J., Hulswar, S., et al.:
23  Understanding Iodine Chemistry over the Northern and Equatorial Indian Ocean. J. Geophys.
24  Res., (x), 0–3. https://doi.org/10.1029/2018JD029063, 2019b.
25
26  Mahajan, A.S., De Smedt, I., Biswas, M.S., Ghude, S.D., Fadnavis, S., Roy, C., van
27  Roozendael, M.: Inter-annual variations in satellite observations of nitrogen dioxide and
28  formaldehyde    over    India.    Atmos.    Environ.    116,    194–201.
29  https://doi.org/10.1016/j.atmosenv.2015.06.004, 2015a.
30
31  Mahajan, A. S., Fadnavis, S., Thomas, M. A., Pozzoli, L., Gupta, S., Royer, S., et al.:
32  Quantifying the impacts of an updated global dimethyl sulfide climatology on cloud
33  microphysics    and    aerosol    radiative    forcing.    J.    Geophys.    Res.,    120,    1–13.
34  https://doi.org/10.1002/2014JD022687, 2015b.
35
36  Mahowald, N. M., Hamilton, D. S., Mackey, K.R.M., Moore, J. K, Baker, A. R., Scanza, R. A.,
37  and Zhang, Y.: Aerosol trace metal leaching and impacts on marine microorganisms. Nat.
38  Commun., 9, 2614, https://doi.org/10.1038/s41467-018-04970-7, 2018.
39
40  Mallik, C., Lal, S., Venkataramani, S., Naja, M., and Ojha, N.: Variability in ozone and its
41  precursors over the Bay of Bengal during post-monsoon: Transport and emission effects. J.
42  Geophys. Res., https://doi.org/10.1002/jgrd.50764, 2013.
43
44  Mandal, T. K., Khan, A., Ahammed, Y. N., Tanwar, R. S., Parmar, R. S., Zalpuri, K. S., et al.:
45  Observations of trace gases and aerosols over the Indian Ocean during the monsoon transition
46  period. J. Earth Syst. Sci., 115(4), 473–484, 2006.
47
48  Manö, S., and Andreae, M. O.: Emission of Methyl Bromide from Biomass Burning, Science,
49  263, 1255-1257, 10.1126/science.263.5151.1255, 1994.
50

1    Martino, M., Mills, G. P., Woeltjen, J., and Liss, P. S.: A new source of volatile organoiodine
2    compounds in surface seawater, Geophys. Res. Lett., 36, L01609, doi:10.1029/2008GL036334,
3    2009.
4
5    Mason, R. P., and Sheu, G.-R.: Role of the ocean in the global mercury cycle, Global
6    Biogeochem. Cy., 16, 40-41-40-14, 10.1029/2001gb001440, 2002.
7
8    Matthews, A. J., Singhruck, P. and Heywood, K. J.: Ocean temperature and salinity components
9    of the Madden–Julian oscillation observed by Argo floats. Clim. Dynam., 35, 1149–1168,
10   https://doi.org/10.1007/s00382-009-0631-7, 2010.
11
12   Meehl, G. A., and J. M. Arblaster: Mechanisms for projected future changes in South Asian
13   monsoon precipitation. Clim. Dynam., 21, 659–675, https://doi.org/10.1007/s00382-003-0343-
14   3, 2003.
15
16   Meenu, S., Rajeev, K., Parameswaran, K., and Suresh Raju, C., Characteristics of the double
17   intertropical convergence zone over the tropical Indian Ocean, J. Geophys. Res., 112, D11106,
18   doi:10.1029/2006JD007950, 2007.
19
20   Mehlmann, M., Quack, B., Atlas, E., Hepach, H., and Tegtmeier, S.: Natural and anthropogenic
21   sources of bromoform and dibromomethane in the oceanographic and biogeochemical regime
22   of the subtropical North East Atlantic, Environ. Sci. Process. Impacts, 22, 679-707,
23   10.1039/c9em00599d, 2020.
24
25   Metzl, N.: Decadal increase of oceanic carbon dioxide in Southern Indian Ocean surface waters
26   (1991–2007), Deep Sea Res. Part II: Topical Studies in Oceanogr., 56, 607-619,
27   https://doi.org/10.1016/j.dsr2.2008.12.007, 2009.
28
29   Mihalopoulos, N., Putaud, J. P., Nguyen, B. C., and Belviso, S.: Annual variation of
30   atmospheric carbonyl sulfide in the marine atmosphere in the Southern Indian Ocean, J. Atmos.
31   Chem., 13, 73–82, https://doi.org/10.1007/bf00048101, 1991.
32
33   Mittermeier, R. A., Turner, W. R., Larsen, F. W., Brooks, T. M., Gascon, C.: Global
34   biodiversity conservation: the critical role of hotspots. Biodiversity hotspots, Berlin,
35   Heidelberg: Springer. pp. 3–22. doi:10.1007/978-3-642-20992-5, 2011.
36
37   Mohan, S. and Bhaskaran, P.K.: Evaluation of CMIP5 climate model projections for surface
38   wind speed over the Indian Ocean region. Clim. Dynam., 53(9-10), 5415–5435, 2019.
39
40   Monks, P. S., Carpenter, L. J., Penkett, S. A., Ayers, G. P., Gillett, R. W., Galbally, I. E., and
41   Meyer, C. P.: Fundamental ozone photochemistry in the remote marine boundary layer: The
42   SOAPEX experiment, measurement and theory. Atmos. Environ., 32(21), 3647-3664, 1998.
43
44   Monks, PS, Archibald, AT, Colette, A, Cooper, O, Coyle, M, Derwent, R, Fowler, D, Granier,
45   C, Law, KS, Mills, GE, Stevenson, DS, Tarasova, O, Thouret, V, von Schneidemesser, E,
46   Sommariva, R, Wild, O and Williams, ML.: Tropospheric ozone and its precursors from the
47   urban to the global scale from air quality to short-lived climate forcer. Atmos. Chem. Phys . 15:
48   8889–8973. DOI: 10.5194/acp-15-8889-2015, 2015.
49

1  Moorthy, K. K., Satheesh, S. K., Babu, S. S., and Dutt, C. B. S.: Integrated Campaign for
2  Aerosols, gases and Radiation Budget (ICARB): An overview, J. Earth Syst. Sci., 117, 243-
3  262, 10.1007/s12040-008-0029-7, 2008.
4
5  Mungall, E. L., J. P. D. Abbatt, J. J. B. Wentzell, A. K. Y. Lee, J. L. Thomas, M. Blais, M.
6  Gosselin, L. A. Miller, T. Papakyriakou, M. D. Willis, and J. Liggio: OVOCs in the
7  summertime marine Arctic atmosphere, Proceedings of the National Academy of Sciences, 114
8  (24) 6203-6208; DOI: 10.1073/pnas.1620571114, 2017.
9
10 Nair, P. R., David, L. M., Girach, I. A., and George, S. K.: Ozone in the marine boundary layer
11 of Bay of Bengal during post-winter period: Spatial pattern and role of meteorology, Atmos.
12 Environ., 45, 4671–4681, 2011.
13
14 Naja, M., Chand, D., Sahu, L., and Lal, S.: Trace gases over marine regions around India, Indian
15 J. Mar. Sci., 33, 95–106, 2004.
16
17 Nalini, K., Uma, K. N., Sijikumar, S., Tiwari, Y. K., and Ramachandran, R.: Satellite- and
18 ground-based measurements of $CO_2$ over the Indian region: its seasonal dependencies, spatial
19 variability,    and    model    estimates,    Int.    J.    Remote    Sens.,    39,    7881-7900,
20 10.1080/01431161.2018.1479787, 2018.
21
22 Naqvi, S. W. A., Jayakumar, D. A., Nair, M., Kumar, M. D., and George, M. D.: Nitrous oxide
23 in the western Bay of Bengal, Marine Chem., 47, 269-278, https://doi.org/10.1016/0304-
24 4203(94)90025-6, 1994.
25
26 Naqvi, S. W. A., Bange, H. W., Gibb, S. W., Goyet, C., Hatton, A. D., and Upstill-Goddard, R.
27 C.: Biogeochemical ocean-atmosphere transfers in the Arabian Sea, Progress Oceanogr, 65,
28 116-144, https://doi.org/10.1016/j.pocean.2005.03.005, 2005.
29
30 Naqvi, S. W. A., Jayakumar, D.A., Narvekar, P. V., Naik, H., Sarma, V. V. S. S., D'Souza, W.,
31 Joseph, S., George, M. D.: Marine hypoxia/anoxia as a source of $CH_4$ and $N_2O$, Biogeosciences
32 7, 2159–2190, 2010a.
33
34 Naqvi, S. W. A., Naik, H., D'Souza, W., Narvekar, P. V., Paropkari, A. L., and Bange, H. W.:
35 Carbon and nitrogen fluxes in the northern Indian Ocean. In: Liu, K.-K., Atkinson, L.,
36 Quiñones, R., Talaue-McManus, L. (Eds.), Carbon and Nutrient Fluxes in Continental Margins:
37 A Global Synthesis. Springer-Verlag, New York, pp. 180–191, 2010b.
38
39 Nayak, R. K., Dadhwal, V. K., Majumdar, A., Patel, N. R., and Dutt, C. B. S.: Variability of
40 atmospheric CO2 over India and Surrounding Oceans and control by Surface Fluxes, Int. Arch.
41 Photogramm. Remote Sens. Spatial Inf. Sci., XXXVIII-8/W20, 96-101, 10.5194/isprsarchives-
42 XXXVIII-8-W20-96-2011, 2011.
43
44 Nieves, V., J. K. Willis, and W. C. Patzert: Recent hiatus caused by decadal shift in Indo-Pacific
45 heating. Science, 349, 532–535, https://doi.org/10.1126/science.aaa4521, 2015.
46
47 Norman, M. and Leck, C.: Distribution of marine boundary layer ammonia over the Atlantic
48 and Indian Ocean during the Aerosols 99 cruise, J. Geophys. Res., 110, D16302,
49 doi:10.1029/2005JD005866, 2005.
50

1   Nowak, J.B., et al.: Gas-phase chemical characteristics of Asian emission plumes observed
2   during ITCT 2K2 over the eastern North Pacific Ocean, J. Geophys. Res. 109, D23S19.
3   doi:10.1029/2003JD004488, 2004.

5   Oetjen, H.: Measurements of halogen oxides by scattered sunlight differential optical
6   absorption spectroscopy, University of Bremen, 2009.

8   Ohara, T., Akimoto, H., Kurokawa, J., Horii, N., Yamaji, K., Yan, X., and Hayasaka, T.: An
9   Asian emission inventory of anthropogenic emission sources for the period 1980–2020, Atmos.
10  Chem. Phys., 7, 4419–4444, https://doi.org/10.5194/acp-7-4419-2007, 2007.

12  Pacyna, J. M., Pacyna, E. G.: Anthropogenic sources and global inventory of mercury
13  emissions. In: Parsons, M.B., Percival, J.B. (Eds.), Mercury: Sources, Measurements, Cycles,
14  and Effects. Short Course Series, vol. 32. Mineralogical Association of Canada, 2005.

16  Palastanga, V., van Leeuwen, P. J., Schouten, M. W., and de Ruijter, W. P. M.: Flow structure
17  and variability in the subtropical Indian Ocean: Instability of the South Indian Ocean
18  Countercurrent, J. Geophys. Res., 112, C01001, doi:10.1029/2005JC003395, 2007.

20  Palmer, P. I., and Shaw, S. L.: Quantifying global marine isoprene fluxes using MODIS
21  chlorophyll observations, Geophys. Res. Lett., 32, 10.1029/2005gl022592, 2005.

23  Pandey, P. C., Khare, N., and Sudhakar, M.: Oceanographic research: Indian efforts and
24  preliminary results from the Southern Ocean, Current Sci., 90, 978-984, 2006.

26  Pant, V., Deshpande, C. G., and Kamra, A. K.: The concentration and number size distribution
27  measurements of the Marine Boundary Layer aerosols over the Indian Ocean, Atmos. Res., 92,
28  381–393, 2009.

30  Pathak, H., Li, C., and Wassmann, R.: Greenhouse gas emissions from Indian rice fields:
31  calibration and upscaling using the DNDC model, Biogeosciences, 2, 113-123, 10.5194/bg-2-
32  113-2005, 2005.

34  Paytan, A., K. R. M. Mackey, Y. Chen, I. D. Lima, S. C. Doney, N. Mahowald, R. Labiosa, A.
35  F. Post: Toxicity of atmospheric aerosols on marine phytoplankton, Proc. Natl. Acad. Sci. USA,
36  106 (12) 4601-4605; DOI: 10.1073/pnas.0811486106, 2009.

38  Peters, G.P., Andrew, R.M., Canadell, J.G. et al.: Carbon dioxide emissions continue to grow
39  amidst slowly emerging climate policies. Nat. Clim. Chang. 10, 3–6,
40  https://doi.org/10.1038/s41558-019-0659-6, 2020.

42  Pfannerstill, E. Y., Wang, N., Edtbauer, A., Bourtsoukidis, E., Crowley, J. N., Dienhart, D.,
43  Eger, P. G., Ernle, L., Fischer, H., Hottmann, B., Paris, J.-D., Stönner, C., Tadic, I., Walter, D.,
44  Lelieveld, J., and Williams, J.: Shipborne measurements of total OH reactivity around the
45  Arabian Peninsula and its role in ozone chemistry, Atmos. Chem. Phys., 19, 11501–11523,
46  https://doi.org/10.5194/acp-19-11501-2019, 2019.

48  Portmann, R.W., J.S. Daniel, and A.R. Ravishankara: Stratospheric ozone depletion due to
49  nitrous oxide: influences of other gases. Philosophical Transactions of the Royal Society
50  London B Biological Sciences 367 (1593): 1256–1264. https://doi.org/10.1098/rstb.2011.0377,
51  2012.

1

2   Prasanna Kumar, S., Muraleedharan, P. M., Prasad, T. G., Gauns, M., Ramaiah, N., de Souza,
3   S. N., Sardesai, S., and Madhupratap, M.: Why is the Bay of Bengal less productive during
4   summer monsoon compared to the Arabian Sea? Geophys. Res. Lett., 29(24), 2235,
5   doi:10.1029/2002GL016013, 2002.

6

7   Prather, M., C. Holmes, and J. Hsu: Reactive greenhouse gas scenarios: Systematic exploration
8   of uncertainties and the role of atmospheric chemistry. Geophys. Res. Lett., 39, L09803, 2012.

9

10  Prather, M. J., Hsu, J., DeLuca, N. M., Jackman, C. H., Oman, L. D., Douglass, A. R., Fleming,
11  E. L., Strahan, S. E., Steenrod, S. D., Søvde, O. A., Isaksen, I. S. A., Froidevaux, L., and Funke,
12  B: Measuring and modeling the lifetime of nitrous oxide including its variability. J. Geophys.
13  Res., 120, 5693– 5705. doi: 10.1002/2015JD023267, 2015.

14

15  Quack, B., Atlas, E., Petrick, G., and Wallace, D.: Bromoform and dibromomethane above the
16  Mauritanian upwelling: Atmospheric distributions and oceanic emissions, J. Geophys.
17  Res.,112, D09312, doi:10.1029/2006JD007614, 2007.

18

19  Quartly, G. D., J. J. H. Buck, M. A. Srokosz, and A. C. Coward: Eddies around Madagascar—
20  The retroflection reconsidered, J. Mar. Syst., 63(3–4), 115–129,
21  doi:10.1016/j.jmarsys.2006.06.001, 2006.

22

23  Quinn, P. K., Coffman, D. J., Johnson, J. E., Upchurch, L. M., and Bates, T. S.: Small fraction
24  of marine cloud condensation nuclei made up of sea spray aerosol. Nat. Geosci., 10(9), 674–
25  679, 2017.

26

27  Raes, E. J., Bodrossy, L., Van de Kamp, J., Holmes, B., Hardman-Mountford, N., Thompson,
28  P. A., McInnes, A. S., and Waite, A. M.: Reduction of the Powerful Greenhouse Gas $N_2O$ in
29  the South-Eastern Indian Ocean, PLOS ONE, 11, e0145996, 10.1371/journal.pone.0145996,
30  2016.

31

32  Rahav, E., Belkin, N., Paytan, A., and Herut, B.: Phytoplankton and Bacterial Response to
33  Desert Dust Deposition in the Coastal Waters of the Southeastern Mediterranean Sea: A Four-
34  Year In Situ Survey. Atmosphere, 9, 305, 2018.

35

36  Rajak, R. and Chattopadhyay, A., Short and long-term exposure to ambient air pollution and
37  impact on health in India: a systematic review, Int. J. Environ. Health Res.,
38  10.1080/09603123.2019.1612042, 2019.

39

40  Ramanathan, V., Crutzen, P. J., Mitra, A. P., and Sikka, D.: The Indian Ocean Experiment and
41  the Asian Brown Cloud, Curr. Sci. India, 83, 947–955, 2002.

42

43  Ramanathan, V., C. Chung, D. Kim, T. Bettge, L. Buja, J. T. Kiehl, W. M. Washington, Q. Fu,
44  D. R. Sikka, M. Wild: Atmospheric brown clouds: Impacts on South Asian climate and
45  hydrological cycle, Proc. Natl. Acad. Sci. USA, 102 (15) 5326-5333; DOI:
46  10.1073/pnas.0500656102, 2005.

47

48  Randel, W. J., Park, M., Emmons, L., Kinnison, D., Bernath, P., Walker, K. A., Boone, C., and
49  Pumphrey, H.: Asian monsoon transport of pollution to the stratosphere, Science, 328, 611–
50  613, doi:10.1126/science.1182274, 2010.

51

1  Rao, S.A., Dhakate, A.R., Saha, S.K., Mahapatra, S., Chaudhari, H.S., Pokhrel, S., and Sahu,
2  S. K.: Why is Indian Ocean warming consistently? Clim. Change 110:709–719,
3  doi.org/10.1007/s1058 4-011-0121-x, 2012.
4
5  Rao, R. R., and Sivakumar, R.: Seasonal variability of sea surface salinity and salt budget of
6  the mixed layer of the north Indian Ocean, J. Geophys. Res., 108(C1), 3009,
7  doi:10.1029/2001JC000907, 2003.
8
9  Raut, N., B. K. Sitaula, L. R. Bakken, R. M. Bajracharya, and P. Dörsch.: Higher $N_2O$ emission
10 by intensified crop production in South Asia. Global Ecology and Conservation 4:176–84.
11 doi:10.1016/j.gecco.2015.06.004, 2015.
12
13 Ravishankara, A., J. S. Daniel, and R. W. Portmann: Nitrous oxide ($N_2O$): The dominant ozone-
14 depleting substance emitted in the 21st century, Science, 326(5949), 123–125,
15 doi:10.1126/science.1176985, 2009.
16
17 Rayman, M. P.: The importance of selenium to human health. Lancet, 356, 233–241, 2000.
18
19 Read, K., A. Mahajan, L. Carpenter, M. J. Evans, B. V. E. Faria, D. E. Heard, J. R. Hopkins, J.
20 D. Lee, S. J. Moller, A. C. Lewis, L. Mendes, J. B. McQuaid, H. Oetjen, A. Saiz-Lopez, M. J.
21 Pilling, and J. M. C. Plane: Extensive halogen-mediated ozone destruction over the tropical
22 Atlantic Ocean. Nature 453, 1232–1235, https://doi.org/10.1038/nature07035, 2008.
23
24 Reppin, J., F. Schott, and J. Fischer: Equatorial currents and transports in the upper central
25 Indian Ocean: Annual cycle and interannual variability, J. Geophys. Res., 104(C7), 15,495 –
26 15,514, 1999.
27
28 Richter, U. and Wallace, D. W. R.: Production of methyl iodide in the tropical Atlantic Ocean,
29 Geophys. Res. Lett., 31(23), 2004.
30
31 Richter, I., and S.P. Xie: Muted precipitation increase in global warming simulations: a surface
32 evaporation perspective. J. Geophys. Res., 113:D24118, doi.org/10.1029/2008J D0105 61,
33 2008.
34
35 Ridderinkhof, H., and W. P. M. de Ruijter: Moored current observations in the Mozambique
36 Channel, Deep Sea Res. Part II, 50, 1933–1955, 2003.
37
38 Rixen, T., Goyet, C., and Ittekkot, V.: Diatoms and their influence on the biologically mediated
39 uptake of atmospheric $CO_2$ in the Arabian Sea upwelling system, Biogeosciences, 3, 1–13,
40 https://doi.org/10.5194/bg-3-1-2006, 2006.
41
42 Rodríguez-Ros, P., Cortés, P., Robinson, C. M., Nunes, S., Hassler, C., Royer, S. J., Estrada,
43 M., Sala, M. M. and Simó, R.: Distribution and drivers of marine isoprene concentration across
44 the Southern Ocean, Atmosphere (Basel)., 11(6), 1–19, doi:10.3390/atmos11060556, 2020.
45
46 Roxy, M. K., Raghu Murtugudde, A. M., Valsala, V., Panickal, S., Prasanna Kumar, S.,
47 Ravichandran, M., et al.: A reduction in marine primary productivity driven by rapid warming
48 over the tropical Indian Ocean. Geophys. Res. Lett., 43, 826–833. doi: 10.1002/2015gl066979,
49 2016.
50

1  Roxy M. K., Ritika K., Terray P., Murtugudde R., Ashok K., Goswami B. N.: Drying of Indian
2  subcontinent by rapid Indian Ocean warming and a weakening land-sea thermal gradient, Nat.
3  Commun., 6:7423. doi.org/10.1038/ncomm s8423, 2015.
4
5  Roxy, M. K., Ritika, K., Terray, P. and Masson, S.: The curious case of Indian Ocean warming.
6  J. Clim. 27, 8501–8509, 2014.
7
8  Roy, R., Pratihary, A., Narvenkar, G., Mochemadkar, S., Gauns, M., and Naqvi, S. W. A.: The
9  relationship between volatile halocarbons and phytoplankton pigments during a
10 Trichodesmium bloom in the coastal eastern Arabian Sea, Estuarine, Coastal and Shelf Science,
11 95, 110-118, https://doi.org/10.1016/j.ecss.2011.08.025, 2011.
12
13 Saha A., Ghosh S., Sahana A. S., and E. P. Rao: Failure of CMIP5 climate models in simulating
14 post-1950 decreasing trend of Indian monsoon, Geophys. Res. Lett., 41:7323–7330.
15 doi.org/10.1002/2014G L0615 73, 2014.
16
17 Sahu, L.K., Lal, S., and Venkataramani, S.: Distributions of $O_3$, CO and hydrocarbons over the
18 Bay of Bengal: a study to assess the role of transport from southern India and marine regions
19 during September-October 2002, Atmos. Environ., 40, 4633–4645, 2006.
20
21 Saiz-Lopez, A., Fernandez, R. P., Ordóñez, C., Kinnison, D. E., Gómez Martín, J. C.,
22 Lamarque, J.-F. and Tilmes, S.: Iodine chemistry in the troposphere and its effect on ozone,
23 Atmos. Chem. Phys., 14(23), 13119–13143, doi:10.5194/acp-14-13119-2014, 2014.
24
25 Saiz-Lopez, A., Baidar, S., Cuevas, C. A., Koenig, T. K., Fernandez, R. P., Dix, B., Kinnison,
26 D. E., Lamarque, J., Rodriguez-Lloveras, X., Campos, T. L. and Volkamer, R.: Injection of
27 iodine to the stratosphere, Geophys. Res. Lett., 42, 6852–6859, doi:10.1002/2015GL064796,
28 2015.
29
30 Saji, N. H., Goswami, B. N., Vinayachandran, P. N., and Yamagata, T.: A dipole mode in the
31 tropical Indian Ocean, Nature, volume 401, 360–363, 1999.
32
33 Sánchez-Pérez, E. D., Marín, I., Nunes, S., Fernández-González, L., Peters, F., Pujo-Pay, M.,
34 Conan, P., Marrasé, C.: Aerosol inputs affect the optical signatures of dissolved organic matter
35 in NW Mediterranean coastal waters, Scientia Marina 80(4), 437-446,
36 https://doi.org/10.3989/scimar.04318.20B, 2016.
37
38 Sardessai, S., Ramaiah, N., Prasanna Kumar, S. and de Sousa, S. N.: Influence of environmental
39 forcings on the seasonality of dissolved oxygen and nutrients in the Bay of Bengal, J. Marine
40 Res., 65, 301–316, 2007.
41
42 Sarma, V. V. S. S., Kumar, N. A., Prasad, V. R., Venkataramana, V., Appalanaidu, S., Sridevi,
43 B., Kumar, B. S. K., Bharati, M. D., Subbaiah, C. V., Acharyya, T., Rao, G. D., Viswanadham,
44 R., Gawade, L., Manjary, D. T., Kumar, P. P., Rajeev, K., Reddy, N. P. C., Sarma, V. V.,
45 Kumar, M. D., Sadhuram, Y., and Murty, T. V. R.: High CO2 emissions from the tropical
46 Godavari estuary (India) associated with monsoon river discharges, Geophys. Res. Lett., 38,
47 10.1029/2011gl046928, 2011.
48
49 Saunois, M., Bousquet, P., Poulter, B., Peregon, A., Ciais, P., Canadell, J. G., Dlugokencky, E.
50 J., Etiope, G., Bastviken, D., Houweling, S., Janssens-Maenhout, G., Tubiello, F. N., Castaldi,
51 S., Jackson, R. B., Alexe, M., Arora, V. K., Beerling, D. J., Bergamaschi, P., Blake, D. R.,

Brailsford, G., Brovkin, V., Bruhwiler, L., Crevoisier, C., Crill, P., Covey, K., Curry, C., Frankenberg, C., Gedney, N., Höglund-Isaksson, L., Ishizawa, M., Ito, A., Joos, F., Kim, H. S., Kleinen, T., Krummel, P., Lamarque, J. F., Langenfelds, R., Locatelli, R., Machida, T., Maksyutov, S., McDonald, K. C., Marshall, J., Melton, J. R., Morino, I., Naik, V., O'Doherty, S., Parmentier, F. J. W., Patra, P. K., Peng, C., Peng, S., Peters, G. P., Pison, I., Prigent, C., Prinn, R., Ramonet, M., Riley, W. J., Saito, M., Santini, M., Schroeder, R., Simpson, I. J., Spahni, R., Steele, P., Takizawa, A., Thornton, B. F., Tian, H., Tohjima, Y., Viovy, N., Voulgarakis, A., van Weele, M., van der Werf, G. R., Weiss, R., Wiedinmyer, C., Wilton, D. J., Wiltshire, A., Worthy, D., Wunch, D., Xu, X., Yoshida, Y., Zhang, B., Zhang, Z., and Zhu, Q.: The global methane budget 2000–2012, Earth Syst. Sci. Data, 8, 697-751, 10.5194/essd-8-697-2016, 2016.

Savoie, D.L., and Prospero, J.M.: Comparison of oceanic and continental sources of non-sea-salt sulphate over the Pacific Ocean, Nature, 339, 685–687, 1989.

Sciare, J., Mihalopoulos, N., Dentener, F. J., and Sciare, L.: Interannual variability of atmospheric dimethylsulfide in the southern Indian Ocean. J. Geophys. Res., 105(D21), 26369–26377, 2000.

Schott, F., and J. P. McCreary, The monsoon circulation of the Indian Ocean, Prog. Oceanogr., 51, 1– 123, 2001.

Schott, F. A., Xie, S.-P., and McCreary, J. P., Indian Ocean circulation and climate variability, Rev. Geophys., 47, RG1002, doi:10.1029/2007RG000245, 2009.

Schouten, M. W., W. P. M. de Ruijter, P. J. van Leeuwen, and H. Ridderinkhof: Eddies and variability in the Mozambique Channel, Deep Sea Res. Part II, 50, 1987–2003, 2003.

Seinfeld, J. H., and S. N. Pandis: Atmospheric Chemistry and Physics: From Air Pollution to Climate Change, 2nd ed., John Wiley&Sons, 2006.

Selin, N. E., Jacob, D. J., Park, R. J., Yantosca, R. M., Strode, S., Jaeglé, L., and Jaffe, D.: Chemical cycling and deposition of atmospheric mercury: Global constraints from observations, J. Geophys. Res., 112, D02308, doi:10.1029/2006JD007450, 2007.

Sharma, S. K., Singh, A. K., Saud, T., Mandal, T. K., Saxena, M., Singh, S., et al.: Measurement of ambient $NH_3$ over Bay of Bengal during W-ICARB campaign. Annales Geophysicae, 30(2), 371–377, https://doi.org/10.5194/angeo-30-371-2012, 2012.

Shaw, S. L., Chisholm, S. W., and Prinn, R. G.: Isoprene production by Prochlorococcus, a marine cyanobacterium, and other phytoplankton, Mar. Chem., 80, 227–245, doi:10.1016/S0304-4203(02)00101-9, 2003.

Shechner, M. and Tas, E.: Ozone Formation Induced by the Impact of Reactive Bromine and Iodine Species on Photochemistry in a Polluted Marine Environment, Environ. Sci. Technol., 51, 24, 14030–14037, https://doi.org/10.1021/acs.est.7b02860, 2017.

Siedler, G., M. Rouault, and J. R. E. Lutjeharms: Structure and origin of the subtropical South Indian Ocean Countercurrent, Geophys. Res. Lett., 33, L24609, doi:10.1029/2006GL027399, 2006.

1   Singh, A., Ramesh, R.: Environmental controls on new and primary production in the northern
2   Indian ocean. Prog. Oceanogr. 131, 138–145, 2015.
3
4   Singh D., Ghosh S., Roxy M. K., and McDermid, S.: Indian summer monsoon: extreme events,
5   historical changes, and role of anthropogenic forcings. Wiley Interdisc. Rev. Clim. Change,
6   doi. org/10.1002/wcc.571, 2019a.
7
8   Singh, K., Panda, J., and Kant, S.: A study on variability in rainfall over India contributed by
9   cyclonic disturbances in warming climate scenario, Int. J. Climatology, doi: 10.1002/joc.6392,
10  2019b.
11
12  Singh, K., Panda, J., Osuri, K.K. and Vissa, N.K.: Progress in tropical cyclone predictability
13  and present status in the North Indian Ocean region. In: Lupo, A.R. (Ed.) Tropical Cyclone
14  Dynamics, Prediction, and Detection. London: Intech Open, https://doi.org/10.5772/64333,
15  2016.
16
17  Simpson, M. D. and Raman, S.: Role of the land plume in the transport of ozone over the ocean
18  during INDOEX (1999), Bound. Lay. Meteorol., 111, 133–152, 2004.
19
20  Sprovieri, F., Pirrone, N., Bencardino, M., D'Amore, F., Carbone, F., Cinnirella, S., Mannarino,
21  V., Landis, M., Ebinghaus, R., Weigelt, A., Brunke, E.-G., Labuschagne, C., Martin, L.,
22  Munthe, J., Wängberg, I., Artaxo, P., Morais, F., Barbosa, H. D. M. J., Brito, J., Cairns, W.,
23  Barbante, C., Diéguez, M. D. C., Garcia, P. E., Dommergue, A., Angot, H., Magand, O., Skov,
24  H., Horvat, M., Kotnik, J., Read, K. A., Neves, L. M., Gawlik, B. M., Sena, F., Mashyanov, N.,
25  Obolkin, V., Wip, D., Feng, X. B., Zhang, H., Fu, X., Ramachandran, R., Cossa, D., Knoery,
26  J., Maruszak, N., Nerentorp, M., and Norstrom, C.: Atmospheric mercury concentrations
27  observed at ground-based monitoring sites globally distributed in the framework of the GMOS
28  network, Atmos. Chem. Phys., 16, 11915–11935, https://doi.org/10.5194/acp-16-11915-2016,
29  2016.
30
31  Srivastava, S., Lal, S., Venkataramani, S., Gupta, S., and Acharya, Y. B.: Vertical distribution
32  of ozone in the lower troposphere over the Bay of Bengal and the Arabian Sea during ICARB-
33  2006: Effects of continental outflow, J. Geophys. Res., 116, D13301,
34  doi:10.1029/2010JD015298, 2011.
35
36  Srivastava, S., Lal, S., Venkataramani, S., Gupta, S., and Sheel, V.: Surface distributions of $O_3$,
37  CO and hydrocarbons over the Bay of Bengal and the Arabian Sea during pre-monsoon season,
38  Atmospheric Environment, 47, 459-467, https://doi.org/10.1016/j.atmosenv.2011.10.023,
39  2012a.
40
41  Srivastava, S. Lal, S. Venkataramani, S., Guha, I., and Bala Subrahamanyam, D.: Airborne
42  measurements of $O_3$, CO, $CH_4$ and NMHCs over the Bay of Bengal during winter, Atmos.
43  Environ., 59, 2012, 597-609, https://doi.org/10.1016/j.atmosenv.2012.04.054, 2012b.
44
45  Stemmler, I., Hense, I., and Quack, B.: Marine sources of bromoform in the global open ocean
46  – global patterns and emissions, Biogeosciences, 12, 1967–1981, https://doi.org/10.5194/bg-
47  12-1967-2015, 2015.
48
49  Streets, D. G., Hao, J., Wu, Y., Jiang, J., Chan, M., Tian, H., and Feng, X.: Anthropogenic
50  mercury emissions in China, Atmos. Environ., 39, 7789-7806,
51  https://doi.org/10.1016/j.atmosenv.2005.08.029, 2005.

1
2  Stuecker, M. F., Timmermann, A., Jin, F. F., Chikamoto, Y., Zhang, W., Wittenberg, A. T.,
3  Widiasih, E., and Zhao, S., Revisiting ENSO/Indian Ocean Dipole phase relationships.
4  Geophys. Res. Lett., 44, 2481–2492. https://doi.org/10.1002/2016GL072308, 2017.
5
6  Sudheesh, V., Gupta, G. V. M., Sudharma, K. V., Naik, H., Shenoy, D. M., Sudhakar, M., and
7  Naqvi, S. W. A.: Upwelling intensity modulates N2O concentrations over the western Indian
8  shelf, J. Geophys. Res., 121, 8551-8565, 10.1002/2016jc012166, 2016.
9
10  Suntharalingam, P., Kettle, A. J., Montzka, S. M., and Jacob, D. J.: Global 3-D model analysis
11  of the seasonal cycle of atmospheric carbonyl sulfide: Implications for terrestrial vegetation
12  uptake, Geophys. Res. Lett., 35, 10.1029/2008gl034332, 2008.
13
14  Suntharalingam, P., Zamora, L. M., Bange, H. W., Bikkina, S., Buitenhuis, E., Kanakidou, M.,
15  Lamarque, J.-F., Landolfi, A., Resplandy, L., Sarin, M. M., Seitzinger, S., and Singh, A.:
16  Anthropogenic nitrogen inputs and impacts on oceanic N2O fluxes in the northern Indian
17  Ocean: The need for an integrated observation and modelling approach, Deep Sea Research
18  Part II: Topical Studies in Oceanogr., 166, 104-113, https://doi.org/10.1016/j.dsr2.2019.03.007,
19  2019.
20
21  Surratt, J. D., Chan, A. W. H., Eddingsaas, N. C., Chan, M., Loza, C. L., Kwan, A. J., Hersey,
22  S. P., Flagan, R. C., Wennberg, P. O., and Seinfeld, J. H.: Reactive intermediates revealed in
23  secondary organic aerosol formation from isoprene, Proc. Natl. Acad. Sci., 107, 6640-6645,
24  10.1073/pnas.0911114107, 2010.
25
26  Swapna P., Krishnan R., and Wallace J.: Indian ocean and monsoon coupled interactions in a
27  warming environment, Clim. Dynam., 42 (2014), pp. 2439-2454, 2014.
28
29  Tadic, I., Crowley, J. N., Dienhart, D., Eger, P., Harder, H., Hottmann, B., Martinez, M.,
30  Parchatka, U., Paris, J.-D., Pozzer, A., Rohloff, R., Schuladen, J., Shenolikar, J., Tauer, S.,
31  Lelieveld, J., and Fischer, H.: Net ozone production and its relationship to NOx and VOCs in
32  the marine boundary layer around the Arabian Peninsula, Atmos. Chem. Phys. Discuss.,
33  https://doi.org/10.5194/acp-2019-1031, in review, 2019.
34
35  Tegtmeier, S., Krüger, K., Quack, B., Atlas, E. L., Pisso, I., Stohl, A., and Yang, X.: Emission
36  and transport of bromocarbons: from the West Pacific ocean into the stratosphere, Atmos.
37  Chem. Phys., 12, 10633–10648, https://doi.org/10.5194/acp-12-10633-2012, 2012.
38
39  Tegtmeier, S., Atlas, E., Quack, B., Ziska, F., and Krüger, K.: Variability and past long-term
40  changes of brominated very short-lived substances at the tropical tropopause, Atmos. Chem.
41  Phys., 20, 7103–7123, https://doi.org/10.5194/acp-20-7103-2020, 2020.
42
43  Tian, H., et al., Global methane and nitrous oxide emissions from terrestrial ecosystems due to
44  multiple environmental changes. Ecosyst. Health, 1(1):4. http://dx.doi.org/10.1890/EHS14-
45  0015.1, 2015.
46
47  Toihir, Abdoulwahab M. et al. Studies on CO variation and trends over South Africa and the
48  Indian Ocean using TES satellite data. S. Afr. j. sci, 111, 9-10, 01-09,
49  http://dx.doi.org/10.17159/SAJS.2015/20140174, 2015.
50

1   Tomsche, L., Pozzer, A., Ojha, N., Parchatka, U., Lelieveld, J., and Fischer, H.: Upper
2   tropospheric $CH_4$ and CO affected by the South Asian summer monsoon during the Oxidation
3   Mechanism Observations mission, Atmos. Chem. Phys., 19, 1915–1939,
4   https://doi.org/10.5194/acp-19-1915-2019, 2019.
5
6   Tokarczyk, R. and Moore, R. M.: Production of volatile organohalo- gens by phytoplankton
7   cultures, Geophys. Res. Lett., 21, 285– 288, https://doi.org/10.1029/94GL00009, 1994.
8
9   Tournadre, J.: Anthropogenic pressure on the open ocean: The growth of ship traffic revealed
10  by altimeter data analysis, Geophys. Res. Lett., 41, 7924-7932, 10.1002/2014gl061786, 2014.
11
12  Tripathi, N., Sahu, L. K., Singh, A., Yadav, R. and Karati, K. K.: High Levels of Isoprene in
13  the Marine Boundary Layer of the Arabian Sea during Spring Inter-Monsoon: Role of
14  Phytoplankton Blooms, ACS Earth Sp. Chem., 4(4), 583–590,
15  doi:10.1021/acsearthspacechem.9b00325, 2020.
16
17  UN-Environment, 2019. Global Mercury Assessment 2018. UN-Environment Programme,
18  Chemicals and Health Branch, Geneva, Switzerland. 59 pp., 2019.
19
20  Van Damme, M., Clarisse, L., Whitburn, S., Hadji-Lazaro, J., Hurtmans, D., Clerbaux, C., and
21  Coheur, P.-F.: Industrial and agricultural ammonia point sources exposed, Nature, 564, 99-103,
22  10.1038/s41586-018-0747-1, 2018.
23
24  Vecchi, G. A., S.-P. Xie, and A. S. Fischer: Ocean-atmosphere co-variability in the western
25  Arabian Sea, J. Climate, 17, 1213–1224, 2004.
26
27  Verver, G. H. L., Sikka, D. R., Lobert, J. M., Stossmeister, G., and Zachariasse, M.: Overview
28  of the meteorological conditions and atmospheric transport processes during INDOEX 1999, J.
29  Geophys. Res., 106, 28399–28413, 2001.
30
31  Wai, K. M., Wu, S., Kumar, A., and Liao, H.: Seasonal variability and long-term evolution of
32  tropospheric composition in the tropics and Southern Hemisphere, Atmos. Chem. Phys., 14,
33  4859–4874, https://doi.org/10.5194/acp-14-4859-2014, 2014.
34
35  Waliser, D. E., Intraseasonal variability. The Asian Monsoon, B. Wang, Ed., Springer, 203–
36  258, 2006.
37
38  Waliser, D. E., and C. Gautier: A Satellite-derived Climatology of the ITCZ. J. Climate, 6,
39  2162–2174, https://doi.org/10.1175/1520-0442(1993)006<2162:ASDCOT>2.0.CO;2, 1993.
40
41  Wang, S., Kinnison, D., Montzka, S. A., Apel, E. C., Hornbrook, R. S., Hills, A. J., et al., Ocean
42  biogeochemistry control on the marine emissions of brominated very short-lived ozone-
43  depleting substances: a machine-learning approach. J. Geophys. Res., 124, 12319– 12339.
44  https://doi.org/10.1029/2019JD031288, 2019.
45
46  Wang, R., Balkanski, Y., Bopp, L., Aumont, O., Boucher, O., Ciais, P., Gehlen, M., Peñuelas,
47  J., Ethé, C., Hauglustaine, D., Li, B., Liu, J., Zhou, F., Tao, S.: Influence of anthropogenic
48  aerosol deposition on the relationship between oceanic productivity and warming, Geophys.
49  Res. Lett., 42, 10,745– 10,754, doi:10.1002/2015GL066753, 2015.
50

Warneck, P.: The relative importance of various pathways for the oxidation of sulfur dioxide and nitrogen dioxide in sunlit continental fair weather clouds, Phys. Chem. Chem. Phys., 1, 5471–5483, 1999.

Watts, S. F.: The mass budgets of carbonyl sulfide, dimethyl sulfide, carbon disulfide and hydrogen sulfide, Atmos. Environ., 34, 761–779, 2000.

Webster, P. J., Moore, A. M., Loschnigg, J. P. and Leben, R. R. Coupled oceanic-atmospheric dynamics in the Indian Ocean during 1997–98. Nature, 401, 356–360, 1999.

Williams, J., Fischer, H., Wong, S., Crutzen, P. J., Scheele, M. P., and Lelieveld, J.: Near equatorial CO and $O_3$ profiles over the Indian Ocean during the winter monsoon: High $O_3$ levels in the middle troposphere and interhemispheric exchange, J. Geophys. Res., 107, 8007, doi:10.1029/2001JD001126, 2002.

Wurl, O., Wurl, E., Miller, L., Johnson, K., and Vagle, S.: Formation and global distribution of sea-surface microlayers, Biogeosciences, 8, 121–135, doi:10.5194/bg-8-121-2011, 2011.

Yamamoto, H., Yokouchi, Y., Otsuki, A., and Itoh, H.: Depth profiles of volatile halogenated hydrocarbons in seawater in the Bay of Bengal, Chemosphere, 45, 371-377, https://doi.org/10.1016/S0045-6535(00)00541-5, 2001.

Yao, S.L., G. Huang, R.-G. Wu, X. Qu, and D. Chen: Inhomogeneous warming of the tropical Indian Ocean in the CMIP5 model simulations during 1900–2005 and associated mechanisms, Clim. Dynam., 2016.

Ye, H., Sheng, J., Tang, D., Morozov, E., Kalhoro, M. A., Wang, S., and Xu, H.: Examining the Impact of Tropical Cyclones on Air-Sea CO2 Exchanges in the Bay of Bengal Based on Satellite Data and In Situ Observations, J. Geophys. Res., 124, 555-576, 10.1029/2018jc014533, 2019.

Yoder, J. A., McClain, C. R., Feldman, G. C., and Esaias, W. E.: Annual cycles of phytoplankton chlorophyll concentrations in the global ocean: A satellite view, Global Biogeochem. Cy., 7, 181-193, 10.1029/93gb02358, 1993.

Yoshida, Y., Ota, Y., Eguchi, N., Kikuchi, N., Nobuta, K., Tran, H., Morino, I., and Yokota, T.: Retrieval algorithm for CO2 and CH4 column abundances from short-wavelength infrared spectral observations by the Greenhouse gases observing satellite, Atmos. Meas. Tech., 4, 717–734, doi:10.5194/amt-4-717-2011, 2011.

Yu, L.: Global variations in oceanic evaporation (1958-2005): the role of the changing wind speed. J. Climate, 20:5376–5390, 2007.

Zavarsky, A., Goddijn-Murphy, L., Steinhoff, T., and Marandino, C. A.: Bubble-Mediated Gas Transfer and Gas Transfer Suppression of DMS and $CO_2$, J. Geophys. Res., 123, 6624-6647, 10.1029/2017jd028071, 2018a.

Zavarsky, A., Booge, D., Fiehn, A., Krüger, K., Atlas, E., and Marandino, C.: The Influence of Air-Sea Fluxes on Atmospheric Aerosols During the Summer Monsoon Over the Tropical Indian Ocean, Geophys. Res. Lett., 45, 418-426, 10.1002/2017gl076410, 2018b.

Atmospheric
Chemistry
and Physics
Discussions

1  Zhang, N., Feng, M., Du, Y., Lan, J., Wijffels, S.E.: Seasonal and interannual variations of
2  mixed layer salinity in the southeast tropical Indian Ocean. J. Geophys. Res., 121(7):4716–
3  4731, 2016.
4
5  Zheng, B., Tong, D., Li, M., Liu, F., Hong, C., Geng, G., Li, H., Li, X., Peng, L., Qi, J., Yan,
6  L., Zhang, Y., Zhao, H., Zheng, Y., He, K., and Zhang, Q.: Trends in China's anthropogenic
7  emissions since 2010 as the consequence of clean air actions, Atmos. Chem. Phys., 18, 14095–
8  14111, https://doi.org/10.5194/acp-18-14095-2018, 2018.
9
10 Zhou, S., Gonzalez, L., Leithead, A., Finewax, Z., Thalman, R., Vlasenko, A., Vagle, S., Miller,
11 L. A., Li, S.-M., Bureekul, S., Furutani, H., Uematsu, M., Volkamer, R., and Abbatt, J.:
12 Formation of gas-phase carbonyls from heterogeneous oxidation of polyunsaturated fatty acids
13 at the air–water interface and of the sea surface microlayer, Atmos. Chem. Phys., 14, 1371–
14 1384, https://doi.org/10.5194/acp-14-1371-2014, 2014.
15
16 Zhou, M., Langerock, B., Vigouroux, C., Sha, M. K., Ramonet, M., Delmotte, M., Mahieu, E.,
17 Bader, W., Hermans, C., Kumps, N., Metzger, J.-M., Duflot, V., Wang, Z., Palm, M., and De
18 Mazière, M.: Atmospheric CO and CH4 time series and seasonal variations on Reunion Island
19 from ground-based in situ and FTIR (NDACC and TCCON) measurements, Atmos. Chem.
20 Phys., 18, 13881–13901, https://doi.org/10.5194/acp-18-13881-2018, 2018.
21
22 Ziska, F., Quack, B., Abrahamsson, K., Archer, S. D., Atlas, E., Bell, T., Butler, J. H.,
23 Carpenter, L. J., Jones, C. E., Harris, N. R. P., Hepach, H., Heumann, K. G., Hughes, C., Kuss,
24 J., Krüger, K., Liss, P., Moore, R. M., Orlikowska, A., Raimund, S., Reeves, C. E.,
25 Reifenhäuser, W., Robinson, A. D., Schall, C., Tanhua, T., Tegtmeier, S., Turner, S., Wang, L.,
26 Wallace, D., Williams, J., Yamamoto, H., Yvon-Lewis, S., and Yokouchi, Y.: Global sea-to-
27 air flux climatology for bromoform, dibromomethane and methyl iodide, Atmos. Chem. Phys.,
28 13, 8915–8934, https://doi.org/10.5194/acp-13-8915-2013, 2013.
29
30 Zou, L.W., Zhou, T.J., Near future (2016–2040) summer precipitation changes over China as
31 projected by a regional climate model (RCM) under the RCP8.5 emissions scenario:
32 comparison between RCM downscaling and the driving GCM. Adv. Atmos. Sci., 30:806–818,
33 2013.
34
35
36